Dissertation zur Erlangung des Doktorgrades
der Fakultät für Chemie und Pharmazie
der Ludwig-Maximilians-Universität München

Engineering a microwell duct-on-chip technology to translate exocrine pancreatic organoids to a cancer model

Sandra Wiedenmann

aus

Stuttgart, Deutschland

2022

Erklärung

Diese Dissertation wurde im Sinne von § 7 der Promotionsordnung vom 28. November 2011 von Frau Prof. Dr. Nina Henriette Uhlenhaut betreut.

Eidesstattliche Versicherung

Diese Dissertation wurde eigenständig und ohne unerlaubte Hilfe erarbeitet.

München, 18.05.2022

Sandra Wiedenmann

……

Dissertation eingereicht am 19.05.2022

1. Gutachterin: Prof. Dr. Nina Henriette Uhlenhaut

2. Gutachter: Prof. Dr. rer. med. Alexander Kleger

Mündliche Prüfung am 23.09.2022

Acknowledgments

I would like to thank *Dr. Matthias Meier* and *Prof. Dr. rer. med. Alexander Kleger* for giving me the opportunity to study this exciting research topic and for supporting me to publish in this interdisciplinary way. Both of them provided me with much professional input and taught and guided me with their respective expertise.

Next, I would like to sincerely thank my supervisor at Ludwig-Maximilians-Universität München *Prof. Dr. Nina Henriette Uhlenhaut,* for advising me during the time of my dissertation. Further, I would like to thank all my thesis committee members: *Prof. Dr. Nina Henriette Uhlenhaut, Prof. Dr. rer. med. Alexander Kleger, Prof. Dr. med. Maximilian Reichert, Prof. Dr. Olivia Merkel, Prof. Dr. Julian Stingele,* and *Prof. Dr. Karl-Peter Hopfner.*

I would also like to thank all my colleagues at Helmholtz Zentrum München in the Helmholtz Pioneer Campus of the Meier group for the great teamwork and scientific as well as emotional support: *Alina Platen, Dr. Scott Atwell, Nina Compera, Johannes Wirth, Jessi Ardila, Simon Rosowski, Daniel Kokotek, Dr. Julius Wiener, Dr. Nico Laumann-Lipp, Dr. Magdalena Motz, Kerstin Kellermann, Julius Perschel, Caroline Brähler, Maren Marder, Munkhtur Otgonbayar, Dr. Michel Moussus, Dr. Misao Akishiba, Dr. Tihomir Georgiev, Johanna Kössel,* and *Tin Wang Wong.*

My special thanks in this regard to *Simon Rosowski*, the second half of Sandmon and the nicest personality ever. He actively assisted me in expanding my skills with his questions on scRNA-seq analysis. Next, I would like to thank *Daniel Kokotek* for often being very spontaneous in helping me with experiments that sometimes extended into the night. Furthermore, without him, I would never have been able to develop my bouldering skills. Together with *Simon Rosowski* and *Johannes Wirth*, he always ensured that I kept my feet on the ground. I would also like to thank Johannes for his support and helpful, constructive criticism. Next, I would like to thank *Nina Compera* for her always cheerful and effective cooperation, she also always gave advice and support. I would also like to thank *Dr. Scott Atwell* and *Dr. Tihomir Georgiev* for always advising me on image data analysis with ImageJ. I also want to thank *Dr. Michel Moussus* for the initial design ideas and instruction in 3D printing techniques. In addition, I want to thank *Dr. Nico Laumann-*

Lipp for the teamwork in the writing process of the review. Further thanks go to *Alina Platen*, who has very reliably supported everyone in cell culture and lab management; without her, the lab would not run as it does.

I sincerely would also like to thank my colleagues at the University Hospital Ulm, Internal Medicine I, AG Kleger for their support in my experiments: *Dr. Meike Hohwieler, Dr. Markus Breunig, Dr. Jessica Merkle, Jana Krüger, Dr. Sandra Heller, Chantal Allgöwer, Ulrike Mayr-Beyrle, Kathrin Köhn,* and *Rashmi Bijegatte*.

Especially I would like to mention *Dr. Meike Hohwieler* and *Dr. Markus Breunig* for the good, efficient and supportive cooperation for which I am very grateful.

Furthermore, I would like to thank *Dr. Christine von Törne* and *Prof. Dr. Stefanie Hauck* for their professional support during the secretome studies. I also acknowledge *Dr. Lucas Schulte, Prof. Dr. Thomas Seufferlein, Dr. Stephanie Ellen Weissinger*, and *Prof. Dr. Peter Möller* for enabling the validation of the biomarker in patient samples. In addition, I would like to thank *Dr. Michael Sterr*, *Ines Kunze*, and *Prof. Dr. Heiko Lickert* for helping me out with manpower and equipment for the single-cell experiments.

Outside of work, credit goes to *Florian Kordon* for his helpful advice and emotional encouragement. He always cheered me up and motivated me to do my best, even late at night. Without him, I would not have been able to write the thesis in such a way.

Next, I would like to thank my father, *Dr. Harald Wiedenmann*, who put much effort into proofreading the manuscript. His input was extremely helpful and aided me, especially with gaps in the thread. I would also like to thank my mother *Birgit Wiedenmann* and my sister *Laura Wiedenmann* for their encouragement.

Finally, I would like to thank my roommate *Roberto Siani* for the constant coffee supply and all my other friends for their interest and support during the progress of my doctoral studies.

Table of Contents

Figure directory

Supplementary data

The supplementary data can be found on the attached USB.

Supplementary Data 1

Top 300 DEGs for the kinetic clusters in **Figure 19c**. *The supplementary data is adapted from Wiedenmann, et al. [1] and used with "author permission rights" from Nature.*

Supplementary Data 2

Dynamical genes for **Figure 23f**. *The supplementary data is adapted from Wiedenmann, et al. [1] and used with "author permission rights" from Nature.*

Supplementary Data 3

Top 300 DEGs for the Louvain clusters in **Figure 27a**. *The supplementary data is adapted from Wiedenmann, et al. [1] and used with "author permission rights" from Nature.*

Supplementary Data 4

PDLO secretome and proteome. *The supplementary data is adapted from Wiedenmann, et al. [1] and used with "author permission rights" from Nature.*

Supplementary Data 5

Results of the ELISA FLNB screening corresponding to **Figure 30h**. *The supplementary data is adapted from Wiedenmann, et al. [1] and used with "author permission rights" from Nature.*

Supplementary Video 1

Live-cell imaging of the 3D cell aggregate formation with hiPSC.

Supplementary Video 2

Live-cell imaging during PDLO differentiation from day 24 until day 31. *The supplementary video is used again from Wiedenmann, et al. [1] and used with "author permission rights" from Nature.*

Glossary Box

General abbreviations

Abbreviation	Definition
2D	Two dimensional
3D	Three dimensional
AA	Ascorbic acid
ADM	acinar-ductal metaplasia
BMP	Bone morphogenetic protein
BSA	Bovine serum albumin
CAFs	Cancer-associated fibroblasts
CAM	Cell adhesion molecule
DDA	Data-dependent acquisition
DEG	Differentially expressed gene
DLP	Digital light processing
DOD	Days of differentiation
ECM	Extracellular matrix
ESC	Embryonic stem cell
FACT	Fast acrylamide free tissue clearing
FAF	Fatty acid free
FASP	Filter aided sample preparation
FGF	fibroblast growth factor
GEMM	genetically engineered mouse model
GFR	Growth factor reduced
GO	Gene ontology
H&E	Hematoxylin and Eosin
HDAC	histone deacetylase
hFB	Human fibroblast
hiPSC	Human induced pluripotent stem cell
HPaSteC	Human pancreatic stellate cell
hPSC	Human pluripotent stem cell
HUVEC	Human umbilical vein endothelial cell
ID	Inner diameter
IF/ICC	Immunofluorescence
IF-p	Immunofluorescence-paraffin
IHC-p	Immunohistochemistry
IPMN	Intraductal papillary mucinous neoplasm
ITPN	Intratubular papillary neoplasm

Abbreviation	Definition
LS-MS/MS	Label-free mass spectrometry
MCN	Mucinous neoplasm
MMP	Multipotent progenitors
mOS	Modified overall survival
NA	Nicotinamid
NGS	Next generation sequencing
NSG	NOD scid gamma
PAGA	Partition-based graph abstraction
PanIN	Pancreatic intraepithelial neoplasm
PB	Peripheral blood
PBS-T	0.5% Triton X-100/PBS
PCA	Principal component analysis
PCO	Pancreatic cancer organoid
PDAC	Pancreatic ductal adenocarcinoma
PDLO	Pancreatic duct-like organoid
PDMS	Polydimethylsiloxane
PDO	Pancreatic ductal organoid
PEG	Poly(ethylene glycol)
PFA	Formaldehyde
PP	Pancreatic progenitor
PSC	pluripotent stem cell
RA	Retinoic acid
rpm	Rounds per minute
scRNA-seq	Single-cell RNA sequencing
SHH	sonic hedgehog
TF	Transcription factor
TFA	Trifluoroacetic acid
TME	Tumor microenvironment
UMI	Unique molecular identifier
UDP	Unipotent ductal progenitors
UMAP	Uniform Manifold Approximation and Projection
WPC	Weeks post-conception
$ZnSO_4$	Zinc sulfate

Gene and Protein abbreviations

Gene/Protein	Definition
ABL1	Tyrosine-protein kinase ABL1
acTUB	Acetylated tubulin
AHNAK	Neuroblast differentiation-associated protein AHNAK
AKT1	RAC-alpha serine/threonine-protein kinase
AMY2A	Pancreatic alpha-amylase
ANXA1	Annexin A1
ANXA2	Annexin A2
ANXA3	Annexin A3
APOA2	Apolipoprotein A-II
APOB	Apolipoprotein B
APOC3	Apolipoprotein C-III
AQP5	Aquaporin-5
AREG	Amphiregulin
ARL13B	ADP-ribosylation factor-like protein 13B
ATF1	Cyclic AMP-dependent transcription factor ATF-1
ATM	Serine-protein kinase ATM
ATR	Serine/threonine-protein kinase ATR
BCLAF1	Bcl-2-associated transcription factor 1
BETA	RAR related orphan receptor B isoform 1
BICC1	Protein bicaudal C homolog 1
BMP	Bone morphogenetic protein
BRCA1	Breast cancer type 1 susceptibility protein
CA2	Carbonic anhydrase 2
CAPN2	Calpain-2 catalytic subunit
CCNA2	Cyclin-A2
CCNB2	Cyclin-B2
CCND1	G1/S-specific cyclin-D1
CDC2	Cyclin-dependent kinase 1
CDH1	Fizzy-related protein homolog
CDH17	Cadherin-17
CDK1	Cyclin-dependent kinase 1
CDK2	Cyclin-dependent kinase 2
CDK4	Cyclin-dependent kinase 4
CDK7	Cyclin-dependent kinase 7
CDKN2A	Cyclin-dependent kinase inhibitor 2A
CDX2	Homeobox protein CDX-2

Gene/Protein	Definition
CEBPB	CCAAT/enhancer-binding protein beta
CFTR	Cystic fibrosis transmembrane conductance regulator
CHD1	Chromodomain-helicase-DNA-binding protein 1
CHGA	Chromogranin-A
CK2ALPHA	Casein kinase II subunit alpha
CLDN1	Claudin-1
CLDN18	Claudin-18
CLDN4	Claudin-4
COL18A1	Collagen alpha-1(XVIII) chain
COL2A1	Collagen alpha-1(II) chain
COL4A2	Collagen alpha-2(IV) chain
COL4A5	Collagen alpha-5(IV) chain
COL4A6	Collagen alpha-6(IV) chain
COL6A1	Collagen alpha-1(VI) chain
CREB1	Cyclic AMP-responsive element-binding protein 1
CREM	cAMP-responsive element modulator
CSNK2A1	Casein kinase II subunit alpha
CSNK2B	Casein kinase II subunit beta
CTRC	Chymotrypsin-C
CXCR4	C-X-C chemokine receptor type 4
DNMT3B	DNA (cytosine-5)-methyltransferase 3B
DPP4	Dipeptidyl peptidase 4
E2F1	Transcription factor E2F1
EED	Polycomb protein EED
ELF1	ETS-related transcription factor Elf-1
ESM1	Endothelial cell-specific molecule 1
EZH2	Histone-lysine N-methyltransferase EZH2
EZR	Ezrin
FGB	Fibrinogen beta chain
FLNB	Filamin-B
FLT1	Vascular endothelial growth factor receptor 1
FOS	Proto-oncogene c-Fos
FOXA1	Hepatocyte nuclear factor 3-alpha
FOXA2	Hepatocyte nuclear factor 3-beta
FOXP3	Forkhead box protein P3
GABPA	GA-binding protein alpha chain
GABPB1	GA-binding protein subunit beta-1
GATA4	Transcription factor GATA-4

Gene/Protein	Definition
GNAS	alpha-subunit of the stimulatory G protein
GP2	Pancreatic secretory granule membrane major glycoprotein GP2
GSK3	Glycogen synthase kinase-3 alpha
GSK3B	Glycogen synthase kinase-3 beta
HCFC1	Host cell factor 1
HDAC2	Histone deacetylase 2
HES1	Transcription factor HES-1
HIST1H3A	Histone H3.1
HIST1H4A	Histone H4
HMGA1	High mobility group protein HMG-I/HMG-Y
HNF1B	Hepatocyte nuclear factor 1-beta
HNF4A	Hepatocyte nuclear factor 4-alpha
IFI16	Gamma-interferon-inducible protein 16
INS	Insulin
IRF1	Interferon regulatory factor 1
IRF8	Interferon regulatory factor 8
JNK2	Mitogen-activated protein kinase 9
JUN	Transcription factor AP-1
JUNB	Transcription factor jun-B
JUND	Transcription factor jun-D
KAT2A	Histone acetyltransferase KAT2A
KAT2B	Histone acetyltransferase KAT2B
Ki-67	Proliferation marker protein Ki-67
KRAS	Kirsten rat sarcoma
KRT19	Keratin, type I cytoskeletal 19
KRT7	Keratin, type II cytoskeletal 7
KRT8	Keratin, type II cytoskeletal 8
LDLR	Low-density lipoprotein receptor
LHX1	LIM/homeobox protein Lhx1
LMO7	LIM domain only protein 7
LYPLA1	Acyl-protein thioesterase 1
MAPK1	Mitogen-activated protein kinase 1
MAPK11	Mitogen-activated protein kinase 11
MAPK14	Mitogen-activated protein kinase 14
MAX	Protein max (Class D basic helix-loop-helix protein 4)
MMP1	Interstitial collagenase
MMP10	Stromelysin-2
MPP	U3 small nucleolar ribonucleoprotein protein MPP10

Gene/Protein	Definition
MST1	Macrophage stimulating 1
MT1E	Metallothionein 1E
MUC1	Mucin-1
MUC13	Mucin-13
MUC15	Mucin-15
MUC5AC	Mucin-5AC
MUC6	Mucin-6
MUCL3	Mucin-like protein 3
MYC	Myc proto-oncogene protein
MYL12B	Myosin regulatory light chain 12B
NCOA3	Nuclear receptor coactivator 3
NFE2L2	Nuclear factor erythroid 2-related factor 2
NFKB1	Nuclear factor NF-kappa-B p105 subunit
NFYA	Nuclear transcription factor Y subunit alpha
NKX6-1	Homeobox protein Nkx-6.1
NOTCH1	Neurogenic locus notch homolog protein 1
NPM1	Nucleophosmin
NRF1	Endoplasmic reticulum membrane sensor NFE2L1
OCT4	POU domain, class 5, transcription factor 1
ONECUT3	One cut domain family member 3
PADI4	Protein-arginine deiminase type-4
PARP1	Poly [ADP-ribose] polymerase 1
PDX1	Pancreas/duodenum homeobox protein 1
PECAM1	Platelet endothelial cell adhesion molecule
PPARGC1A	Peroxisome proliferator-activated receptor gamma coactivator 1-alpha
PRKCD	Protein kinase C delta type
PRMT1	Protein arginine N-methyltransferase 1
PROM1	Prominin-1
PSL1	Signal peptide peptidase-like 2B
PTF1A	Pancreas transcription factor 1 subunit alpha
RB1	Retinoblastoma-associated protein
RBBP4	Histone-binding protein RBBP4
RBL1	Retinoblastoma-like protein 1
RBL2	Retinoblastoma-like protein 2
RELA	Transcription factor p65
REST	RE1-silencing transcription factor
RING1	E3 ubiquitin-protein ligase RING1

Gene/Protein	Definition
RPS6KA1	Ribosomal protein S6 kinase alpha-1
S100A10	Protein S100-A10
S100A14	Protein S100-A14
SCTR	Secretin receptor
SDCBP2	Syntenin-2
SKP2	S-phase kinase-associated protein 2
SMAD3	Mothers against decapentaplegic homolog 3
SMAD4	Mothers against decapentaplegic homolog 4
SMARCA4	Transcription activator BRG1
SMARCC1	SWI/SNF complex subunit SMARCC1
SMARCC2	SWI/SNF complex subunit SMARCC2
SOX2	Transcription factor SOX-2
SOX4	Transcription factor SOX-4
SOX9	Transcription factor SOX-9
SP1	Transcription factor Sp1
SP3	Transcription factor Sp3
SPI1	Transcription factor PU.1
SPP1	Sphingosine-1-phosphate phosphatase 1
SST	Somatostatin
STAT1	Signal transducer and activator of transcription 1-alpha/beta
STAT3	Signal transducer and activator of transcription 3
TAF1	Transcription initiation factor TFIID subunit 1
TAF4	Transcription initiation factor TFIID subunit 4
TAX1BP1	Tax1-binding protein 1
TBP	TATA-box-binding protein
TCF3	Transcription factor E2-alpha
TFAP2A	Transcription factor AP-2-alpha
TFF1	Trefoil factor 1
TFF3	Trefoil factor 3
TIMP2	Metalloproteinase inhibitor 2
TIMP3	Metalloproteinase inhibitor 3
TOP2	Topoisomerase 2
TOPBP1	DNA topoisomerase 2-binding protein 1
TP53BP1	TP53-binding protein 1
TTYH1	Protein tweety homolog 1
USF1	Upstream stimulatory factor 1
USF2	Upstream stimulatory factor 2
VTN	Vitronectin

Gene/Protein	Definition
XIAP	E3 ubiquitin-protein ligase XIAP
XRCC5	X-ray repair cross-complementing protein 5
YY1	YY1-associated protein 1
ZEB1	Zinc finger E-box-binding homeobox 1
ZMIZ1	Zinc finger MIZ domain-containing protein 1
ZNF384	Zinc finger protein 384
ZO1	Tight junction protein ZO-1

Publications during the doctoral studies

During the period of the doctoral studies, the following papers have been published or are in the publishing process:

[1] Markus Breunig*, Jessica Merkle*, Martin Wagner, Michael K Melzer, Thomas F E Barth, Thomas Engleitner, Johannes Krumm, **Sandra Wiedenmann**, Christian M Cohr, Lukas Perkhofer, Gaurav Jain, Jana Krüger, Patrick C Hermann, Maximilian Schmid, Tamara Madácsy, Árpád Varga, Joscha Griger, Ninel Azoitei, Martin Müller, Oliver Wessely, Pamela G Robey, Sandra Heller, Zahra Dantes, Maximilian Reichert, Cagatay Günes, Christian Bolenz, Florian Kuhn, József Maléth, Stephan Speier, Stefan Liebau, Bence Sipos, Bernhard Kuster, Thomas Seufferlein, Roland Rad, Matthias Meier#, Meike Hohwieler#, Alexander Kleger#: *Modeling plasticity and dysplasia of pancreatic ductal organoids derived from human pluripotent stem cells*. ***Cell Stem Cell 28***, 1105-1124 e1119, doi:10.1016/j.stem.2021.03.005 (2021).[2]

[2] **Sandra Wiedenmann***, Markus Breunig*, Jessica Merkle, Christine von Toerne, Tihomir Georgiev, Michel Moussus, Lucas Schulte, Thomas Seufferlein, Michael Sterr, Heiko Lickert, Stephanie Ellen Weissinger, Peter Möller, Stefanie M. Hauck, Meike Hohwieler#, Alexander Kleger# & Matthias Meier#. *Single-cell-resolved differentiation of human induced pluripotent stem cells into pancreatic duct-like organoids on a microwell chip.* ***Nature Biomedical Engineering 5***, 897-913, doi:10.1038/s41551-021-00757-2 (2021).[1]

[3] Simon T. Rosowski; Caroline Brähler; Maren Marder; Misao Akishiba; Alina Platen; Siegfried Ussar; Fabian Theis; **Sandra Wiedenmann#**, Matthias Meier#: *Single-cell characterization of neovascularization using hiPSC-derived endothelial cells in a 3D microenvironment*, ***bioRxiv,*** 2022.02.15.480506; doi:10.1101/2022.02.15.480506 and submitted to ***eLife***[3]

[4] **Sandra Wiedenmann**, Nico Laumann-Lipp, Alexander Kleger, Matthias Meier#: *Engineering technologies for translating human exocrine pancreas into pancreatic cancer models*, manuscript in final preparation and will be submitted to ***Molecular Systems Biology***

* contributed equally

corresponding author

Parts of this doctoral thesis have already been published in Wiedenmann, et al. [1].

Zusammenfassung

Das duktale Adenokarzinom der Bauchspeicheldrüse (PDAC) ist eine der tödlichsten Erkrankungen der exokrinen Bauchspeicheldrüse, für die uns relevante Frühdiagnosemarker fehlen. Um PDAC-Marker zu identifizieren, werden *in vitro* kultivierte exokrine Pankreasmodelle aus dem frühestmöglichen, präkanzerösen Stadium benötigt. Die Übertragung der Pankreasgang-Differenzierung von humanen pluripotenten Stammzellen (hiPSCs) in *in vitro*-Krankheitsmodelle erfordert ein umfassendes Verständnis der Entwicklungsbahnen von pankreasspezifischen Zelltypen.

In dieser Arbeit wurde eine Microwell-Chip-Technologie mit definierten mikrostrukturierten Strukturen entwickelt, um aus hiPSC differenzierte Vorläuferzellen des Pankreas (PP) in einer 3-dimensionalen Zellkultur zu assemblieren. Die Vorteile der Chip-Plattform sind i) die parallele Bildung von Hunderten gleichgroßer 3D-Zellaggregate, ii) eine Matrigel-freie Mikroumgebung, iii) die Kompatibilität mit hochauflösender Bildgebung, iv) die einfache Anwendbarkeit für verschiedene nachfolgende Analysen mit minimaler Störung und v) die Möglichkeit, Ko-Kulturen zu etablieren. Der Chip wurde verwendet, um in weniger als 6 Stunden tausende von 3D-Zellaggregaten aus etwa 600 PPs zu bilden. In den folgenden 14 Tagen wurden die 3D-PP-Kulturen mit einem definierten Wachstumsfaktorprotokoll in pankreatische dukt-ähnliche Organoide differenziert.

Zeitaufgelöste Einzelzell-Transkriptionsprofile und Immunfluoreszenz von gereinigten dukt-ähnlichen Organoiden der Bauchspeicheldrüse zeigten die Entstehung von zwei Arten von duktalen Vorläufern, Zwischenstufen, und reifen duktalen Zellen und wenigen nicht-duktalen Zelltypen. Entsprechende dynamische Transkriptionsstadien wiesen auf definierte Differenzierungsrouten der duktalen Zellen hin, die in zwei entweder *CFTR*$^{+}$ oder *Mucin*$^{+}$ Subpopulationen resultieren. Diese Subpopulationen wurden bereits in primären Einzelzelltranskriptomen des Pankreas gefunden[4]. Die Integration unseres Einzelzelldatensatzes mit drei primären Pankreasdatensätzen[4-6] zeigte, dass unsere dukt-ähnlichen Zellen zusammen mit primären duktalen Zellen zu den beiden Subpopulationen clustern. Außerdem konnten die Marker der Subpopulationen in einem reanalysierten Primärdatensatz[5] erneut identifiziert und in menschlichem Primärgewebe

angefärbt werden. Darüber hinaus wurde die Duct-on-Chip-Plattform genutzt, um Organoid-Ko-Kulturen mit humanen Stellat-Zellen zu etablieren. Als zusätzliche Anwendung ermöglichte die Matrigel-freie Chip-Technologie die Entnahme des Sekretoms und Proteoms der Organoide. In Verbindung mit dem Einzelzell-Transkriptom und der klinischen Validierung ermöglichten uns diese Sekretomstudien die Entdeckung eines beispielhaften frühen PDAC-Marker namens FLNB, welcher sowohl in Biopsien als auch im peripheren Blut von Patienten im Frühstadium nachweisbar ist.

Zusammenfassend zeigt diese Arbeit die erfolgreiche Herstellung von Pankreas dukt-ähnlichen Organoiden aus hiPSCs, die ein Reifestadium aufweisen, welches mit dem des fötalen Pankreas vergleichbar ist. Durch die Kombination von zeitaufgelöster Einzelzelltranskriptomik mit verschiedenen Analysemethoden, Sekretomstudien, Proteomstudien und klinischer Validierung auf unserem Microwell-Chip wurde ein patientenspezifisches Duktmodell und ein potenzielles Krebsdiagnoseinstrument entwickelt.

Summary

Pancreatic ductal adenocarcinoma (PDAC) is one of the most severe diseases of the exocrine pancreas, for which relevant early diagnostic markers are still missing. To identify PDAC biomarkers, experimental models employing *in vitro* cultivation of exocrine pancreas models require as early as possible precancerous stages. The translation of pancreatic ductal differentiation of human pluripotent stem cells (hiPSCs) into *in vitro* disease models requires a comprehensive understanding of the developmental trajectories of pancreas-specific cell types.

In this study, a microwell chip technology exhibiting defined microstructured patterns to assemble hiPSC-derived pancreatic progenitor cells (PP) into a 3-dimensional cell culture was developed. The advantages of the chip platform are i) the parallel formation of hundreds of equally sized 3D cell aggregates, ii) a Matrigel-free microenvironment, iii) the compatibility with high-resolution imaging, iv) simple applicability for several downstream analyses with minimal perturbation, and v) the possibility to establish co-cultures. The chip was used to generate thousands of 3D cell aggregates from approximately 600 PPs, in less than six hours. For the following 14 days, the 3D PP cultures were differentiated towards pancreatic ductal-like organoids by employing defined growth factor protocols.

Time-resolved single-cell transcriptional profiling and immunofluorescence of cleared pancreatic duct-like organoids revealed the emergence of two types of ductal progenitors, intermediates, mature duct-like cells, and a few non-ductal cell types. Corresponding dynamic transcriptional stages indicated defined differentiation routes of duct-like cells, cumulating in two either *CFTR*$^{+}$ or *mucin*$^{+}$ subpopulations, which have been found before in primary single-cell transcriptomes of the pancreas[4]. The integration of the PDLO single-cell dataset into three primary pancreas datasets[4-6] showed that the duct-like cells clustered together with primary ductal cells into the two subpopulations. Furthermore, the markers of the subpopulations could be reidentified in a reanalyzed primary dataset[5] and subjected to confirmation by immunofluorescence in primary human tissue. Additionally, the duct-on-chip platform was exploited to establish organoid co-cultures with stellate cells. As an additional application, the Matrigel-free chip technology allowed the characterization of secretome and proteome. Together with the single-cell transcriptome

and clinical validation, these secretome studies revealed an exemplary early PDAC marker, called FLNB, which is detectable in biopsies and early-stage patients' peripheral blood.

In conclusion, this study reports the successful engineering of pancreatic duct-like organoids from hiPSCs, which show a maturation stage comparable to the fetal pancreas. By combining time-resolved single-cell transcriptomics with different analysis methods, secretome, proteome and clinical validation on our microwell chip, a patient-specific duct model and a potential cancer diagnostic tool was developed.

1 Introduction

1.1 The Pancreas

1.1.1 Pancreatic function

The pancreas is located in the upper abdomen and is one major organ contributing to digestion and hormone balance (**Figure 1a,b**). The different cell types of the pancreas can be grouped into two functional compartments, i.e., the endo- and exocrine pancreatic tissue. Cells of the endocrine functional unit form the islets of Langerhans and regulate the blood glucose level (**Figure 1c**). While β-cells reduce high glucose levels by secreting the hormone insulin, α-cells promote an increase in glucose levels upon glucagon

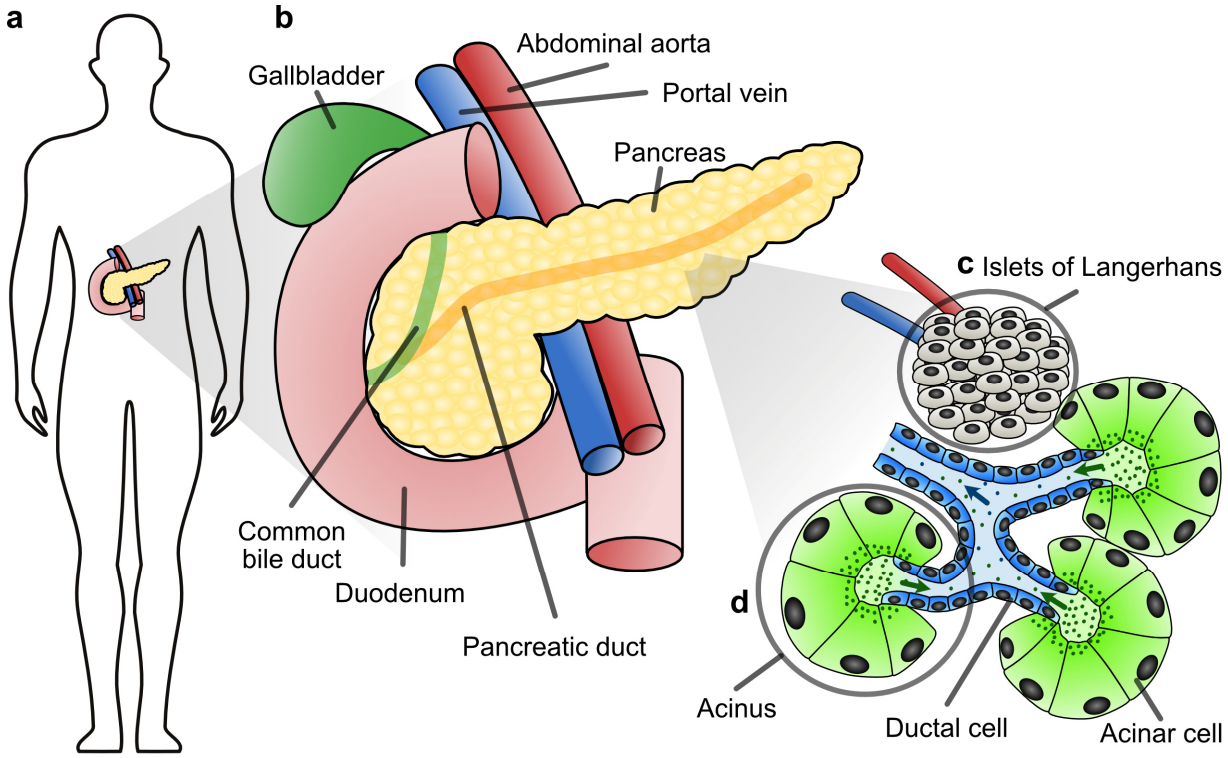

Figure 1 | Scheme of the location and structure of the pancreas.

a, Schematic location of the pancreas within the body. **b**, Representation of the location of the pancreas and surrounding tissue. **c**, The endocrine compartment of the pancreas: the blood glucose level-regulating islets of Langerhans. **d**, The exocrine part of the pancreas: the acini produce and transport the digestive enzymes through the branched network of tubular pancreatic ducts to the duodenum.

secretion. Besides α- and β-cells, the islets of Langerhans contain the hormone-producing δ-, γ-, and ε- cells[7]. The exocrine functional unit, representing more than 95% of the pancreas, produces and transports inactivated digestive enzymes into the duodenum (**Figure 1d**)[8]. Within the exocrine part, the acinar cells produce inactive digestive enzymes, including proteases, pancreatic lipases, and amylase[9]. Subsequently, the digestive enzymes are secreted through the apical side of the acinar cells into the acinus lumen. Upon contact with the digestive enzymes, ductal cells secrete bicarbonate and release water into their branched tubular network[10]. The secretion process neutralizes the pH of the gastric acid and initializes the flow of pancreatic juice[11]. The pancreatic juice is then transported through the branched ducts to the main pancreatic duct and its destination in the duodenum (**Figure 1b**)[12]. The digestive enzymes are activated in the intestine and process proteins, lipids, and carbohydrates[13].

1.1.2 Pancreatic diseases and pancreatic ductal adenocarcinoma

Dysfunction of endocrine and exocrine cells causes various diseases with serious health consequences. The most common endocrine disease is diabetes mellitus, caused by a loss of β-cells through an autoimmune reaction, impaired insulin secretion or insulin resistance[14,15]. Diseases of the exocrine pancreas like pancreatitis, cystic fibrosis or exocrine pancreatic insufficiency translate into the destruction of exocrine cells and lead to an impaired supply of pancreatic juice[16-18]. In addition to several other risk factors, diabetes mellitus and chronic pancreatitis can lead to pancreatic cancer, one of the most lethal cancer types[19].

The most common pancreatic cancer type is pancreatic adenocarcinoma (PDAC), which can arise from both exocrine cell types[20]. Despite intense research efforts over the last decades, the survival probability for PDAC patients still remains low. The 5-year survival rate after diagnosis is currently less than 8%[19,21]. To date, the only possible treatment is surgery with subsequent chemotherapy. While this raises the probability of survival to 20-23%, it can only be used in about 15% of patients[22]. This extremely poor prognosis has several reasons. First, due to unspecific symptoms in the early stages, more than half of the patients are only diagnosed at late disease stages when the tumor is inoperable[23]. Second, the development of possible tailored treatment methods remains rather poor due to the genetic complexity and high degree of intra- and intertumoural

heterogeneity[24,25] (**Figure 2**). Moreover, PDAC is hallmarked by the remarkable plasticity of epithelial cells[26], involving cell fate transitions during acinar-ductal metaplasia (ADM)[27] and the formation of premalignant lesions (**Figure 2**).

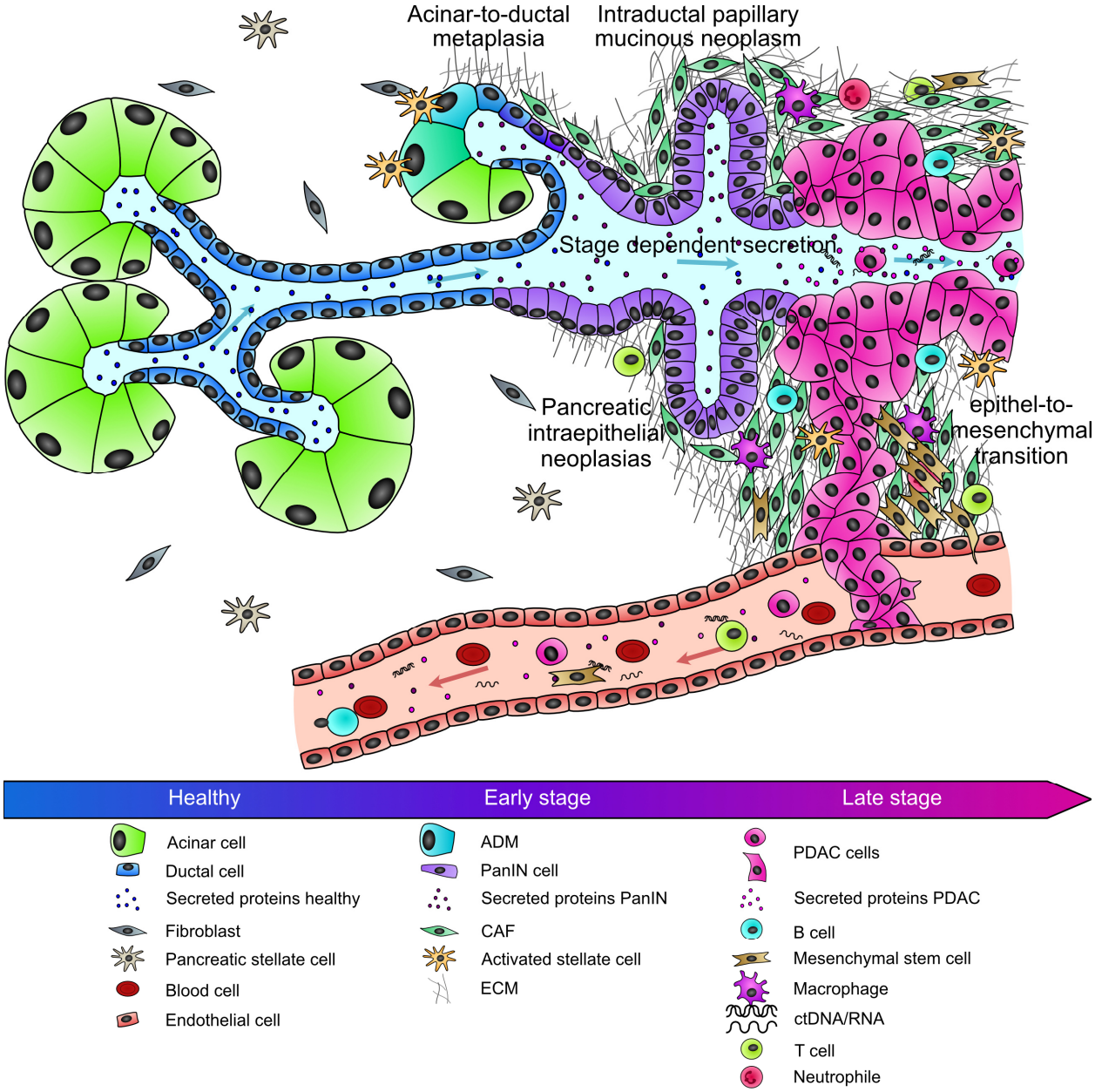

Figure 2 | The complex development of PDAC.

The schematic development from early to late-stage PDAC with diverse and complex characteristics. The figure is replicated according to Samandari, et al. [28].

These precursor lesions can be classified into four types: pancreatic intraepithelial neoplasms (PanINs), intraductal papillary mucinous neoplasms (IPMNs), mucinous

neoplasms (MCNs), and intratubular papillary neoplasms (ITPNs)[29-34]. However, the intimate molecular mechanisms leading to cellular reprogramming in early pancreatic cancer are poorly understood. In addition, the complex and dense consistency of the tumor microenvironment is associated with the presence of cancer-associated fibroblasts (CAFs) and immature myeloid and macrophages. Consequently, the rigid and poorly perfused extracellular matrix (ECM) promotes tumoral growth[35-38] while hampering drug delivery and chemotherapy[38] (**Figure 2**). Therefore, the development of new and efficient treatment methods and an earlier diagnosis with a possible preventive medical check-up is urgently needed. Diseases can be broken down into less complex aspects and new therapeutic strategies can be explored in a controlled environment with the help of *in vitro* models.

1.2 3D cell cultures to tackle PDAC from different angles *in vitro*

The restricted accessibility of human fetal and adult pancreatic tissues represents an obstacle for *ex vivo* replication and thorough investigations of human pancreas development and disease. Previously, knowledge of pancreatic development was achieved with genetically engineered mouse models (GEMMs), patient-derived xenografts, and 2D cell culture experiments. These experimental settings have characterized key signaling pathways in development, cancer progression mechanisms, and potential drug targets [39-41]. However, these model systems are associated with several constraints, such as the labor-intensive generation of GEMMs. Thus, it renders GEMMs inappropriate for high throughput drug screenings. Moreover, the entire genetic heterogeneity within and between human PDAC tumors can only be partially reproduced by GEMMs, since these models only focus on single oncogenes[25,39]. Failure to recapitulate the complex tumor microenvironment (TME) with its various cancer-associated cell types is another major caveat of patient xenografts[42]. Lastly, the commonly used pancreatic cancer cell lines are mostly established from metastases and do not represent the primary PDAC or PanINs[43]. These cell lines do not reconstruct the tumor complexity and lack the expression profiles found in patient tumors or xenografts[44,45].

Given the above, an ideal PDAC investigation model should i) accurately replicate the development of PDAC from the earliest stages, ii) mirror different PDAC characteristics,

iii) mimic heterogeneity, iv) relay the same response to stimuli or drugs as *in vivo*, v) be reproducible and reliable, vi) be easily implementable, and vii) be non-intrusive. While such a model has not been established yet, several attempts to approach it have been made.

1.2.1 Primary tissue-derived exocrine pancreatic organoids

More recently, the PDAC research field directed its focus on organoid models to delineate development, drug response prediction and personalized medicine for this deadly disease[46]. Organoids are self-organizing 3D structures that recapitulate their corresponding organ cells' composition, identity, and function *in vitro*[47]. They can be generated from primary cells, embryonic stem cells (ESCs) or pluripotent stem cells (PSCs) using cells' self-assembling properties[48]. Organoids can be cultured and passaged for a long time[49,50]. A major milestone was set by Sato and colleagues[51] by generating self-organizing intestinal organoids from adult tissue-specific stem cells in mice. Thereby, the media composition is essential for organoid formation and differentiation, long-term culture, and cell type preservation. Supplementation of media with organ-specific niche factors was not only crucial for the preservation of intestinal stem cells' ability to self-renew but also facilitated their differentiation into organoids with the 3D intestinal crypt architecture[51-54].

The first pancreatic organoid model featuring the ability to propagate murine adult bi-potent pancreas progenitors was established by Huch, et al. [55] in 2013. Subsequently, Boj, et al. [35] reported a modified media formulation aiding the differentiation of adult mouse pancreatic fragments into pancreatic ductal organoids (PDOs). The culture medium was supplemented with generic stem cell niche factors (R-spondin 1, EGF, and noggin) and pancreatic progenitor cell proliferation factors (FGFs)[51,56,57]. Mouse PDOs were able to undergo long-term clonal expansion *in vitro* and expressed transcription factor SOX-9 (SOX9), cytokeratin 19 (KRT19), and mucin-1 (MUC1) markers specific for ductal cell identity[35]. In the same attempt, Boj, et al. [35] could generate the first human pancreatic organoid model from normal and cancer tissue biopsies. The organoids recapitulated healthy human PDOs and pancreatic cancer organoids (PCOs), resembling the different stages of PDAC[35,58-60] (**Figure 3**). Long-term expansion and a

high degree of genomic stability render the PDOs with luminal physiology attractive for disease models and drug screening approaches.

PCOs exhibiting ductal and disease-stage-specific characteristics are eligible for several PDAC models. Transplantation of PCOs recapitulated different stages of PDAC and offered new insights into the implicated mediators and genetic and cell heterogenity[58,61-63]. Co-cultivation with other PDAC-related cells further helped to understand the complex communication, microenvironment, and progression in the different stages[64]. The possibility of long-term culture with genomic stability enables the compilation of a pancreatic cancer patient-derived organoid library[63,65]. PCOs are a powerful tool for developing new drugs or executing drug screening tailored to the progression stage and genetic or patient background[61].

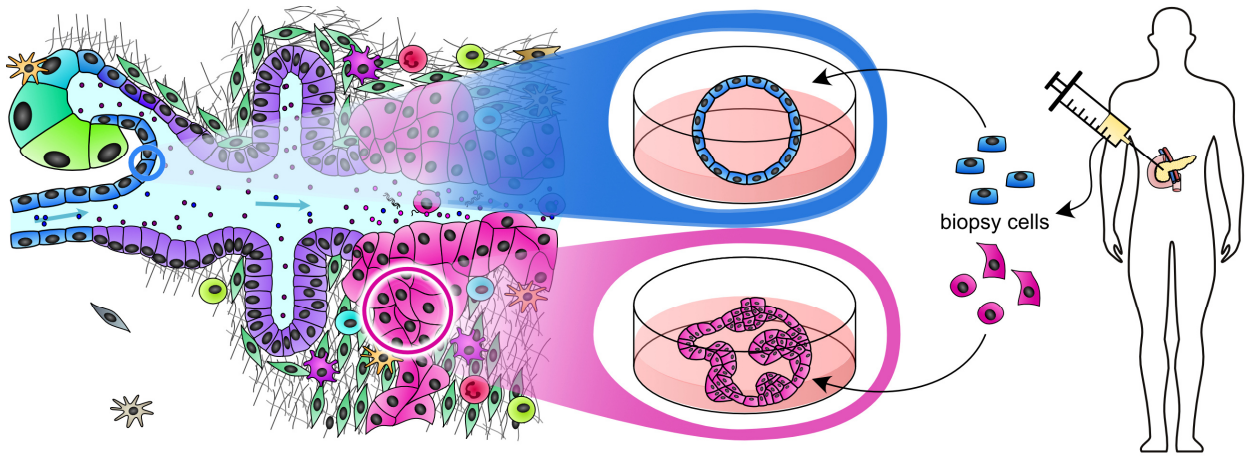

Figure 3 | Primary-derived PDOs and PCOs for *in vitro* research of PDAC.

Schematic representation of the retrieval of biopsy cells for generation and cultivation of PDO and PCO. Detail of **Figure 2** with the region of interest for PDAC modeling is shown.

Although the generation of PDOs and PCOs is possible, prior attempts to establish pancreatic acinar organoids (PAO) from pancreatic tissue have so far been unsuccessful. A major hurdle in PAO generation is the high plasticity of acinar cells[66]. Upon injury, acinar cells can regenerate the pancreas and undergo ADM, transdifferentiating into a progenitor- or duct-like state[27,67] (**Figure 2**). ADM is usually reversible and can assist the regeneration process with rebuilding acini[68,69]. However, it becomes irreversible upon oncogenic signaling and stress, leading to PanIN lesions and ultimately to PDAC[34,70]. Therefore, both human and murine primary acinar cells and cell clusters

transdifferentiate to progenitor or ductal marker-expressing cells *in vitro*[71-76]. Stable PAOs could serve as a model for ADM and thus give insight into the essential priming and reprogramming in early PanIN and PDAC progression.

1.2.2 Bioengineering PDAC models

Although we gained substantial knowledge of organoid cultures, the advances in treatment methods and survival probability still remain insufficient[19,21]. In addition, the classical hydrogel organoid model lacks essential *in vivo*-like properties, such as correct ECM composition, which translates into changes in components and stiffness during cancer progression[71,77-81]. Moreover, remodeling complex cell contacts, communication, signaling, and media drug supplementation not resembling realistic drug delivery are crucial challenges. Biopsy samples from healthy tissue are ethically restricted, and therefore the genetically controlled progression of cancer from a healthy stage is not possible. In recent years, various bioengineering strategies have been developed to improve organoid cultures further to mimic the complexity of PDAC more accurately.

1.2.2.1 Engineering synthetic hydrogels to resemble tumor microenvironment

The classical 3D organoid culture uses Matrigel as a basement membrane surrogate. Importantly, Matrigel is a batch variable mixture of ECM components derived from a murine cancer cell line, including growth factors, and does not replicate the *in vivo* pathological TME[71,77-80]. Poly(ethylene glycol) (PEG) hydrogels were designed to optimize the culture of intestinal organoids and overcome these obstacles[79,82-84]. Detailed aforegoing pancreatic tumor ECM studies[85,86] allowed Below, et al. [81] in 2021 the engineering of a fully synthetic PEG hydrogel to imitate the essential characteristics of pancreatic tumor ECM (**Figure 4**). This improved hydrogel allowed not only successful cultivation of murine and human PDOs and PCOs but also revealed new relevant ECM interactions, e.g., laminin and integrin, that contribute to enhancing PCO and cancer-related cell survival or invasion[81,87]. Further, the engineered hydrogel allowed minute stiffness adjustments according to the different PDAC changes and co-cultivation with stromal cells[81]. Thus, the engineering of this hydrogel allowed the recapitulation of a highly controlled synthetic TME[81].

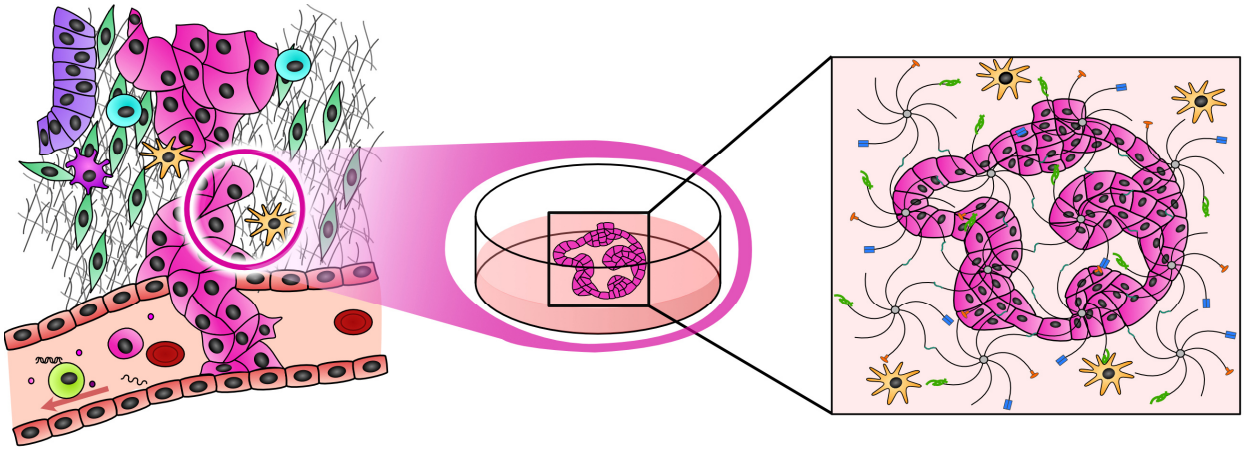

Figure 4 | Engineering fully synthetic hydrogels to model stiffness changes upon ECM secretion during PDAC progression.

Schematic representation of fully synthetic PEG hydrogel developed by Below, et al. [81] to rebuild TME with the possibility of stiffness adaption and co-cultivation of PDAC-related stromal cells. Detail of **Figure 2** with the region of interest for PDAC modeling is shown.

1.2.2.2 Drug delivery simulation through artificial vessels

After diagnosis, pancreatic cancer patients are usually treated with gemcitabine, which unfortunately only helps in a few cases[88]. Many patients rapidly develop drug resistance to chemotherapy, which can be traced to several different tumor-related issues[89]—for example, the inappropriate drug delivery through the vasculature in cancer. However, classical 2D or 3D organoid cultures and similar approaches cannot reconstruct clinical drug delivery via the vasculature system. Earlier studies showed that a combination of epithelial tumor cells, stromal cells, and endothelial cells results in augmented drug resistance of the cancerous cells[90-92]. Further studies with this chip might give more detailed insights into cancer angiogenesis. While recapitulation of the *in vivo* TME complexity of PDAC was attempted in animal studies, species-dependent differences in drug response may occur, resulting in a need for more realistic human *ex vivo* PDAC models.

The lately developed organ-on-a-chip technology enabled the creation of cell cultures that mimic cell microenvironment similar to the human body through precise microfluidic control. They can be used for organ- or disease-specific modeling, allowing not only the

possibility for drug screening and personalized medicine but also the replacement of animal testing.

Lai, et al. [93] developed 2017 the InVADE platform to form an artificial blood vessel with a surrounding Matrigel-based hydrogel, including growing tumor organoids and other cells. Three years later, Lai, et al. [94] revealed the possibility of drug delivery through a vascularized pancreatic epithelium with a tri-culture system of PCOs, human fibroblasts (hFB) and human umbilical vein endothelial cells (HUVECs) (**Figure 5**). With this PDAC TME model, Lai, et al. [94] established a microfluidic approach for an *in vivo*-like drug delivery system. This study demonstrated that synergistic contact between PCOs and activated hFBs results in the formation of up to six times stiffer TME. Thus it approaches the human PDAC hallmarks[95], which impedes the exposure to gemcitabine and ultimately the drug resistance in patients[94].

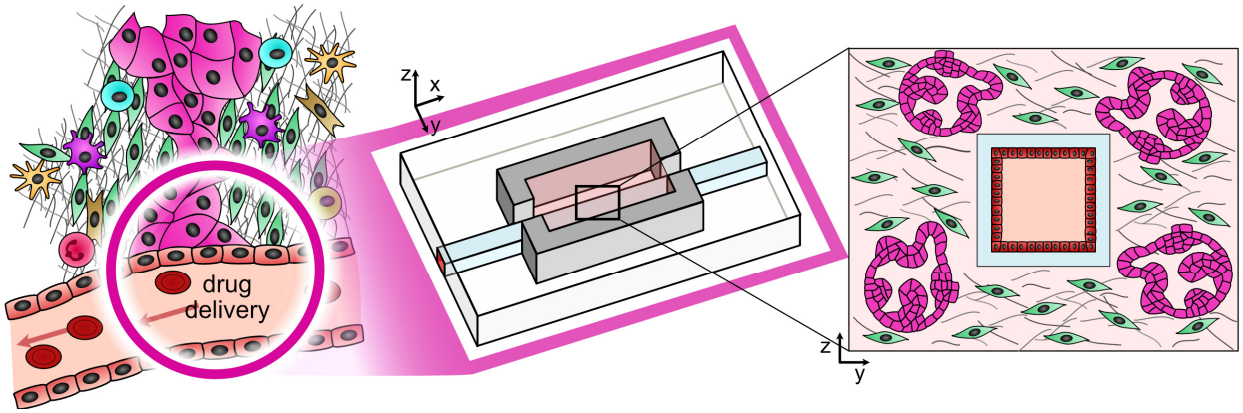

Figure 5 | Microfluidic chip to model drug delivery and resistance in PDAC.

Schematic representation of the microfluidic chip developed by Lai, et al. [93] and Lai, et al. [94] to model the drug delivery to PDAC cells and the development of drug resistance within patients. Detail of **Figure 2** with the region of interest for PDAC modeling is shown.

1.2.2.3 Recapitulation of PDAC hypovascularization

Another cause for PDAC drug resistance and subsequent metastatic events is hypovascularity[96-98]. During the progression of PDAC, cancer cells invade the vascular system (intravasation), spread to remote sites through the bloodstream, and leave the vessels (extravasation) before invading, growing and forming micrometastases[98]. This metastatic progression occurs in the early stages, followed by the ablation of vessels by

cancer cells, inhibiting the drug delivery[26,99]. Intravasation and extravasation have already been addressed in microfluidic chips with perfusable 3D vessels for other cancer types[100-102].

Nguyen, et al. [103] developed a pancreatic cancer on-chip to study the migration from PDAC cells towards vessels and the subsequent ablation of endothelial cells (**Figure 6**). Thus, two perfusable cylindrical channels are embedded in a collagen hydrogel, each mimicking an artificial vessel and a murine PDAC lumen[103]. Branching of the PDAC cells towards the vessel lumen was induced by creating a gradient through flushing FBS into the endothelial channel[103]. The tumor sprouts reached and wrapped around the biomimetic vessel before growing along, invading, occupying and abating it[103]. Thereby, the vessel was assimilated to a tumor-filled luminal structure consistent with patient studies[103,104]. The invasion and occupancy of artificial vessels by the cancer cells combined with the ablation of the endothelial vessel cells could explain circulating cancer cells, metastatic rate of PDAC and hypovascularity[103].

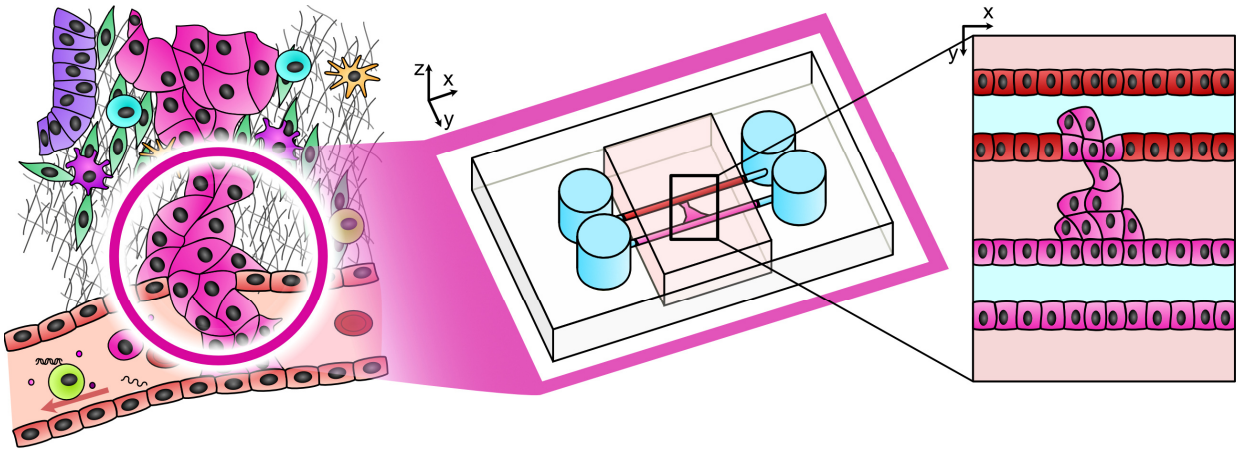

Figure 6 | Modeling hypovasularization during PDAC *in vitro*.

Schematic representation of the microfluidic chip developed by Nguyen, et al. [103] to model hypovasularization and ablation of endothelial cells during PDAC progression. Detail of **Figure 2** with the region of interest for PDAC modeling is shown.

1.2.3 hPSC-derived exocrine pancreatic organoids

Pancreas-derived organoids maintain the cellular heterogeneity of the human pancreas and can be deployed for functional testing or biomarker screening for PDAC

in vitro[105,106]. However, pancreatic cancer-derived organoids also have limitations. First, they have an undefined genetic background; being generated from a tumor renders challenging the generation of an accurate general organoid model. Second, organoids resembling the cancer end-stage are unsuitable for biomarker discovery in the earliest stages of pancreatic dysplasia[107]. Moreover, organoids of the adult human pancreas[60,108] are difficult to establish and cultivate in an untransformed stage. In addition, they cannot mimic intermediate stages of human pancreas development. Pancreatic ductal cells derived from human pluripotent stem cells (hPSCs) could provide an alternative pancreatic organoid source capable of overcoming these barriers[109,110].[1]

1.2.3.1 Human induced pluripotent stem cells

hPSCs can differentiate into all cell types of the human body except trophectoderm[111]. Thereby, hPSCs serve as an optimal tool for *in vitro* tissue development and disease modeling. In 2006, Takahashi and Yamanaka [112] revolutionized stem cell research by reprogramming somatic mouse cells with *Oct4*, *Sox2*, *Klf4*, and *Myc* into induced pluripotent stem cells. Takahashi and colleagues[113] reprogrammed human fibroblasts to generate human induced pluripotent stem cells (hiPSCs) in the following year. The generation of hiPSCs from somatic cells advanced the stem cell field by enabling the replacement of ethically critical human ESCs as a resource for almost indefinitely self-renewing stem cells. Also, hiPSCs can be retrieved from patients and thus enable patient-derived organoid studies. Therefore, hiPSCs can serve as an optimal starting material for controlled organoid differentiation to mimic human development and disease *in vitro*.

1.2.3.2 Resembling pancreas development from stem cells to pancreatic progenitors

The prerequisites for engineering and implementing ductal disease models are represented by a comprehensive mechanistic understanding of the *in vitro* differentiation landscape, cell-type composition, and functionality at the ductal stage. The knowledge of embryonic ductal development in humans, however, is insufficient. Preliminary rodent research has demonstrated that all cell lineages of the pancreas develop from a common

cell type[114], namely the pancreatic progenitor (PP) cell, which derives from the endoderm of the pancreas.[1]

Differentiation of pluripotent stem cells into the multipotent PPs requires a multistep protocol employing various growth factors and small molecule inhibitors, mainly based on murine pancreatic development[77,115,116]. Such a protocol is associated with activation and inhibition of signaling pathways during various developmental stages and therefore needs to be well-timed and systematically tested. After the publication of the first protocol to differentiate PSCs into PPs by D'Amour, et al. [117] in 2006, today's protocols feature different shades of variation traced back to different PSC cell lines[118], culture conditions or media compositions.

With the activation and inhibition of several pathways (protocol details, similarities, and differences in **Figure 7**), PSCs can be differentiated into PPs. During the first stage of embryogenesis, PSCs express the pluripotency markers POU domain, class 5, transcription factor 1 (*OCT4)* and transcription factor SOX-2 (*SOX2*)[119] (**Figure 7**). PSCs subsequently develop into the three germ layers: endoderm, mesoderm, and ectoderm. The pancreas-relevant definitive endoderm expresses hepatocyte nuclear factor 3-alpha (*FOXA2)*, transcription factor SOX-*17 (SOX17)*, and C-X-C chemokine receptor type 4 (*CXCR4)* and can also develop further to, e.g., intestine and lung[120,121] (**Figure 7**). The succeeding stage, the gut tube endoderm, has the potential to develop into, e.g., liver and stomach, in addition to pancreatic development[122]. The next developmental stage is the first specific to the pancreatic linage, called pancreatic endoderm, and expresses pancreatic/duodenal homeobox protein 1 (*PDX1*)[123]. The last step of the four-stage protocol, in which multipotent pancreas progenitors are formed, highly differs from the final differentiation step described by other protocols (**Figure 7**). The differentiation efficiency is validated by the coexpression of *PDX1* and Homeobox protein NKX-6.1 (*NKX6-1*)[124]. The expression of pancreas transcription factor 1 subunit alpha (*PTF1A)*, *SOX9*, hepatocyte nuclear factor 1-beta *(HNF1B)*, and glycoprotein 2 (*GP2)* shows the potential of multipotent PPs to develop into all pancreas cell types (**Figure 7**)[125].

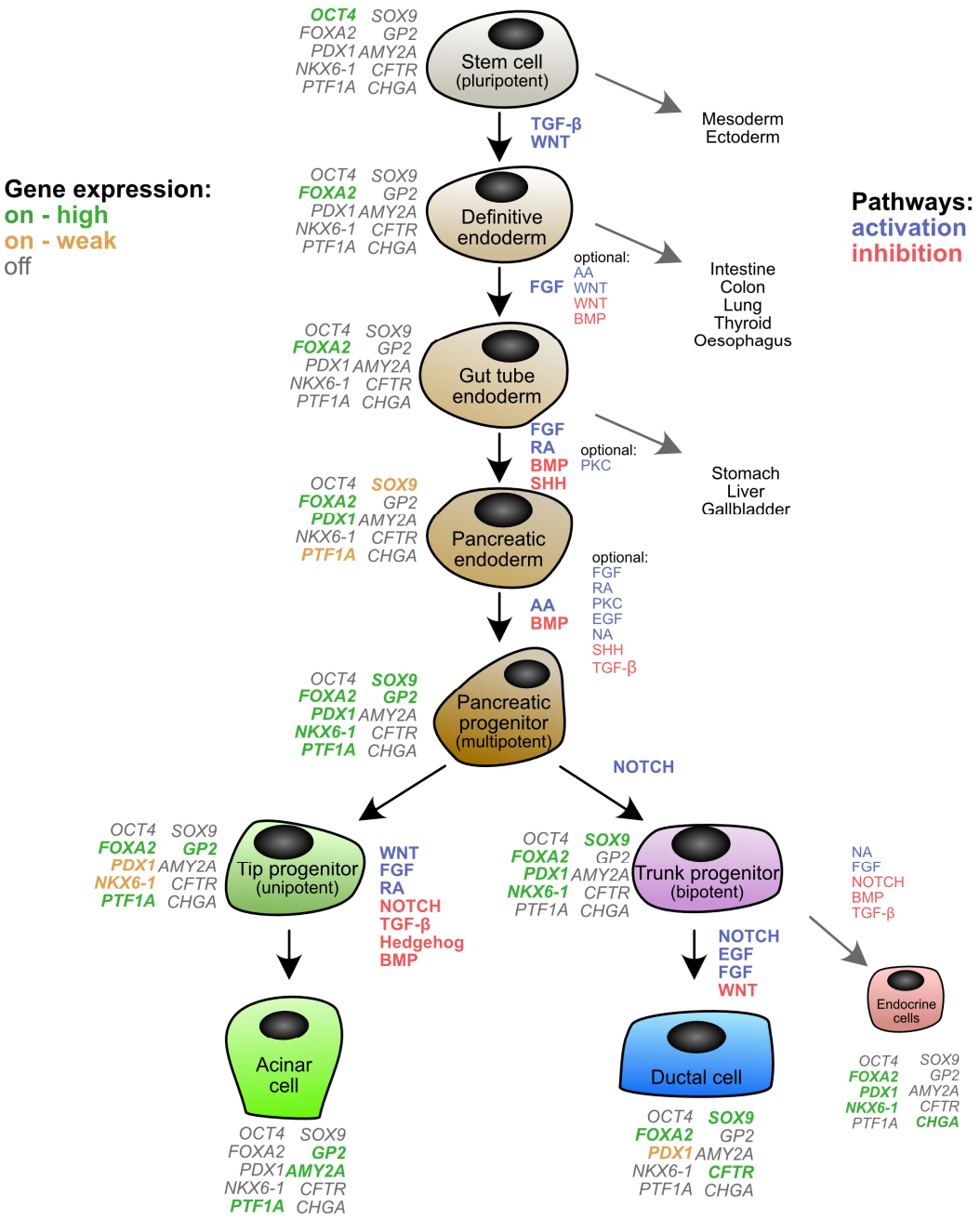

Figure 7 | Pancreas development and differentiation from stem cells into the distinct exocrine and endocrine cell types.

The lineage-committed pancreas cell type development scheme with highlighted gene expression and pathway regulations in the various stages and differentiation protocols is presented [2,109,117,118,126-136].

The murine pancreas development continues with the tip (reduce expression of *PDX1* and *NKX6-1*) and trunk (reduce expression of *GP2* and *PTF1A*) patterning (**Figure 7**).

While unipotent tip cells develop into acinar cells (expressing pancreatic alpha-amylase (*AMY2A*)), bipotent trunk progenitors differentiate into the ductal (expressing cystic fibrosis transmembrane conductance regulator (*CFTR*)) and endocrine cells (expressing chromogranin-A (CHGA)) that subsequently separate[137,138]. Using time-resolved immunostaining of developing human embryos, Jennings, et al. [139] hypothesized similar developmental routes for human pancreatic cell types. Only recently, Breunig, et al. [2] and Huang, et al. [136] established a differentiation protocol to induce hPSCs development into pancreatic duct-like organoids (PDLOs)[2,136] and pancreatic acini-like organoids (PALOs)[136].

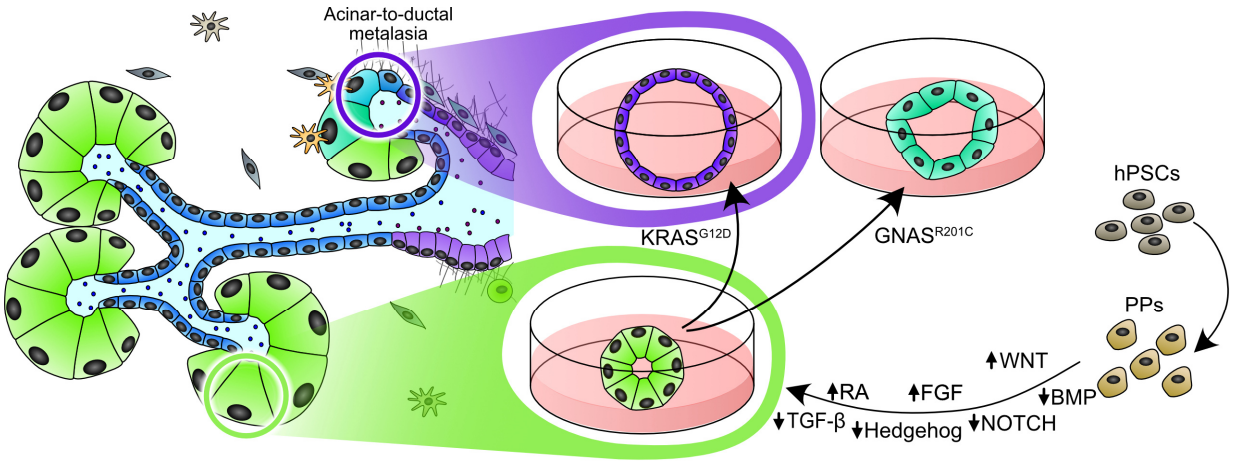

Figure 8 | Remodeling acini and PDAC development with genetically defined oncogene induction.

Schematic representation of the hPSC differentiation into PALOs. The controlled activation of the oncogene *KRAS^{G12D}* modeled ADM[136]. The induction of oncogene *GNAS^{R201C}* resulted in a lumen expansion. Detail of **Figure 2** with the region of interest for PDAC modeling is shown.

1.2.3.3 Engineering hPSC-derived acinar organoids for genetically customized PDAC induction

In 2021, Huang, et al. [136] published the first protocol for differentiating hPSC-derived pure acinar organoids. Differentiation of hPSCs to PPs, based on a protocol by Pagliuca, et al. [140], was followed by a four-stage protocol to promote PALO development (**Figure 7**, **Figure 8**). In order to achieve an acinar-like specification, activation of WNT and FGF pathways was paralleled by retinoic acid (RA) addition, and inhibition of hedgehog,

NOTCH, bone morphogenetic protein (BMP), and TGF-β pathways[136]. The PALOs displayed amylase and lipase activity and expression of the acinar markers PTF1A, CTRC, and CPA1[136]. In addition, PALOs' maturity was comparable to the human fetal or neonatal pancreas[136]. The possibility of PALOs generation and long-term cultivation enabled studies of acinar development and disease modeling *in vitro*[136].

Although PDAC is highly heterogonous, mutated Kirsten rat sarcoma (*KRAS*) was documented in 84% of PDAC patients[141] and more than 80% of PanIN lesions[142]. $KRAS^{G12D}$ is the predominant mutation of all PDAC-related *KRAS* mutations[141]. Within the precursor IPMNs lesions, guanine nucleotide-binding protein (*GNAS*) mutations are widespread, and codon 201 is the most frequently affected[143,144]. To investigate *KRAS* and *GNAS* mutations *in vitro*, Huang, et al. [136] engineered hPSC cell lines with doxycycline-inducible $KRAS^{G12D}$ and $GNAS^{R201C}$ and induced the oncogenes at PALO stage. While the $GNAS^{R201C}$ induction did not show PDAC-related *in vivo* changes in PALOs, $KRAS^{G12D}$ induced acinar-to-ductal metaplasia-like alterations (**Figure 8**)[136].

1.2.3.4 Engineering hPSC-derived ductal organoids for genetically customized PDAC induction

Very recently, Breunig, et al. [2] and Huang, et al. [136] designed a protocol for generating PDLOs from hPSCs. Breunig, et al. [2] applied a two-stage protocol to PPs differentiated according to Nostro, et al. [145] and Hohwieler, et al. [146]. In contrast, Huang, et al. [136] employed a four-stage protocol to PPs, differentiated based on the protocol of Pagliuca, et al. [140] (**Figure 9**). Both ductal induction protocols employed activation of NOTCH, FGF, and EGF pathways and inhibition of WNT pathways. Additionally, Breunig, et al. [2] added zinc sulfate ($ZnSO_4$) and nicotinamide (NA), whereas Huang, et al. [136] supplemented the media with RA and inhibited TGF-β and histone deacetylase (HDAC) signaling.

The PDLOs, forming a one-layered ring-like epithelial structure, expressed in both approaches ductal cell markers like KRT19, CFTR, SOX9, HNF1B, and carbonic anhydrase II (CA2)[2,136]. Furthermore, PDLOs exhibited apical-in and basal-out polarity and were fully functional, as demonstrated by CA2 and CFTR activities[2,136]. The PDLOs achieved a ductal maturation similar to the fetal ductal pancreas. Notably, Breunig, et al.

[2] further matured the PDLOs into more complex PDLO structures by orthotopic transplantation. Taken together, Breunig, et al. [2] and Huang, et al. [136] developed a protocol to generate PDLOs that can be employed as a tool for pancreas developmental studies and disease modeling.

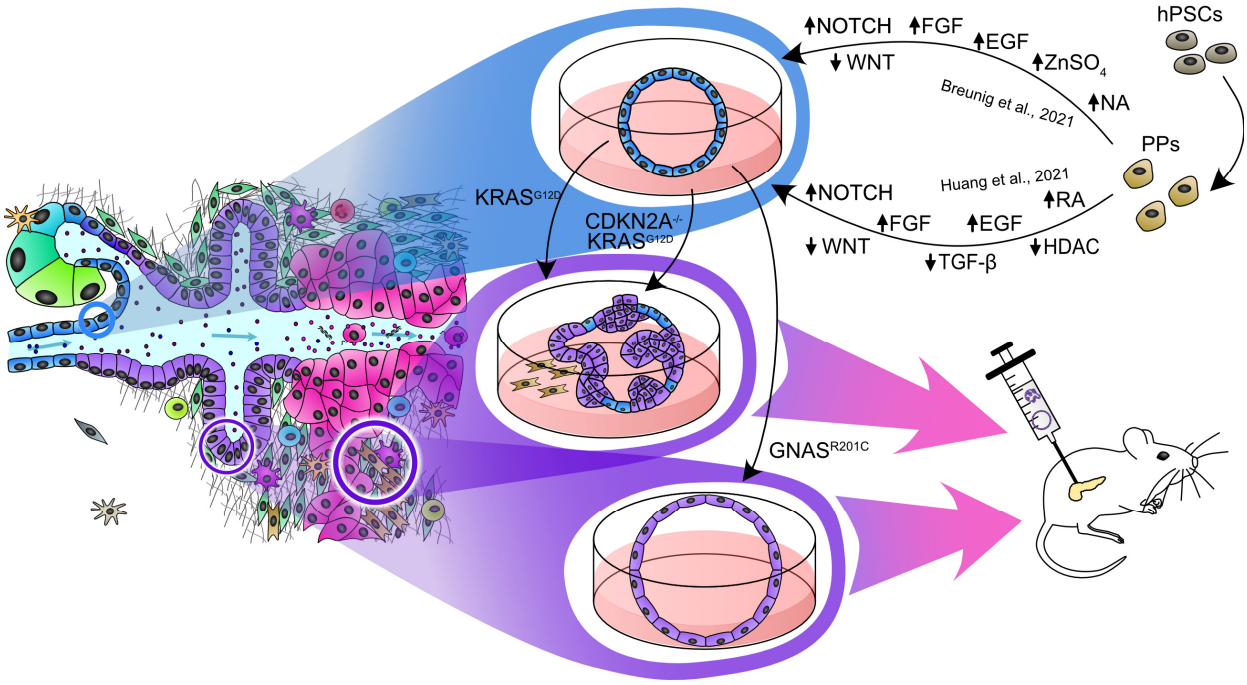

Figure 9 | hPSC-derived PDLOs resemble pancreatic ductal development and allow the controlled study of different oncogenes.

Schematic representation of the hPSC differentiation to PDLOs with relevant pathway regulation from the two distinct protocols of Breunig, et al. [2] and Huang, et al. [136]. The controlled activation of the oncogene *KRAS*^{G12D} (and *CDKN2A*$^{-/-}$) models EMT and (de-) differentiated PDAC upon transplantation[2,136]. The induction of oncogene *GNAS*$^{R201C/H}$ induced cyst formation and IPMN formation upon transplantation[2,136]. Detail of **Figure 2** with the region of interest for PDAC modeling is shown.

The *in vitro* induction of oncogenic *GNAS*^{R201C} and *GNAS*^{R201H} in PDLOs leads to a morphological change toward a cyst structure, proliferation, and expression of IMPN-related mucin-2 (MUC2) (**Figure 9**)[2,136]. After orthotopic transplantation, PDLOs formed IPMN-like structures[2,136]. Thus, the model featuring inducible GNAS oncogenes could emphasize the role of GNAS$^{R201C/H}$ as a key player in cystic neoplastic growth in pancreatic ducts[2,147,148].

In addition, oncogenic *KRAS*^{G12D} caused lumen filling and proliferation within the PDLOs from Huang, et al. [136] (**Figure 9**). Likewise, PDLOs expressing oncogenic *KRAS*^{G12D} showed lumen filling and were additionally marked by an inhibited proliferation within the study of Breunig, et al. [2]. Moreover, the *KRAS*^{G12D}-expressing PDLOs displayed EMT-specific changes[2]. Orthotopic transplantation of these organoids led either to the formation of heterogenous dysplastic lesions or PDAC[2,136]. The combination of genetic covariance upon tumor suppressor cyclin-dependent kinase inhibitor 2A (*CDKN2A*) loss and *KRAS*^{G12D} overexpression resulted in growth arrest, lumen filling, and EMT-like changes, including migrational cell behavior within PDLOs[2].

Altogether, the hPSC-derived PDLOs provide an untransformed genetic background, resembling healthy pancreatic ductal development with intermediates[2,136]. Thus, PDLOs enable genetically customized studies of pancreatic dysplasia *in vitro* and cancer formation upon orthotopic transplantation *in vivo*[2,136].

1.3 Methodic background - Microsystem tools for engineering exocrine pancreatic organoids on a microwell chip

1.3.1 Microwell array chips

Organ-on-chips are 3D microfluidic cell culture technologies that simulate organs' mechanics, functions, and physiological behavior with 3D organoids[149]. Organ-on-chip technologies are generated by combining various engineering approaches like microenvironment engineering, tissue engineering, and microfluidic engineering. The chip models became of greater interest than traditional 2D cell cultures, as they provide a higher organoid or tissue structure, resulting in a more physiological behavior and maturation [149]. Furthermore, the low-cost technology is adaptable to organ and research requirements to model *in vitro* multicellular function, development and disease without animal testing[149].

Today, thousands of different chip platforms have been developed and every chip platform is customized to specific research needs. Microwell array chips are the most simplistic form of chips, forming hundreds or thousands of organoids in parallel[1,150-156]. Since different sizes and shapes of microwells and cell type and number compromise aggregation, these properties need to be systematically tested[152,156]. An open platform

format further allows cell seeding without shear stress and easy sample retrieval without organoid disruption.

1.3.2 Soft-lithography molding of chips with polydimethylsiloxane

Polydimethylsiloxane (PDMS) is a transparent, flexible, low-cost, gas-permeable, and biocompatible polymer, making it attractive for various cell culture approaches[157]. PDMS is commonly used for microfluidic chip prototyping and manufacturing[157]. After mixing PDMS with a cross-linking agent, it can be poured onto microstructured molds and cured with heating to produce microfluidic chips. PDMS molding enables rapid chip design change and mass production from a single mold. However, PDMS can also absorb and release small molecules, requiring prior verification of media constituents and making most drug screening approaches impossible[158].

1.3.3 3D printing for customized chip molds

The most commonly used chip fabrication method is soft-lithography. The molds for chips are usually produced with photolithography to produce high-resolution micro-structures. However, these molds are limited in the z-dimension with a maximum thickness of 100 µm. To overcome this limitation, 3D printing is mainly limited by a maximum aspect ratio of 37:1[159]. Printing chip molds with a digital light processing (DLP) desktop 3D printer allows fast adaptable prototyping with an x-y-resolution going down to 25 µm. The minimum z-resolution depends on the print resist. 3D DLP printers have been used before to produce 3D molds for soft-lithography of microfluidic chips[160-162].

1.3.4 Engineering apical-out organoids for secretome studies

To model a secretory organ such as the pancreas and its early stages of diseases, measurement of changes in secreted proteins could be applied to trace early changes within pancreatic cancer and possible liquid-biopsy early biomarkers[163,164]. In classical Matrigel or hydrogel culture, the accessibility of the embedded organoids for downstream analysis is limited[82]. Additionally, PDOs and PCOs exhibit an apical-in, basal-out polarity and are thereby secreting to their inner lumen[2,35,60,136,165]. Secreted proteins trapped inside the organoid or hydrogel are not or hardly analyzable. Usually, the matrix is dissolved, or organoids are disaggregated for the downstream analysis and can not be traced or analyzed in their original culture conditions[166]. Suppose that some of the

secreted proteins can be measured in the hydrogel; in this case, a standard cell medium contains serum or other proteins in high concentrations that cannot be washed out of the solid matrix for secretion analysis and thus strongly impede it. Co, et al. [166] reported a reversible polarity switch upon suspension culture within epithelial organoids to measure secretion. Combining the polarity switch with genetically adaptable hPSC-derived PDLOs[2,136] would be a convenient starting organoid type to measure the earliest possible stages of PDAC and their secretome.

1.4 Methodic background - Validation and investigation of newly generated organoid types and their development

Differentiating organoids from stem cells for the first time on-chip requires a detailed charting of the PDLOs. Methods such as recording cell identity at the single-cell level at various time points as transcriptome and proteome are suitable for characterization.

1.4.1 Single-cell RNA sequencing

In recent years, next-generation sequencing (NGS), created for high-throughput RNA bulk analysis, has been further developed to capture the transcriptome of single cells[167]. The development of single-cell mRNA sequencing (scRNA-seq) took the analyzing possibilities to the next level through the unbiased high-resolution recording of the transcriptomic cell state[167]. Briefly e.g., droplet-based scRNA-seq methods capture single cells together with gel beads within oil on a microfluidic chip to barcode their mRNAs with a unique molecular identifier (UMI)[168]. After cDNA-library preparation and sample barcoding, the transcriptome is sequenced with NGS methods. The reads are then quality filtered and annotated to the corresponding genome, and the expressed genes are allocated to the individual cells with the UMIs[169]. Bioinformatic analysis of scRNA-seq allows, e.g., uncovering new and unexpected biological processes, cell types, cell interactions, and developmental trajectories[169].

1.4.2 High-resolution immunofluorescence imaging

Due to scRNA-seq being elaborate, expensive, and does not resolve spatial information, it is usually applied to previously validated cells. Therefore, the expression of cell- or organoid-specific common proteins is usually examined. Specific antibodies bind to their

antigen in immunofluorescence (IF) staining and label the protein of interest with fluorophores. For example, IF stainings can be applied to single cells to validate or sort them according to their protein expression via flow cytometry. In addition, it can be applied to cell cultures and tissue slices and captured with fluorescence microscopes to validate and locate the expressed proteins. Combining scRNA-seq with high-resolution IF imaging allows i) the prior validation of known cell markers, ii) the morphological and structural charting of proteins, iii) the comparison and validation of the transcriptomic and proteomic cell state, and iv) the cellular localization of scRNA-seq-derived findings.

1.4.3 Measurement of secretome and transcriptome with mass spectrometry

In combination with mass spectrometry, liquid chromatography can separate, identify, and quantify different molecules with high specificity and sensitivity. In clinics, liquid chromatography-tandem mass spectrometry (LC-MS/MS) is usually used for diagnostics[170]. In research, LC-MS/MS can be used to chart the proteome of secretome or lysed cell samples[171]. Applying LC-MS/MS onto the lysed PDLOs can further prove ductal identity and allow the possibility of comparing the transcriptomic and proteomic states of the PDLOs. Further, the measurable protein, protein levels, and protein isoforms can identify highly sensitive differences upon cancer induction within the secretome of PDLOs.

1.5 Research question – Engineering a chip for biomarker discovery

1.5.1 Thesis background

Given the poor effect of the current pancreatic cancer medication, removing the affected part of the pancreas by surgery still remains the only option for improving survival. However, only a few patients are eligible for this option[172], as the tumor is usually diagnosed too late due to its non-specific symptoms[173]. In order to tackle pancreatic cancer from different angles, it is necessary to improve *in vitro* modeling for new treatment methods and find ways to diagnose PDAC in the early stages[22].

1.5.2 Thesis aims

This thesis aimed to develop an *in vitro* model with hiPSC-derived PDLOs with the possibility of screening for early PDAC biomarkers. In order to accomplish this goal, the following assignments were required to be fulfilled consecutively:

i) Engineer an easy and fast adaptable system to optimize starting and ending conditions and allow straightforward access for downstream analysis with the application possibilities to i) reproducibly aggregate a defined cell number to homogeneous 3D cell cultures, ii) have an adequate number of organoids on the chip, iii) enable live-cell imaging, iv) generate a PDLO type, which is applicable to secretome studies for early biomarker detection within a matrix-free approach, v) easily apply downstream analysis, like IF imaging and sample retrieval for sequencing or proteomics, and vi) enable co-culturing of different cell types.

ii) Perform an in-depth validation and investigation of the correct organoid type and development. Therefore, different methods should be applied to resolve transcriptomic and proteomic changes within the differentiation and further compare the organoids to the primary human pancreas.

iii) Execute an *in vivo* proof-of-concept of the developed cell culture format to show the applicability of the chip system as a potential pancreatic cancer model.

1.5.3 Thesis content

In this doctoral thesis, I engineered a microwell duct-on-chip technology to generate matrix-free hiPSC-derived pancreatic duct-like organoids (**Figure 10**). Time-resolved single-cell RNA sequencing together with immunofluorescence imaging and proteome analysis gave a deep understanding of PDLO developmental routes and cell type composition *in vitro*. Within the PDLO transcriptome, a *CFTR*- and a *mucin*-rich ductal subcluster could be identified and *in vivo* validated. Finally, I challenged the microwell duct-on-chip technology to measure secretome in order to identify and validate prognostic cancer markers. Accordingly, the microwell duct-on-chip technology is applicable for future ductal disease modeling.[1]

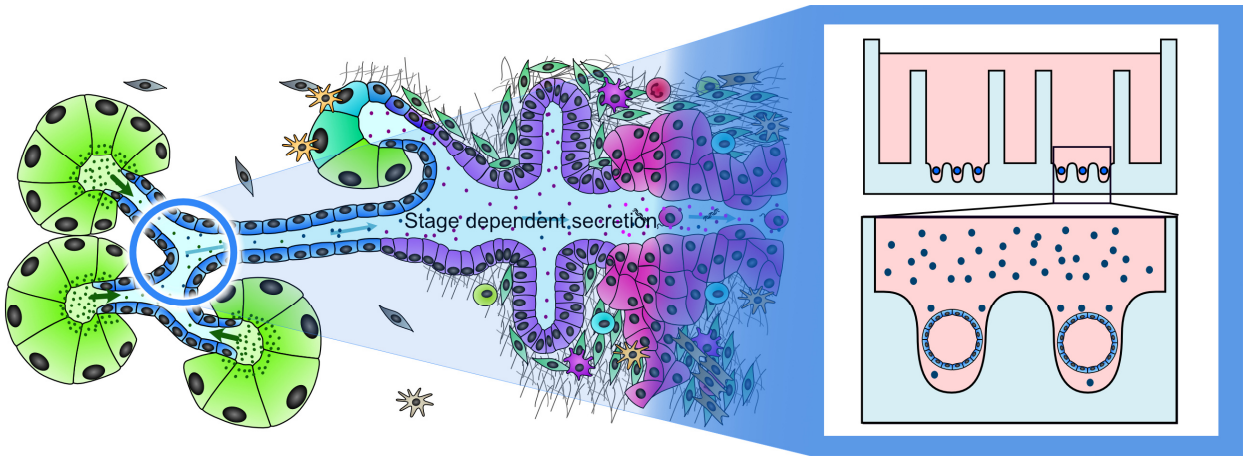

Figure 10 | Engineering microwells for PDAC biomarker discovery.

Schematic representation of the PDLO microwell chip to model and measure ductal secretion. Detail of **Figure 2** with the region of interest for PDAC modeling is shown.

2 Material and Methods

Parts of this chapter are quoted verbatim from the author's manuscript of Wiedenmann, et al. [1] with minimal corrections. A detailed description of my participation in the experiments and analysis can be found in **Chapter 8.3**.

2.1 Microwell duct-on-chip technology

2.1.1 Design of the negative microwell mold

"All microwell chips used within this study consisted of four hexagonal microwell arrays surrounded by 12 pillars. Each pillar had a diameter of 0.6 mm and a height of 4 mm. The three different microwell chips had a well diameter of 150 µm, 300 µm, and 600 µm with 251, 61, and 19 wells per array, respectively. The well's diameter-to-depth ratio on each microwell chip was 1:1.5."[1]

2.1.2 3D printing of the negative microwell mold

"Molds of the PDMS microwell chips were printed using the Freeprint® mold (Detax) resin in a DLP 3D printer (Asiga PICO2 HD 27) with a slice thickness of 10 µm. After washing the prints twice with isopropanol for 10 min, molds were incubated at 80°C for 1 h. Post-curing of the parts was achieved with an Otoflash G171 (NK-Optik) unit by exposing each side of the mild to 2000 flashes under a nitrogen environment. To ensure complete evaporation of isopropanol, molds were incubated at 80°C overnight."[1]

2.1.3 PDMS microwell chip molding

"PDMS microwell chips were produced by standard soft-lithography. In short, 3D printed molds were precoated with 0.1% hydroxypropylmethylcellulose (Fluka Analytical) dissolved in 0.2 M sodium phosphate (Sigma) (pH=3, adjusted with 0.1 M citric acid (Sigma) for 10 min) based on a protocol by Gitlin, et al. [174]. The 3D printed molds were washed with deionized water and under a nitrogen atmosphere. 1:10 PDMS (SYLGARD™ 184 Silicone Elastomer Kit, Dow Chemical Company) was cast and degassed in a vacuum chamber. A glass substrate was placed onto the microwell chip spacer structures and the PDMS was cured for 1.5 h at 80°C (**Figure 11,** steps 1-3)."[1]

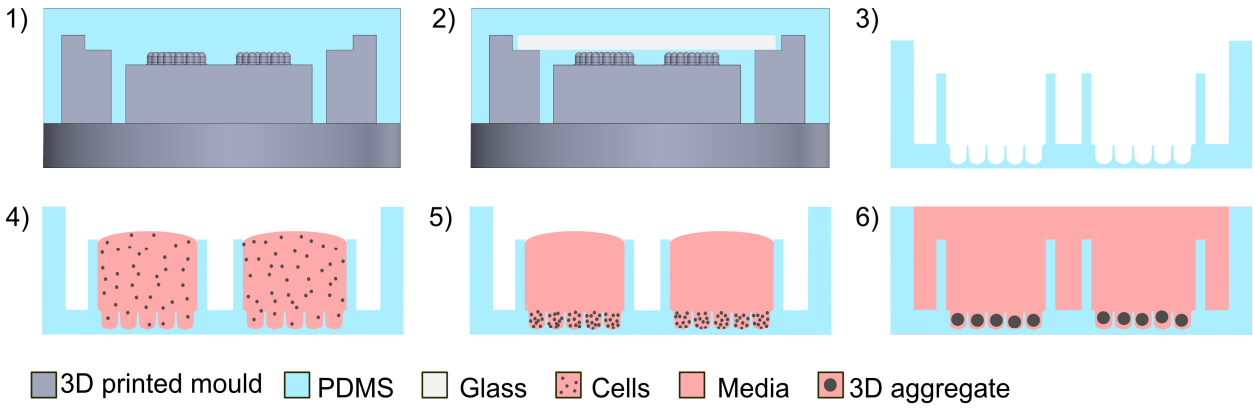

Figure 11 | Design, production, and use of the microwell duct-on-chip technology.

"Schematic of the microwell chip fabrication (steps 1–3) and cell seeding process (steps 4–6). Step 1: PDMS is poured into the 3D printed mold. Step 2: A glass slide is aligned to imprinted spacers of the mold. Step 3: PDMS is released from the mold and glass. Step 4: After passivation of PDMS with the hydrophobic co-block polymer pluronic-F127, cells resuspended in 20–40 µl of media are pipetted into the microwell arrays held by surface tension due to the 12 surrounding pillars. Step 5: Cells settle into the microwells within 30 min. Step 6: The microwell chip is filled up to 800 µl of media and cells aggregate within 4 h."[1] *The figure is adapted from Wiedenmann, et al. [1] and used with "author permission rights" from Nature.*

2.2 Cell experiments

2.2.1 Cell seeding onto the microwell duct-on-chip technology

"Before cell seeding, microwell chips were coated with 10% Pluronic F-127 (Sigma) overnight and sterilized for 30 min using 254 nm UV light (NK-Optik). On the next day, microwell chips were washed twice with Dulbecco's Phosphate Buffered Saline (PBS) (Gibco) and once with DMEM:F12 (Gibco). For ductal differentiation on microwell chips, PPs were washed with PBS, then incubated for 3-8 min with TrypLE Select (Gibco) at 37°C for detachment. PPs were centrifuged at 200 g for 5 min and then seeded in 35 µl PDLO medium per array (**Figure 11 step 4**). The surface tension on top of the arrays allowed an equal distribution of the cell suspension. After the cells settled at 37°C for 45 min (**Figure 11 step 5**), additional 660 µl of PDLO medium was carefully added to the side of the microwell chip (**Figure 11 step 6**). The cells formed 3D aggregates within a few hours. For preliminary determination of the ideal cell number for organoid formation,

hiPSCs were seeded on the microwell chip in mTeSR1 medium, supplemented with 10 µM ROCK inhibitor Y-27632 (abcam) during the first 24 h (**Supplementary Video 1**).“[1]

2.2.2 Culture of hiPSCs

“Generation and culturing of the hiPSC line has been described previously[109]. Briefly, hiPSCs were cultured on hESC Matrigel-precoated plates according to the manufacturer’s recommendations (Corning) in mTeSR1 medium (Stemcell Technologies) at 5% CO_2, 5% O_2, and 37°C with daily medium change. The general scientific use of the cells was approved by the local Ethics Committee at Ulm University (reference no. 68/11-UBB/bal.). The isolation method, culture and pancreatic differentiation of hiPSCs, as well as the study of hiPSC derivatives was approved by the local Ethics Committee at Ulm University (reference no. 159/19) under informed consent of donors.“[1]

2.2.3 HiPSC differentiation to PDLOs

“HiPSCs were differentiated into PPs in a monolayer culture based on a fused protocol from two previously published studies[109,145]. In brief, 2.5x 10^5 hiPSCs were seeded in mTeSR1 with 10 µM Rock inhibitor per well of a 24-well plate, precoated with growth factor reduced (GFR) Matrigel (1:18 in DMEM:F12, Corning). For the first 6 days, cells were differentiated in the backbone media BE1: MCDB131 (Invitrogen) supplemented with 1% Glutamax (Gibco), 0.8 g/L glucose (Sigma), 1.174 g/L sodium bicarbonate (Sigma), and 5 g/L fatty acid-free (FAF) bovine serum albumin (BSA) (Proliant). While 100 ng/ml Activin A (PeproTech) and 2 µM GSK3β-inhibitor (CHIR99021) (Axon MedChem) were added for 24 h, the medium contained 100 ng/ml Activin A and 5 ng/ml bFGF (Novoprotein) for the following two days. From day 3 until day 6 the BE1 media was complemented with 50 ng/ml FGF10 (R&D), 0.75 µM dorsomorphin (Sigma), and 3 ng/ml mouse Wnt3a (PeproTech). The subsequent backbone media BE3 was composed of MCDB131, 1% glutamax, 3.3 g/L glucose, 1,754 g/L sodium bicarbonate, 20 g/L FAF-BSA, and 0.5% insulin-transferrin-selenium-X (Gibco). From day 6 until day 9 50 ng/ml FGF10, 200 nM LDN-193189, 0.25 µM SANT-1, 2 µM retinoic acid, and 0.044 g/L L-ascorbic acid (all Sigma) were added. From day 9 until day 13, BE3 media

was supplemented with 200 nM LDN-193189, 100 ng/ml EGF (R&D), 10 mM nicotinamide (Sigma), 330 nM indolactam V (StemCell Technologies), and 0.044 g/L L-ascorbic acid. The media was freshly prepared and changed every day. At day 3 (definitive endoderm), day 9 (pancreatic endoderm), and day 13 (pancreas progenitor stage) the differentiation efficiencies were analyzed by flow cytometry. Pancreas progenitors were only used when at least 70% of the cells were PDX1 and NKX6-1 double-positive.“[1]

“For differentiation from PPs to PDLOs, cells were transferred on the microwell duct-on-chip technology facilitating a 3D cell culture. For the first seven days on the microwell chip, BE3 medium was supplemented with 1% Penicillin/Streptomycin (Sigma), 10 mM nicotinamide, 10 µM $ZnSO_4$ (Sigma), 50 ng/ml EGF, 50 ng/ml FGF10, 50 ng/ml KGF (PeproTech), 50 nM MSC2530818 (SelleckChem), and 0.044 g/L L-ascorbic acid (PDLO medium phase I). 10 µM Rock inhibitor was additionally added for the transfer of PPs on the microwell chip. From day 20 on, cells were differentiated in BE3 containing 1% Penicillin/Streptomycin, 10 mM nicotinamide, 10 µM $ZnSO_4$, 50 ng/ml EGF, 50 n/ml FGF10, and 0.044 g/L L-ascorbic acid (PDLO medium phase II). The media was changed twice a week. The complete differentiation scheme from hiPSCs to PDLOs is displayed in **Figure 14a**.“[1]

2.2.4 Differentiation quality control via flow cytometry

“Differentiation efficiencies were controlled on days 3, 9, and 13. The percentage of definitive endoderm cells was assessed by staining the surface marker CXCR4 and c-KIT on day 3. Pancreatic endoderm and pancreas progenitor cells were fixed in formaldehyde (4% PFA) (Thermo Fisher Scientific) on days 9 and 13 for intracellular staining of PDX1, and PDX1/NKX6-1, respectively. Details of the staining procedure have been previously described by Hohwieler, et al. [109].“[1]

2.2.5 Matrigel culture

“For studying niche-dependent polarity changes, microwell chip-derived PDLOs were harvested and transferred to a Matrigel 3D culture. After pipetting PBS directly on top of the microwells, PDLO cells on day 27 were washed in BE3 medium and PDLOs from ¼ array were resuspended in 50 µl (-Matrigel. Domes of 50 µl were seeded on 24-well plate

wells and after solidification for 10 min at 37 °C, PDLO medium phase II supplemented with 10 µM Y-27632 was added. After 14 days of culture with medium change (PDLO medium phase II) every 2-3 days, PDLOs were fixated with 4% PFA with 10% Sucrose for histological analysis and processed as described in later sections.“[1]

2.2.6 Mouse model

“NOD scid gamma (NSG) mice (NOD.Cg-Prkdc^{scid} Il2rgtm1Wjl/SzJ strain (Charles River); RRID:BCBC_4142) were used for xenotransplantation of PDLOs into the pancreas with permission of the “Regierungspräsidium Tübingen” (TVA-1406). All animal work was performed under ethical and animal protection regulations of the German animal protection law. Husbandry was performed in standardized hygiene barrier rooms with reduced pathogen microorganism burden. 10-week-old females were used for xenotransplantation experiments. Housing was performed in groups of two to four mice per cage.“[1]

2.2.6.1 Orthotopic transplantation of PDLOs

“Microwell chip-derived PDLOs at day 27 were harvested and singularized. After pipetting PBS directly on top of the microwells, cells were washed two more times with PBS and singularized with Accutase (Sigma) at 37°C for 30min. The enzymatic reaction was neutralized with DMEM/F12 (Gibco), supplemented with 1% BSA (Proliant) and 1% P/S (Thermo). Thereafter, cells were washed in BE3 medium and resuspended in PDLO medium phase II supplemented with 20 µM Y-27632 and GFR-Matrigel in a 1:1 ratio. Aliquots with cell/Matrigel mixture were kept on ice until transplantation. Mice were pain-mediated starting three days before transplantation by addition of 1 mg/ml Tramadol (Grünenthal) to the drinking water. To improve efficacy when transplanting low number of PDLO cells, acute pancreatitis was induced using caerulein (Sigma). 10 µl of 5 µg/ml Caerulin 0.9% NaCl solution was injected intraperitoneally every hour six times prior to transplantation. After anesthesia with isoflurane, a small cutaneous midline incision was followed by a small incision into the peritoneum. A volume of 50 µl containing 100,000 cells was delivered orthotopically to every mouse into the pancreatic tail. Carefully, pancreas and spleen were repositioned in the abdomen before the peritoneum was closed by medical sewing using 5-0 polyglactin-coated vicryl suture (Ethicon). Surgical

staples were used for closing the skin and removed one week after transplantation., Tramadol treatment was stopped at this moment. After eight weeks, mice were sacrificed and pancreata were collected, fixed with 4% PFA at 4°C o/n, before being processed for histological analysis. All animal experiments were performed in compliance with the institutional guidelines, under ethical and animal protection regulations of Ulm University.“[1]

2.2.7 Pancreatic stellate cells

“Human pancreatic stellate cells (HPaSteCs), isolated from a chronic pancreatitis resection and immortalized by SV40 large T antigen and the catalytic subunit of hTERT[175], were kindly provided by Prof. Matthias Löhr (Karolinska Institute). Cells were cultured in DMEM supplemented with 10% FCS and 1% P/S and split using 0.05% Trypsin-EDTA (Sigma) twice a week in a 1:6 ratio“[1] by my colleagues of the Kleger lab.

2.2.8 PDLO/Stellate co-culture

“PDLOs and HPaSteCs were seeded on a fluidic hexagonal microwell duct-on-chip technology facilitating paracrine signaling between PDLOs and HPaSteCs in the same microwell chip without direct cellular contact. For this, 150 cells were seeded per well following the procedure described above (**Figure 29a**). The PDLOs were derived on the upscaled microwell duct-on-chip technology (**Figure 30a**), harvested at day 31, and transferred onto two arrays of the microwell chip (**Figure 12**). The microwell chip was filled with phase II ductal media and co-cultured for three days without media change. The 3D HPaSteC aggregates and PDLOs were harvested on day 34. Briefly, media was removed, and drops of 40 µl PBS were delivered on top of each array. Utilizing surface tension, the HPaSteC aggregates and PDLOs were harvested without cross-contamination before being washed three times with PBS. The 3D HPaSteCs aggregates and PDLOs were centrifuged with 200g for 5 min after each 10 min the washing steps. The dry pellet was frozen and stored at -80 °C before sample preparation for proteomic measurements.“[1]

2.3 Imaging experiments

2.3.1 Live Imaging

“For live-cell imaging, PDLOs were imaged every 2 hours from day 24 to 31 of differentiation with a Zeiss Axio Observer Z1 microscope. The PDLOs on microwell chip were kept in cell culturing conditions with a stage top incubator (Tokai Hit).“[1]

2.3.2 Forskolin swelling assay

“For the swelling assay, organoids were transferred to a bright field imaging microwell chip, which was composed of microwells with a diameter of 300 µm and a flat bottom to allow improved bright field imaging. Cells were stimulated on day 28 with either 20 µM forskolin (Abcam) and 100 µM 3-Isobutyl-1-methylxanthine (Sigma) (forskolin treatment) or 1:1000 DMSO (control) in DMEM:F12 medium. Live cell imaging was performed on a Zeiss Axio Observer Z1 microscope for 18 h after treatment. Images of 16 different positions were taken for each sample every 20 min.“[1]

2.3.3 Fast acrylamide free tissue clearing and immunofluorescence staining

“To allow imaging of whole organoids on microwell chips, the organoids were cleared with a protocol based on fast acrylamide free tissue clearing (FACT)[176]. Therefore, organoids were washed once with PBS and then PFA fixed for three days at 4°C. Washing with PBS was followed by incubation at 37°C for 1-3 h with 8% ultra-pure SDS (Invitrogen) in PBS for actual clearing. After two washing steps with PBS and PBS-T (0.01% Tween 20 (Roth)), the organoids were subjected to blocking and permeabilization with 1% BSA (Roche), 22.52 mg Glycin (Roth), and 0.1% Tween 20 for 1 h. The primary antibody was diluted in 1% BSA and 0.1% Tween 20 and samples were stained for 3 days at 4°C. After washing twice with TBS-T (Duolink), organoids were incubated with the secondary antibody diluted in 1% BSA overnight at 4°C. The organoids were washed twice with TBS (Duolink) before incubation with 1 µg/ml DAPI (Sigma) for 15 min. Subsequently, the organoids were washed twice with TBS-T and fixed for 30 min with 4% PFA. During confocal imaging (Zeiss Axio Observer LSM 880), organoids were kept on microwell chips in X-CLARITY Mounting Solution (Logos Biosystems).“[1]

A detailed list of the employed antibodies with their dilution and conditions can be found in supplement chapter **8.1.1**.

2.3.4 Paraffin embedding of PDLOs

“PDLOs were harvested with PBS as described in the Matrigel culture section. Harvesting was followed by fixation of PDLOs in 4% PFA with 100 mM sucrose. After incubation at 4°C o/n, PFA was removed carefully and PDLOs were washed twice with PBS. Samples were pre-embedded in 2% agarose (Sigma) and further processed according to standard histology procedures. After serial dehydration, PDLOs were embedded in paraffin and 4 µm sections were prepared. Tissue slices were mounted on SuperFrost Ultra Plus microscope slides (Thermo). Pancreatic tissue from transplantation experiments were fixed, embedded, and sectioned as described above without pre-embedding in 2% agarose.“[1]

2.3.5 Histological standard techniques

“Histological stainings, including Hematoxylin and Eosin (H&E) staining, were performed according to standard protocols. Paraffin sections of PDLOs or pancreatic tissue were rehydrated in ethanol series followed by either heat-mediated or enzymatic antigen retrieval, depending on the antibody (supplement chapter **8.1.1**). Tris buffer (pH=9) or Citrate buffer (pH 6, both Vector Laboratories) were used for heat-mediated antigen retrieval in a steamer, while a self-made Citrate buffer (pH=6, 1.9 g/l citric acid; Sigma) was used in the pressure cooker. To continue with immunofluorescence-paraffin (IF-p) staining, tissue permeabilization was performed with 0.5% Triton X-100/PBS (PBS-T) for 30 min at RT. After washing twice, slides were incubated o/n at 4°C in a wet chamber with the primary antibodies diluted in Antibody Diluent (Zytomed). After washing three times with PBS-T for 5 min, slides were stained with Alexa Fluor secondary antibodies (Thermo) and 500 ng/ml DAPI diluted in Antibody Diluent for 90 min at RT in the dark. Slides were washed three times with PBS-T and finally with dH_2O before sections were mounted with Fluoromount-G (SouthernBiotech).“[1]

2.3.6 IHC staining on paraffin tissue sections

“Immunohistochemistry (IHC-p) staining of filamin b (FLNB) was performed on a comprehensive human PDAC patient cohort consisting of 86 available tissues from

resected PDACs[177-179] on a fully automated OMNIS staining device (Dako) using Envision FLEX HRP Magenta high pH kit (Dako, GV900) according to manufacturer's recommendations. Briefly, paraffin slides were incubated with primary FLNB (rabbit, 1:50, Merck, HPA004886) antibody for 30 min at RT in a wet chamber, secondary reagent for 10 min, polymer reagent for 20 min and chromogen for 5 min for color development. Washing steps were performed as described in the manufacturer's recommendations. Nuclei were counterstained with 20% haematoxylin (Dako, GC808).“[1]

“The probes were graded according to PDAC and PanIN cells. The intensity of FLNB was denoted from 0 to 3 (0 negative, 3 strongly positive). The percentage of positive FLNB cells within cancerous structures was graded from 1 to 5 (1 denotes 20% and 5 100% of FLNB positive cells). All healthy ductal cells were slightly positive and rated with 5 (number of positive cells) and 1 (intensity).“[1]

“The H-score[180,181] was calculated by multiplication of intensity scores (intensity of staining) with percentage scores (number of positive cells) in PDAC, PanIN, and healthy cells. For the Kaplan-Meier plots, the maximal H-Score per lesion was used for each patient. The patients with non-tumor-related death were treated as alive. For the bar plot in **Figure 30e,** a Mann-Whitney-U Test was used to calculate statistical significance.“[1]

2.3.7 Image analysis

“IF, IHC and bright-field images were cropped, rotated, aligned, enlarged (with black background to unify the picture size), and brightness and contrast edited with ImageJ. The measurements of organoid diameters for the comparison of different cell numbers and well diameters were performed in ImageJ. In **Figure 12e** at least 58 3D PP aggregates from three different microwell duct-on-chip arrays were measured for each condition. In **Figure 13b,** 3D hiPSC aggregates from four technical replicates were measured over three days. One-sided students t-test was used to analyze size changes in R. Normal distribution was confirmed by the Shapiro-Wilk test. For image analysis and editing, ImageJ version 1.52p was used[182].“[1]

2.4 Single-cell transcriptome experiments

2.4.1 Sample preparation for scRNA-seq

“While PPs at day 13 were harvested with TrypLE Select as described above, organoids on the microwell chip were harvested on days 14, 16, 20, 23, 27 (samples from experiment 2: 600 cells, 300 µm microwell diameter), and 31 (samples from experiment 1: 300 cells, 300 µm microwell diameter and 600 cells, 600 µm microwell diameter) by washing the microwell chip three times with PBS. For the dissociation of PDLOs into single cells, organoids were incubated in Accutase for 30-45 min at 37°C. In experiment 2, single cells were cryo-preserved in DMEM with 10% heat-inactivated FBS (Thermo Fisher Scientific) and 10% DMSO based on a previously described scRNA-seq sample preparation protocol[183]. For sequencing, cryo-preserved cells were thawed in DMEM:F12 and then live-dead filtered as described in the 10x Genomics protocol CG000093. Experiment 1 (Figure 14a) cells were not cryo-preserved or filtered but directly processed for actual scRNA-seq measurements. An RNA library was generated using Chromium Single Cell 3’ library and gel bead kit v3.1 (10x Genomics). The amplified cDNA library was sequenced on a NovaSeq 6000 S2 flow cell from Illumina. The number of the sequenced cells is presented in **Figure 20b**.“[1]

2.4.2 ScRNA-seq data pre-processing

“Raw sequencing data files were demultiplexed, aligned (reference genome hg38_ensrel96), filtered, barcodes and UMIs counted, and subjected to a quality filter with CellRanger (10xGenomics). The pre-processing and downstream analysis were performed with the package ‘Scanpy API’[184] in python with default parameters, if not stated differently. First, dead or stressed cells were eliminated, identified by a percentage of mitochondrial genes higher than 15%. Next, cells with less than 1,200 or more than 10^4 expressed genes and genes expressed in less than three cells were excluded. Afterward, the datasets of different days and experiments were concatenated, normalized to 10^4 gene counts per cell and log-transformed. Batch effects were corrected using ComBat. Further on, the top 4,000 highly variable genes were used for the downstream analysis. As discussed by Luecken and Theis [169], the total gene counts, percentage of mitochondrial genes, and the cell cycle distribution of S, G2 and M phase

were corrected to investigate differentiation-dependent changes on the transcriptome level.“[1]

2.4.3 Dimensionality reduction, clustering, and cell-type annotation

“The single-cell neighborhood graph was computed with the first 50 principal components and ten nearest neighbors and the cells were clustered with the Louvain algorithm[185] at a resolution of 0.4. For visualization, the dimensionality of the data was reduced using Uniform Manifold Approximation and Projection (UMAP)[186]. For cell type annotation, 300 DEGs for each of the nine Louvain clusters were calculated by ranking the clusters against all remaining cells with the t-test method (**Supplementary Data 1**). The clusters were then annotated based on known marker genes.“[1]

2.4.4 RNA velocity through dynamical modelling

“To study developmental trajectories, RNA velocity was calculated and directional dynamic gene information was recovered by splicing kinetics. Information like clustering and UMAP coordinates were retrieved from the Scanpy analysis. The preprocessing and downstream analysis were performed with scVelo[187] using default parameters. Splice variants and cells were filtered, normalized, and set to log scale with the function scv.pp.filter_and_normalize (parameters: min_cells=3, min_counts=200, min_shared_counts=20, n_top_genes=500). In a next step, the moments, based on the connectivity, were calculated with 30 PCAs and 30 neighbors. After recovering the dynamics, the latent time was calculated with a root cell from day 13. Based on this latent time, the velocity was calculated as a dynamical model[187].“[1]

“For the poly fit presented in **Figure 23e**, the endocrine and the endothelial cell clusters, as well as all cells from the progenitor clusters with a latent time higher than 0.5 were excluded. Thereby mainly excluding the progenitor cells present at late time points. Afterward, the cells were sorted by their latent time and the gene expression was fitted to a 3rd degree polynomial, following the code published by Bastidas-Ponce, et al. [188].“[1]

2.4.5 Enriched gene expression of gene sets

“The gene enrichment UMAP plots from **Figure 25**, **Figure 26**, and **Figure 30c** were generated using the scanpy command sc.tl.score_genes. The score function subtracts

the average expression of a set of genes with a reference gene set expression, randomly sampled from the whole gene pool. The gene lists for the pathway analysis were downloaded with the R package KEGGREST.“[1]

2.4.6 Integration of primary pancreas datasets

“For the integration of the primary pancreas, three human datasets were used. While GSE84133[4] (human samples GSM2230757, GSM2230759 and GSM2230760) and GSE81547[6] mainly focused on endocrine cells, GSE131886[5] described the ductal cell types. Before concatenation, the datasets were preprocessed, clustered, and aligned as described for the PDLO scRNA-seq data. For calculation of the neighborhood graph, 32 PCAs (based on an elbow plot) and 20 nearest neighbors were considered. For integration and correction of the datasets, bbknn was applied to the datasets (neighbors_within_batch=5, n_pcs=32, trim=0, copy=True) before reclustering of cells with the Louvain algorithm[185] at a resolution of 1.3.“[1]

2.4.7 Reclustering of the GSE131886[5] dataset

“In order to further investigate the markers featuring the duct-like cell cluster, the GSE131886[5] dataset was re-clustered similar to our main analysis. Cells with less than 800 different genes and more than 15% of mitochondrial counts were filtered out. For the re-clustering, a Louvain algorithm at a resolution of 0.06 was applied, and 2000 variable genes and 27 PCs were taken into account.“[1]

2.5 Proteome and secretome experiments

2.5.1 PDLO Secretome – Sample preparation for mass spectrometry

“For determination of PDLOs secretome, an upscaled microwell chip was manufactured. The chip contained 1196 microwells with a well diameter of 400 µm, a well depth of 600 µm. A total of 600 cells were seeded per well (**Figure 30a**). On day 28 of differentiation, PDLOs were washed three times with DMEM:F12 medium without supplements. 10 min incubation time between the washing steps ensured the settling of eventually floating PDLOs. Then, 700 µl blank DMEM:F12 was added and the supernatant was retrieved after 8 h for subsequent analysis by mass spectrometry. For the parallel PDLO proteome characterization, PDLOs were harvested at the end and

washed twice with ice-cold PBS and then subjected to lysis for 15 min on ice in 200 µl RIPA buffer (Thermo Fisher Scientific). For disruption of the DNA, samples were additionally sonicated and then incubated for another 15 min on ice. Protein lysates were centrifuged at 13,000 rpm for 5 min at 4°C and the supernatant was collected. 10 µg lysate and 20 µg supernatant were subjected to tryptic digestion by applying a modified filter-aided sample preparation (FASP) procedure as described[189]. Peptides were collected by centrifugation (10 min at 14,000 rpm) and acidified with 0.5% trifluoroacetic acid (TFA) and stored at -20°C.“[1]

2.5.2 Mass spectrometric measurements

“LC-MS/MS analysis was performed in data-dependent acquisition (DDA) mode. MS data were acquired on a Q-Exactive HF-X mass spectrometer (Thermo Scientific), each online coupled to a nano-RSLC (Ultimate 3000 RSLC; Dionex). Tryptic peptides were automatically loaded on a C18 trap column (300 µm inner diameter (ID) × 5 mm, Acclaim PepMap100 C18, 5 µm, 100 Å, LC Packings) at 30 µl/min flow rate. For chromatography, a C18 reversed-phase analytical column (nanoEase MZ HSS T3 Column, 100 Å, 1.8 µm, 75 µm x 250 mm, Waters) at 250 nl/min flow rate in a 95-min non-linear acetonitrile gradient from 3 to 40% in 0.1% formic acid was used. High-resolution (60,000 full width at half-maximum) MS spectrum was acquired with a mass range from 300 to 1500 m/z with an automatic gain control target set to $3x\ 10^6$ and a maximum of 30 ms injection time. From the MS pre-scan, the 15 most abundant peptide ions were selected for fragmentation (MS/MS) if at least doubly charged, with a dynamic exclusion of 30 s. MS/MS spectra were recorded at a resolution of 15,000 with an automatic gain control target set to $5x\ 10^2$ and a maximum of 50 ms injection time. The normalized collision energy was 28, and the spectra were recorded in profile mode.“[1]

2.5.3 Data Processing – Protein Identification

“Proteome Discoverer 2.4 software (Thermo Fisher Scientific; version 2.4.1.15) was used for peptide and protein identification via a database search (Sequest HT search engine) against Swissprot human database (Release 2020_02, 20349 sequences). Full tryptic specificity was considered, allowing for one missed tryptic cleavage sites, precursor mass tolerance 10 ppm, and fragment mass tolerance 0.02 Da. Carbamidomethylation

of Cys was set as a static modification. Dynamic modifications included deamidation of Asn, Gln, oxidation of Met; and a combination of Met loss with acetylation on protein N-terminus. Percolator was used for validating peptide spectrum matches and peptides, accepting upon only the top-scoring hit for each spectrum, and satisfying the cut-off values for FDR <1%, and posterior error probability <0.01. The final list of proteins complied with the strict parsimony principle.“[1]

2.5.4 Data processing – Label-free quantification

“Proteins were quantified based on abundance values for unique peptides. For this, abundance values were first normalized to each sample's total amount of peptides to account for sample loading errors. The abundance of proteins was calculated by summing up the abundance values for admissible peptides. In the following, only proteins with more than one unique peptide hit were used for downstream analysis.“[1]

“The secretome data were filtered as follows: First, only proteins not detected in the parallel recorded proteome or scRNA transcriptome datasets of the duct-like clusters were filtered. Secondly, proteins that were never detected before in the pancreas were filtered out. Therefore, the protein list “not detected proteins in the pancreas” of the Human Protein Atlas project[190] was used. To determine the fraction of actively secreted proteins, the PDLO secretome was matched against the refined human secretome[191]. Here, only proteins with the label blood secretion and extracellular space were used.“[1]

“The changes in protein abundance within the co-culture experiment were calculated by normalizing the proteomes to the mean abundance levels. The PCs were calculated on the normalized abundances. In the following, log2 fold changes of the proteins were calculated between individual and co-culture. The upregulated proteins in co-culture experiments versus the respective separately cultured PDLOs or HPaSteCs were further subjected to overrepresentation analyses. Enrichment of upregulated proteins with gene sets in common databases (Gene Ontology, KEGG, Reactome) was tested using the browser tool g:Profiler (version: e100_eg47_p14_7733820)[192]. EnrichR[193,194] enabled the analysis extension to a collective EnrichR database comprising transcription factor-protein interaction networks. The co-culture signaling networks were generated using X2Kweb[195].“[1]

2.6 Filamin B validation experiments

2.6.1 Patient material

“Samples of FFPE material and clinical data from clinical reports originate from a previously published ULM cohort which included 122 patients with resected PDAC [178,179]. Data collection was conducted retrospectively and included cases from 1997 to 2008. The study was approved by the local Ethics Committee at Ulm University (reference no. #67, 105/98, 211/2002 and 268/2008).“[1]

“Blood plasma of patients with metastasizing PDAC was provided by the biobank of Ulm University Hospital. A group of healthy subjects was used as controls. The study was approved by the local Ethics Committee at Ulm University (reference no. 159/19). Written informed consent of all patients was given for material extraction and scientific use.“[1]

2.6.2 Enzyme-linked immunosorbent assay

“The level of human filamin B in PDAC patient serum was run using the FLNB ELISA kit (MyBioSource, MBS731914) according to manufacturer’s guidelines. Before assaying, plasma was centrifuged at 1000 x g for 15 min at 4 °C and the undiluted supernatant was added in duplicates to the ELISA plate. Absorbance at 450 nm was measured with Tecan Infinite M200 Pro plate reader. The concentration of the samples was interpolated from the standard curve that was determined within the same experiment run. The results and patient characteristics can be found in **Supplementary Data 5**. Statistical significance between the control patients and PDAC patients with grading 2 and 3 was calculated with a t-test (**Figure 30h**). One patient with a tumor grading of 2-3 was excluded for the calculation of statistical significance.“[1]

2.7 Software specifications

“The scRNA-seq alignment was run in CellRanger version 3.0.1. The analyses were run in python 3.7.4 with Scanpy API version 1.4.4 or 1.5.1, anndata version 0.6.22 or 0.7.4, umap version 0.3.10, numpy version 1.17.4, scipy version 1.5.1, pandas version 0.25.3 or 1.0.5, scikit-learn version 0.22, statsmodels version 0.10.1, python-igraph version 0.7.1, louvain version 0.6.1, scvelo version 0.1.26 development, matplotlib version 3.2.1,

seaborn version 0.9.0, loompy version 3.0.6, XlsxWriter version 1.2.6, bbknn version 1.3.6 and scrublet version 0.2.1.“[1]

“The plots from **Figure 12**, **Figure 30**, **Figure 13** and **Figure 31** were generated in RStudio with R version 3.6.0 with the R packages readxl version 1.3.1, ggplot2 version 3.3.0, dplyr version 1.0.4, survminer version 0.4.8, ggpubr version 0.4.0, reshape2 version 1.4.4, survival version 3.1-12 and ggsignif version 0.6.0. Dot plots in **Figure 30e** and bar graphs in **Figure 31b** were generated using GraphPad Prism version 8.4.3. PCs (**Figure 29b**) were calculated with stats version 3.6.0 and plotted with factoextra version 1.0.7.“[1]

2.8 Data availability

“The data supporting the results in this study are available in the thesis and its supplementary. Raw data, read counts and the analyzed datasets from scRNA-seq can be accessed from the Gene Expression Omnibus repository using the accession code GSE162547. Mass spectrometry data have been deposited on the PRIDE database and can be accessed with the identifier PXD024461.“[1]

2.9 Code availability

“The code for scRNA-seq analysis is available on Zenodo at https://doi.org/10.5281/zenodo.4738625[196].“[1]

3 Results

3.1 Design of a microwell chip for the formation and differentiation of 3D PP aggregates

In this study, a microwell chip technology was designed and engineered to allow the long-term cultivation of duct-like organoids from hiPSC-derived PPs. The microwell chip's pourable negative molds (**Figure 12a**) were designed with 3D CAD software and printed with a 3D DLP printer, thus enabling an easy and fast adaption to the design

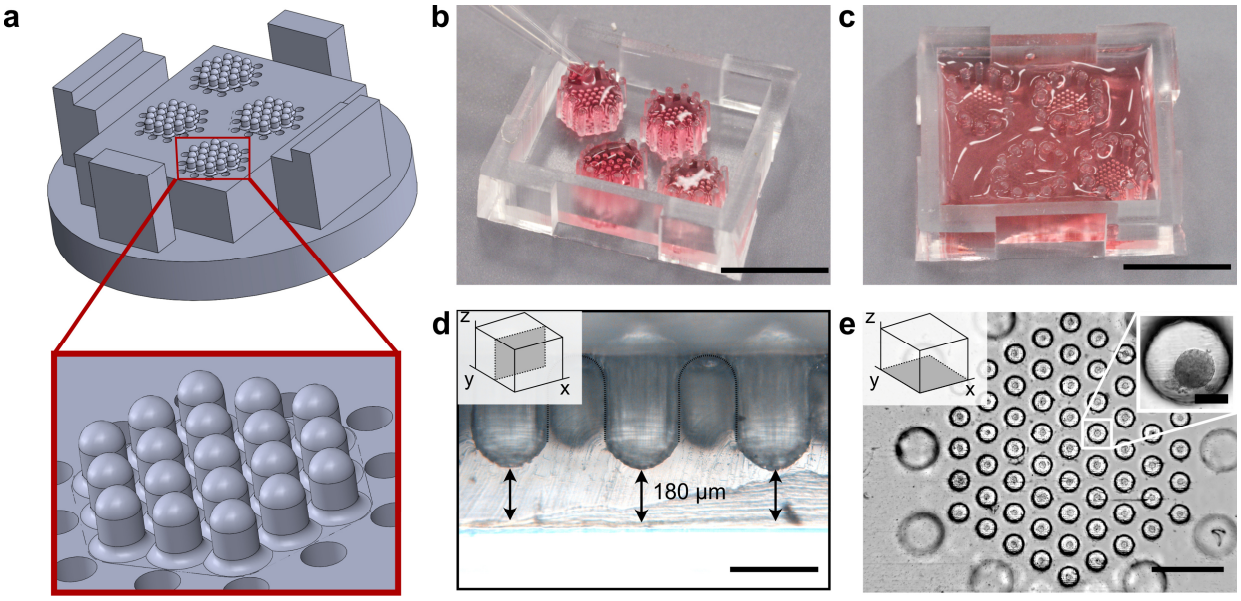

Figure 12 | Engineering a 3D microwell chip to generate, cultivate, and differentiate 3D cell aggregates.

a, Example illustration of the 3D printed castable negative mold design of the microwell chip with a well diameter of 600 µm and 19 microwells per array. **b,** The casted microwell chip with the four hexagonal arrays during cell seeding. The twelve pillars around the arrays hold the medium droplet of 20 - 40 µl containing the cells over the array with the help of surface tension. Scale bar denotes 1 cm. **c**, Image of the chip after filling up to 800 µl medium for long-term cultures and differentiation. Scale bar denotes 1 cm. **d**, Cross-section of the microwell chip to illustrate the microwell shape and the 180 µm thin bottom. Scale bar denotes 300 µm. **e**, Bottom-up view of a microwell chip array with hiPSC-derived 3D PP aggregates formed from 600 cells in a microwell chip with a well diameter of 300 µm. Scale bar denotes 1 mm and 100 µm for the magnification.[1] *The figure is adapted from Wiedenmann, et al. [1] and used with "author permission rights" from Nature.*

requirements. The 3D printed molds were then used to produce the microwell chips by soft-lithography with PDMS. Each of the microwell chips featured four hexagonal arrays of conical microwells surrounded by twelve round pillars. Using surface tension, these pillars captured an aqueous droplet (20-40 µl) on top of the array (**Figure 12b**). This enabled the seeding of a defined cell number per well and the possibility of studying up to four different conditions or cell types on the microwell chip. The microwell chip was filled with differentiation or co-culturing media, connecting all wells and arrays for long-term cultivation (**Figure 12c**). The four arrays allowed staining of up to four different antibody combinations on-chip. High-resolution imaging of the entrapped organoids was enabled by the 180-µm thin PDMS bottom layer (**Figure 12d**). The combination of the roundings between the wells and the pillars allowed an accurate and homogeneous cell seeding process in the absence of blind cell spots (**Figure 12d,e**). For a detailed description of the production workflow and cell seeding and cultivation process, please refer to **Figure 11** within the material and methods section.[1]

It is known that the shape, size, and (cell) material of the microwells and the 3D cell aggregates can influence the formation, survival, and differentiation efficiency[150,152,156,197,198]. Cell number and well size were systematically altered to provide the best starting conditions. Initially, the viability of 3D hiPSC aggregates in microwells of different sizes (150, 300 and 600 µm diameter) was examined by measuring the growth rates of the 3D hiPSC aggregates (**Figure 13a,b**). Formation of hiPSC aggregates was observed within four hours on the microwell chip (**Supplementary Video 1**) with a homogeneous size corresponding to the different well diameters and cell numbers (**Figure 13a,c**). Few numbers of cells (<50 cells/well) did not aggregate in the microwells. 3D aggregates with a diameter lower than 50 µm were associated with either substantial cell death or slowly growing over three days. To avoid insufficient nutrient diffusion, the aggregates were maintained smaller than ~250 µm in size[199]. Subsequently, to optimize the formation of PP aggregates from hiPSC, the starting cell number and the size of the microwells were systematically tested. An average 3D PP aggregate size of 96 µm (600 cells in 300 µm diameter microwells) was chosen as the initial size for following ductal differentiation if not stated differently (**Figure 13c**).[1]

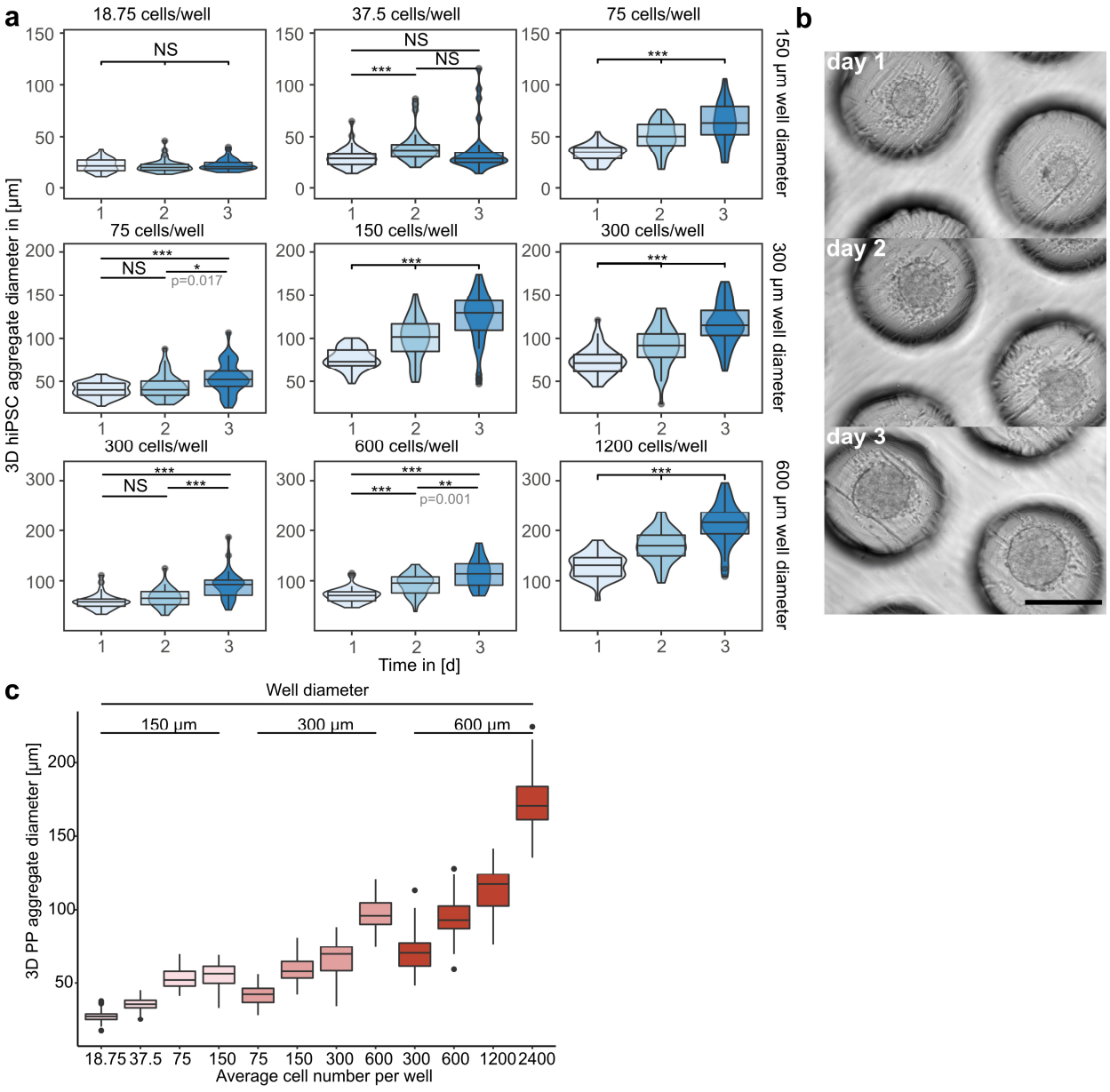

Figure 13 | Dependence of formation and growth of 3D aggregates of hiPSC on well diameter and cell number.

a, The diameter size distribution of 3D aggregates formed from hiPSC after one, two, and three days post-seeding in microwells with a 150, 300, and 600 µm diameter. 52 3D aggregates were measured for each condition from three different microwell arrays. The boxplots show the median with the first and third quartiles. The whiskers represent the 1.5 x interquartile ranges and outliers as dots. Significance levels were calculated with a two-sample Welch test and are given as follows: *: $p < 0.05$; **: $p < 0.01$; ***: $p < 0.001$. **b**, Bright-field images of 3D-hiPSC aggregates with an initial cell number of 150 per well and a well diameter of 300 µm on the first, second and third day after seeding. Scale bar denotes 200 µm. **c**, The size distribution of the diameter of 3D

aggregates formed from hiPSC-derived PPs after 24 hours. At least 58 3D aggregates of pancreatic progenitor cells from three different microwell arrays were measured. The boxplots show the median with the first and third quartiles. The whiskers represent the 1.5 x interquartile ranges and outliers as dots.[1] *The figures are adapted from Wiedenmann, et al. [1] and used with "author permission rights" from Nature.*

3.2 Differentiation of pancreatic duct-like organoids from hiPSC-derived 3D PP aggregates on the microwell chip

3.2.1 Morphologic progression during the PDLO differentiation

The microwell chip was used to differentiate 3D pancreas progenitor aggregates into PDLOs. PPs generated in 2D culture aggregated on the microwell chip within a few hours. Subsequently, a two-step differentiation protocol with specific growth factors was applied to mimic ductal development (**Figure 14a**). Consequently, substantial morphological transformations occurred in the 3D PP aggregates, as the representative bright-field images showed (**Figure 14a-c**). The initially formed homogeneous round structure of the 3D PP aggregates was broken down during the first phase of ductal induction (day 13 to 20). The cells reassembled into multiple epithelial-like layers, formed micro-lumen within the aggregates, and protrusions developed (**Figure 14b**). The number of layers of multi-layered epithelial organoids underwent reduction. Simultaneously, cystic organoids were secreted from the PDLOs' outer epithelial layer (**Figure 14b**). Of note, on day 31 of differentiation, a few cystic PDLO structures were still attached to the multi-layered epithelial PDLOs. The morphological reorganization of the PDLOs was visualized in **Supplementary Video 2**. The video and the brightfield images display the formation of both organoid types from the same 3D PP aggregate. High-resolution immunofluorescence images of cleared organoids showed cellular reorganization into micro-lumens, reduction of the multi-layered epithelial structure toward the end of phase 1, and formation of cystic PDLOs in phase 2 (**Figure 15a,b**).[1]

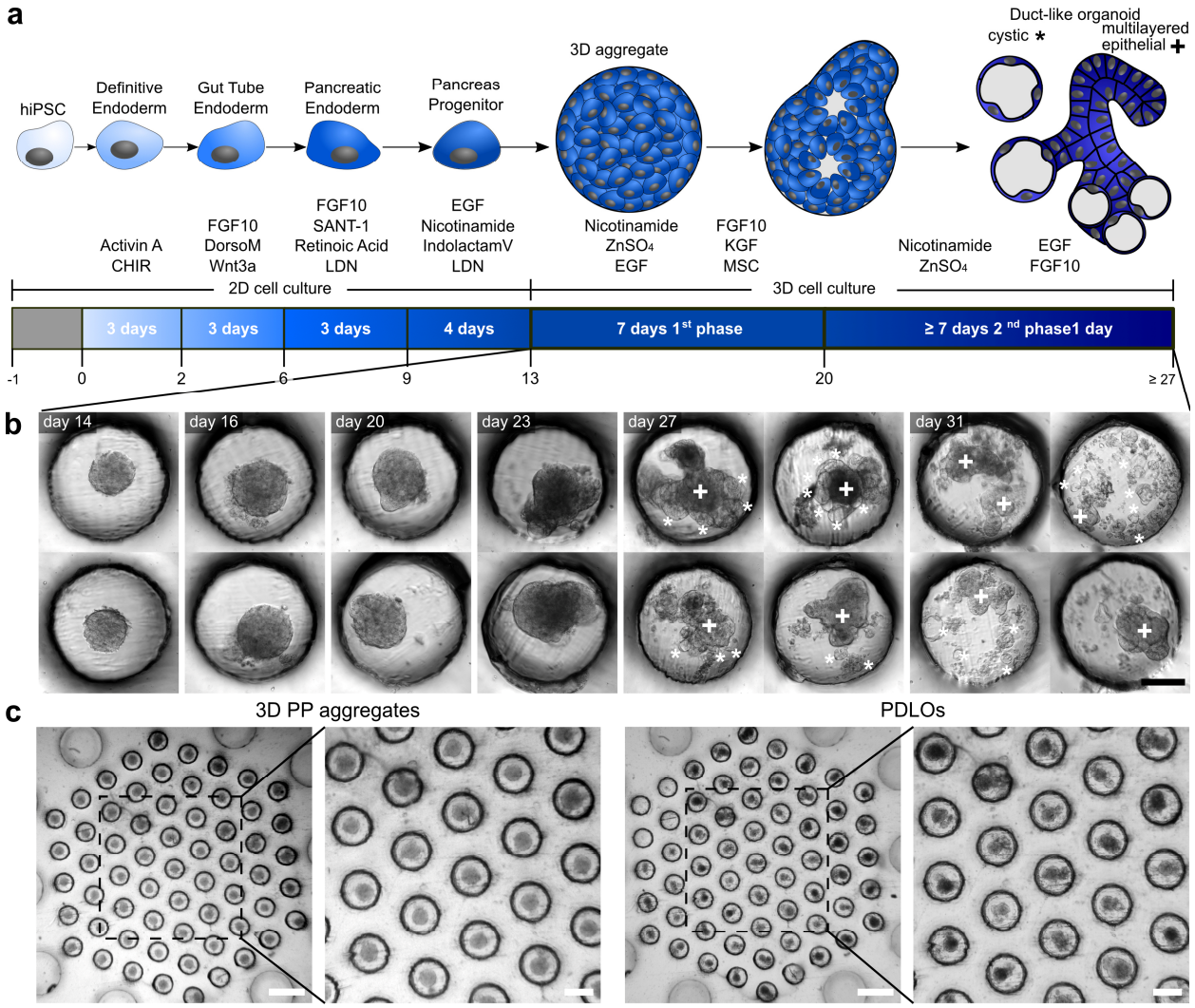

Figure 14 | Differentiation 3D PP aggregates to PDLOs in the microwell chip.

a, Schematic overview of growth factor-induced cell differentiation of hiPSCs to PDLOs. **b,** Bright-field images of representative 3D PP aggregates on the microwell chip after 14, 16, 20, 23, 27, and 31 days of differentiation (DOD). The characteristic morphological changes of the first and second differentiation phases are presented. Two morphologically distinct PDLO types arose from the same 3D PP aggregate at the end of the second phase. Multi-layered epithelial PDLOs are indicated with a + and cystic PDLOs with a *. **c**, Representative bright-field images of a microwell chip array for five independently performed differentiations of 3D PP aggregates at day 14 and day 27 of differentiation. Scale bar denotes 500 µm and 200 µm for the magnification.[1] *The figure is adapted from Wiedenmann, et al. [1] and used with "author permission rights" from Nature.*

3.2.2 Expression of pancreatic ductal markers within the PDLOs

To validate the correct development of the PDLOs, various ductal, epithelial, PP, and control marker proteins were analyzed during the PDLO differentiation. The analysis of progenitor proteins on the chip confirmed the expected starting cell type at day 13, the stability over the differentiation, and the correct expression in the PDLO stage. SOX9, HNF1B, PDX1, and cytokeratin (KRT8) were constantly expressed (**Figure 15a-d**). The progenitor marker NKX6-1, expected to be only present in the progenitor and endocrine cells, either decreased or completely absent in the PDLO stage (**Figure 15d**). While stemness and pluripotency markers SOX2 and OCT4 were not expressed at the PDLO stage, they showed the expected positive immunoreactivity within the hiPSCs (**Figure 15e**).[1]

The epithelial cell type was confirmed by the upregulation of E-cadherin (CDH1) (**Figure 15b**). In the final phase, the ductal identity of the cells was further verified using KRT19, CA2, CFTR, aquaporin 5 (AQP5), claudin 1 (CLDN1), and cytokeratin 7 (KRT7) (**Figure 15a,c**). In addition, PDLOs were stained for several control proteins to ensure no other cell types evolved during the differentiation. Although no evidence of acinar cells (AMY2A) was found, a small subset of cells showed endocrine markers such as CHGA (**Figure 15f**). Simultaneously, while a homogenous expression of epithelial cell marker CDH1 could be observed, no detection of the mesenchymal marker zinc finger E-box-binding homeobox 1 (ZEB1) could be documented (**Figure 15f**). While after 28 days of differentiation, only a few cells showed the proliferation marker protein Ki-67 (Ki-67) expression in the PDLOs, the gastric and dysplasia marker mucin-5AC (MUC5AC) and intestinal marker MUC2 were absent. (**Figure 15f**). Furthermore, pancreatic ductal indicator mucin-6 (MUC6) expression was widespread in PDLOs.[1]

Taken together, the PDLOs on the microwell chip showed the correct exocrine pancreatic ductal marker expression with no evidence of stem, mesenchymal, acinar, dysplastic or intestinal cells.[1]

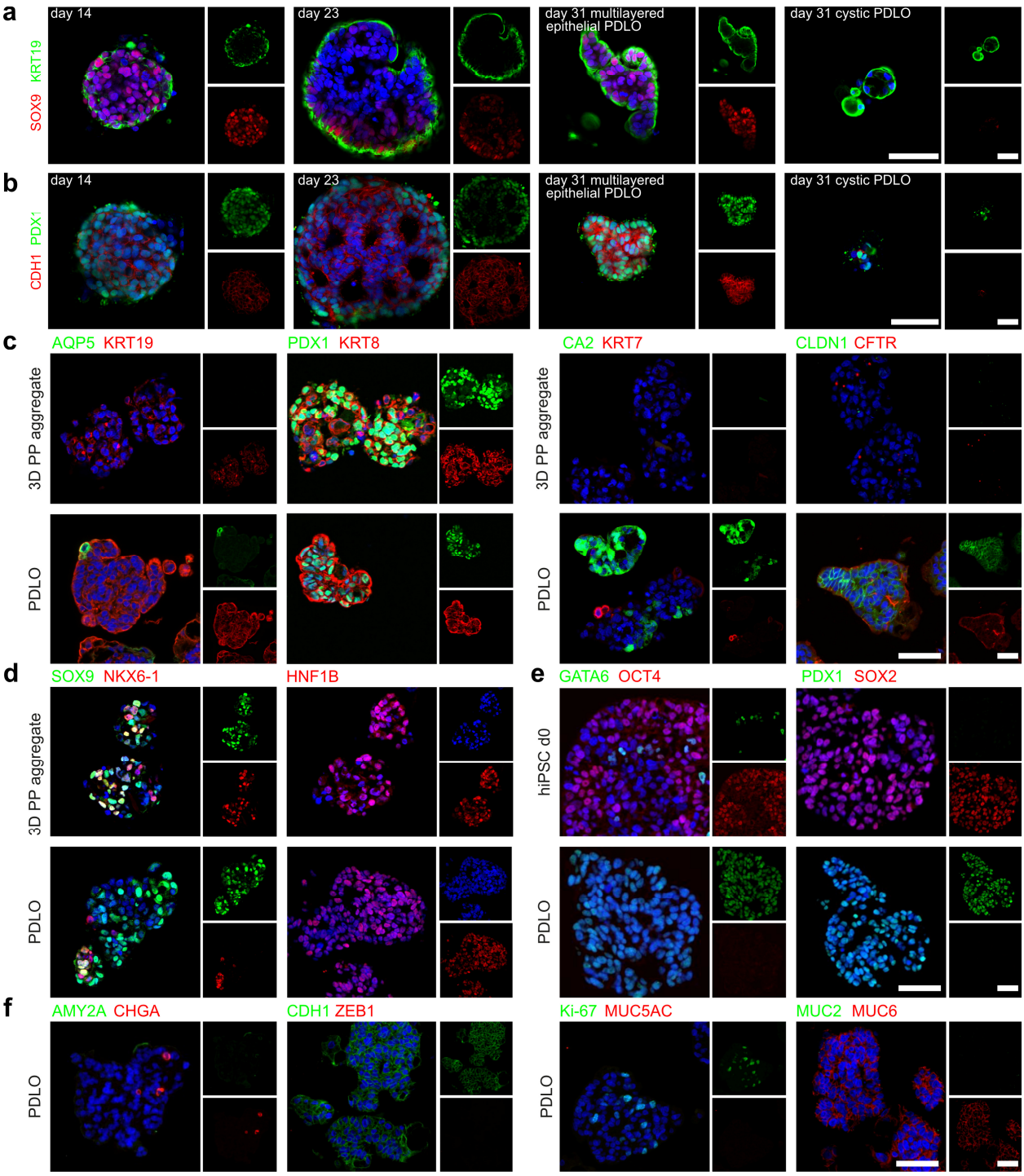

Figure 15 | Characterization of developing microwell-derived PDLOs.

a-b, High-resolution fluorescence images of cleared organoids on-chip during the time course with SOX9, KRT19, PDX1, and CDH1, respectively. **c-f**, High-resolution fluorescence images of day 28-PDLOs with appropriate controls, stained with: **c**, AQP5, KRT19, PDX1, KRT8, CA2, KRT7, CLDN1, and CFTR; **d**, NKX6-1 and HNF1B; **e**, OCT4 and SOX2; **f**, AMY2A, CHGA, ZEB1,

CDH1, Ki-67, MUC5AC, MUC2, and MUC6. **a-f**, The nuclei were counterstained with DAPI. All Scale bars denote 50 µm.[1] *The figures are adapted from Wiedenmann, et al. [1] and used and used with "author permission rights" from Nature.*

3.2.3 PDLOs differentiated on the microwell chip exhibit an apical-outside polarity

The pancreatic duct exhibits an apical-in and basal-out polarity within the pancreas to maintain the pancreatic juice transport function. In order to investigate the polarity during the development of the PDLOs, the expression of apical proteins such as tight junction protein-1 (ZO1) and CLDN1, as well as the basement membrane basal protein collagen IV (COL4A1), were interrogated in immunofluorescence stainings (**Figure 16**). No clear polarity could be observed at the beginning and intermediate stages of the differentiation. On day 31, when most organoids were dichotomized into the two subtypes, the apical markers ZO1 and CLDN1 displayed mainly an apical outside localization. At the same time, the basal marker COL4A1 was mainly expressed inside the multi-layered epithelial PDLOs. Within the cystic PLDOs, no clear polarity could be observed.

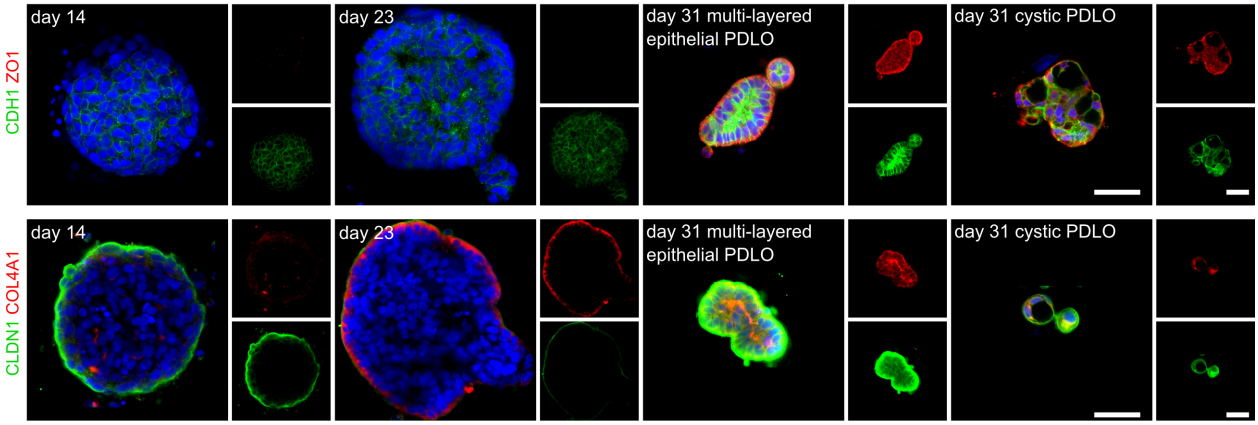

Figure 16 | PDLOs develop an apical-out polarity during differentiation on the microwell chip.

High-resolution fluorescence images of cleared organoids on-chip during the time course with apical polarity markers ZO1 and CLDN1 (apical), basal polarity marker COL4A1 and unpolarized CDH1. The nuclei were counterstained with DAPI. Scale bars denote 50 µm.[1] *The figures are adapted from Wiedenmann, et al. [1] and used with "author permission rights" from Nature.*

To investigate the reverse polarity and the lineage commitment of the microwell chip-derived PDLOs in more detail, day 27-PDLOs were orthotopically engrafted into the pancreas of immunocompromised mice or transferred to Matrigel (**Figure 17a**). After eight weeks, PDLO transplants were forming tube-shaped, duct-like tissue (**Figure 17b**). The transplanted PDLOs showed positive immunoreactivity for the classical pancreatic ductal markers SOX9, KRT19, AQP5 and CDH1 with no evidence of endocrine (CHGA and NKX6-1), progenitor (NKX6-1), or mesenchymal (VIM) markers (**Figure 17c**).[1]

To compare the polarity between transplanted, Matrigel, and chip organoids, day 27-PDLOs were subjected to immunostainings with several polarity markers. In the experimental setup, predicted PDLOs exhibited mainly apical-out polarity. However, ZO1, the cilia marker acetylated tubulin (acTUB), and ADP-ribosylation factor-like protein 13B (ARL13B) were also detectable on the opposite side of the membrane in a few cases. Thus, suggesting a small lumen within the organoid (**Figure 16** and **Figure 17d,e**). A polarity change from apical-out to apical-in was observed after the transfer of microwell chip-derived PDLOs into a 3D Matrigel culture or post-engraftment (**Figure 17d,e)**. The occurrence of PDLOs with the apical-out polarity can be explained by the absence of extracellular matrix (ECM) deposition in suspension cultures[200-202]. Consequently, an artificial "basement membrane" mimicked by Matrigel could facilitate the development of an apical-in organization epithelium.[1]

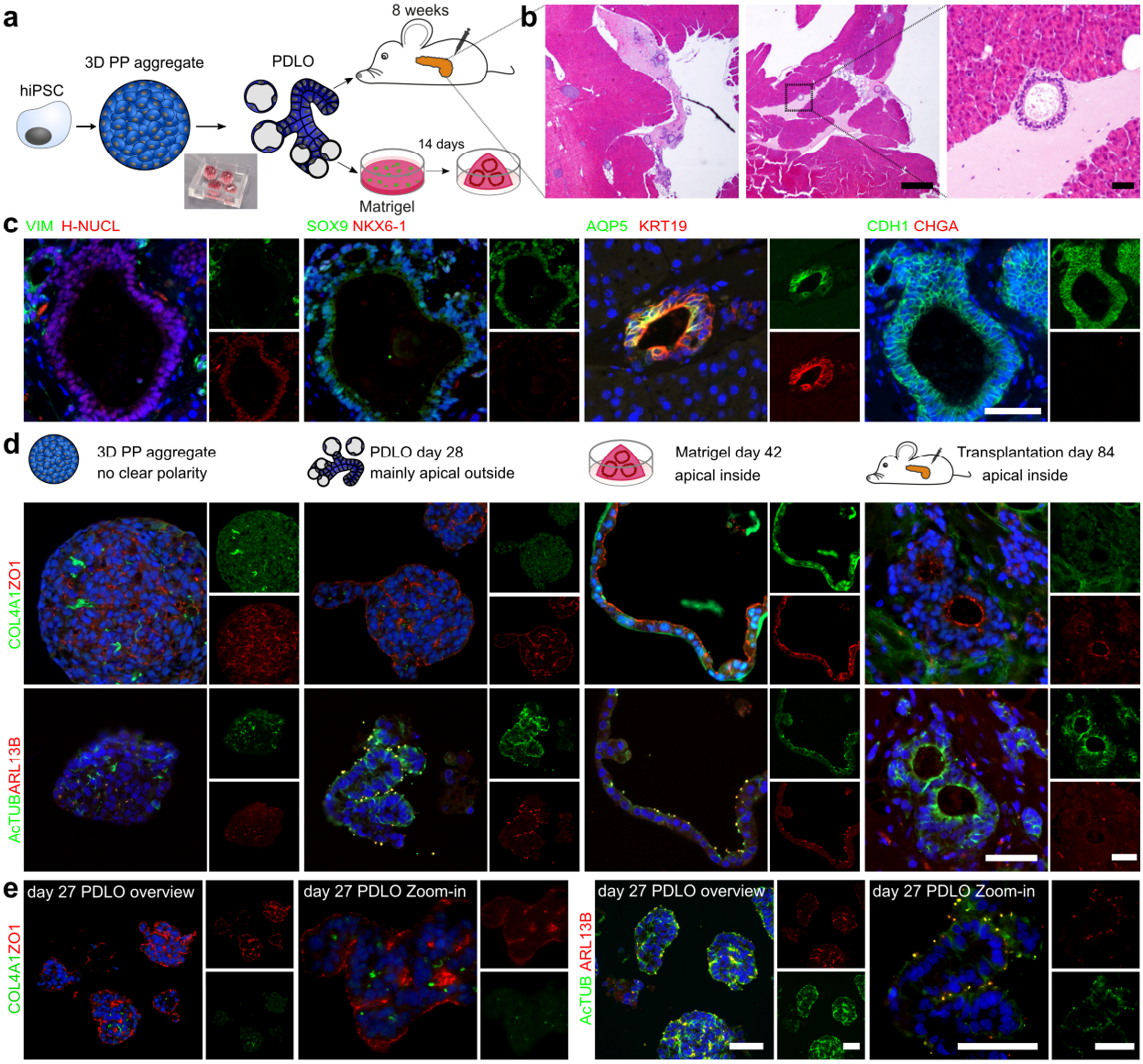

Figure 17 | Microwell chip-derived PDLOs' apical-out polarity switched to apical-in after orthotopic grafting or Matrigel embedding.

a, Overview of the Matrigel and orthotopic transplantation experiment. 27-days old PDLOs were transplanted in nude mice. Animals were sacrificed eight weeks later. **b**, Overview and magnification images of hematoxylin-eosin (HE) staining of the transplantation site of the two mice. Scale bar denotes 500 µm and 50 µm for the magnification. **c**, Upon transplantation, PDLOs formed human epithelial duct-like tissues *in vivo*. The nuclei of the organoids were immunostained with H-NUCL (human-specific nucleoli). **d**, The IF images of apical (ZO1 and AcTUB) and basal (COL4A1 and ARL13B) markers on 3D PP aggregates, PDLOs, Matrigel PDLOs, and engrafted PDLOs are shown. **e**, Overview and magnification of the PDLO images displayed in **d**. **c-e**, The nuclei were counterstained with DAPI. Scale bars denote 50 µm.[1] *The*

figures are adapted from Wiedenmann, et al. [1] and used with "author permission rights" from Nature.

3.2.4 Ductal functionality of the PDLOs

The validation of the pancreatic ductal markers revealed the expression of functional proteins within the PDLOs. CFTR controls one of the major functions of the pancreas, namely the anion efflux into the apical lumen of the duct upon contact with the secreted gastric acid of the acinar cells. Once CFTR is activated by phosphorylation, Cl^- and HCO_3^- are secreted to control the pH and the osmotic fluid secretion[203]. Treatment of PDLOs with forskolin triggers CFTR activation, which results in organoids' swelling[109]. While the forskolin-stimulated PDLOs indeed showed swelling within some areas, this event could not be observed in the control samples (**Figure 18**). Thus, the swelling supported the hypothesis that the PDLOs maintain some apical-in regions.

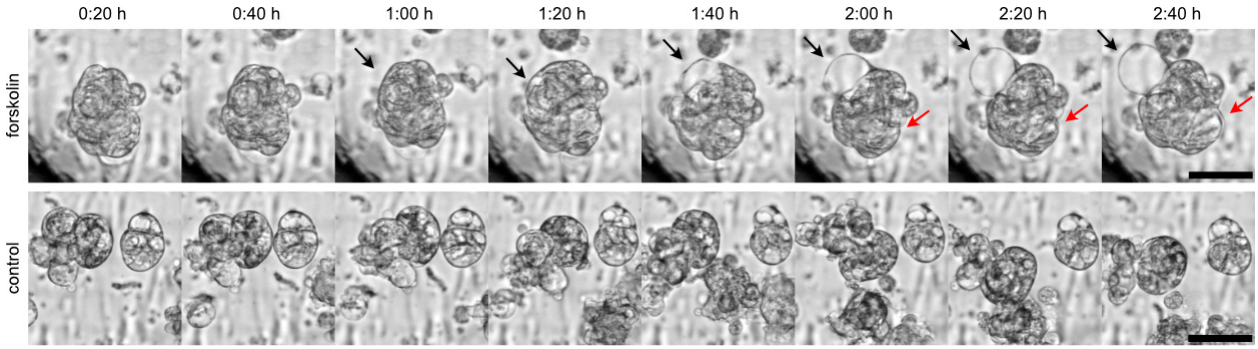

Figure 18 | PDLOs show partial functional swelling upon forskolin stimulation.

Live imaging on the microwell chip of PDLOs after stimulation with forskolin and IBMX. For the control experiment, H_2O was added. The swelling of the organoids is indicated by arrows. Scale bar denotes 50 µm.[1] *The figures are adapted from Wiedenmann, et al. [1] and used with "author permission rights" from Nature.*

3.3 Charting PDLO differentiation at single-cell transcriptomic level

For a detailed analysis of the PDLO development on the microwell chip, 14,811 cells were analyzed in a time-resolved single-cell RNA sequencing approach. The scRNA-seq data allowed analysis of the final cell types' transcriptional identity and the cell type composition across differentiation. The probes were collected and sequenced at seven time points during the differentiation of PPs to PDLOs on-chip (**Figure 19a**).

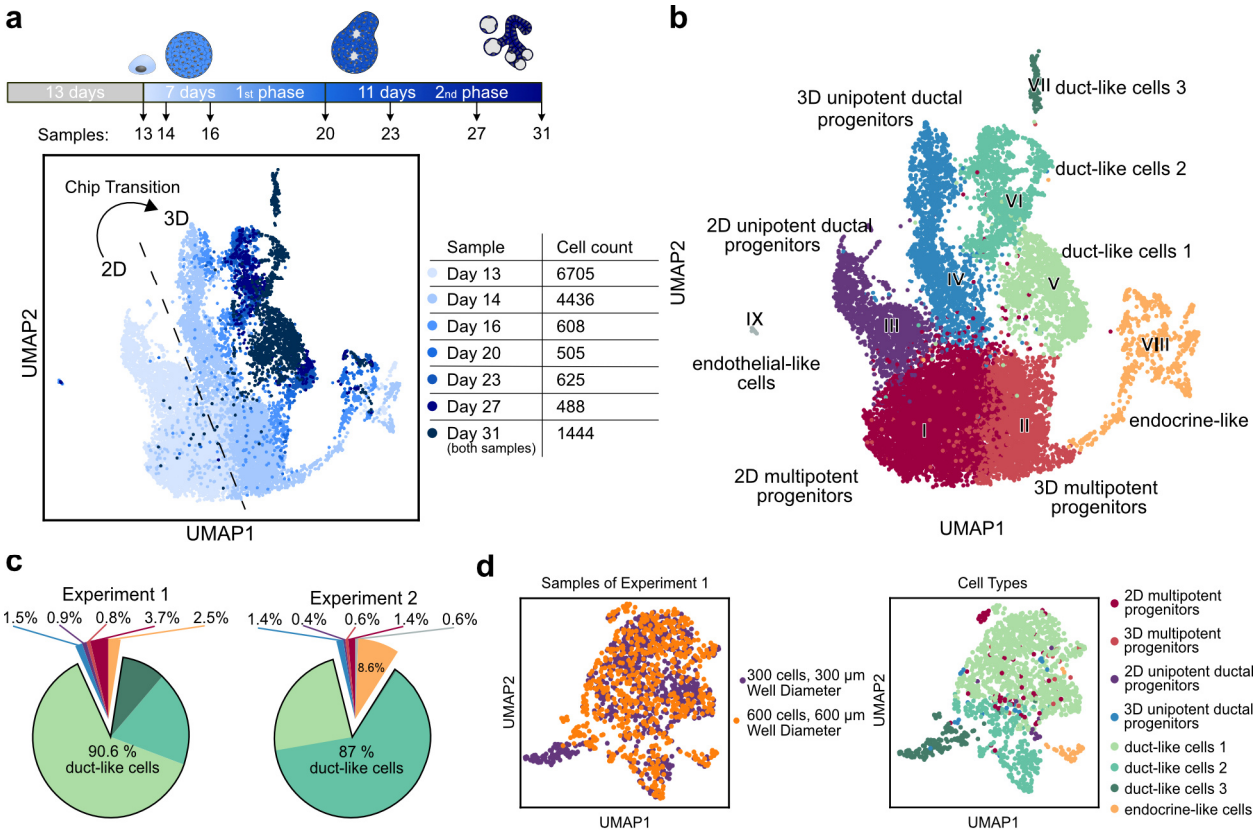

Figure 19 | Uncovering cellular heterogeneity over the differentiation time from PP to PDLOs on-chip using scRNA-seq.

a, Scheme showing sample timing during ductal differentiation with single-cell count numbers for cells and UMAP representation. Light to dark blue color shading indicates sampling time points. **b,** UMAP plot of the nine Louvain clusters found within the scRNA-seq data. Each cluster was assigned to a specific cell type. **c,** Pie charts of cell-type distribution at the end of differentiation of two independent experiments show differentiation efficiency close to 90% in both. **d**, UMAP plot of two PDLO cell differentiations with different starting conditions at day 31 without batch correction. The first condition was 300 cells per well in a 300 µm diameter microwell, and the second was 600 cells per well in a 600 µm diameter microwell. In the second UMAP plot, the same cells are stained according to the previously determined clusters.[1] *The figures are adapted from Wiedenmann, et al. [1] and used with "author permission rights" from Nature.*

Two-dimensional Uniform Manifold Approximation and Projection (UMAP) of the individual cells of the time points showed major transcriptional changes already on the first-day on-chip, at the transition from 2D to 3D (**Figure 19a**). The cells of the late time points of differentiation were located in the top right part of the UMAP image. Nine distinct cell clusters were identified by Louvain clustering (**Figure 19b**). The occurrence over

time of the different cell clusters further demonstrated the significant time-dependent change in transcriptional cellular identity caused by the growth factor-induced differentiation process (**Figure 19a,b**).[1]

By screening for known pancreatic developmental genes in the differentially expressed genes (DEGs) in the respective clusters, each cell cluster could be assigned to a specific cell type (**Figure 19b; Supplementary Data 1**). The distinct cell clusters were classified into three duct-like, four progenitor-like, one endocrine-like, and one endothelial-like cell cluster. Single-cell sequencing of mRNA samples from end-stages of two independent experiments was performed to test the differentiation's reproducibility. Approximately 90% of PPs developed into cells with a characteristic transcriptomic profile for duct-like cell types in both cell differentiations (**Figure 19c**). PDLO RNA was sequenced at the end-stage from two different well diameters and starting cell numbers to test whether different starting conditions on the microwell chip affected differentiation. Homogeneous superposition of cells from the two conditions in a non-batch corrected UMAP plot showed that doubling the initial cell number of PP aggregates or well size did not affect the outcome of ductal differentiation (**Figure 19d**).[1]

To assign each cell cluster to a specific cell type, the top 300 DEGs of the clusters were examined for pancreas developmental specific genes. Three of the determining DEGs for cluster assignment are displayed in the violin plot (**Figure 19b**). The cells of clusters I-IV were identified as four putative progenitor cell types. Cluster VIII could be assigned to an endocrine-like cell population and cluster IX to a non-pancreatic endothelial-like cell population. The three remaining clusters V-VII are subdivided into three types of duct-like cells.[1]

Interestingly, the initial cell population of PPs could be separated into two different cell types based on their transcriptional profile, into multipotent (cluster I) and unipotent ductal (cluster III) progenitor cells. In both types, commonly known progenitor markers such as *PDX1*, *HNF1B* and *SOX9* were found to be expressed (**Figure 20a-c**). Cluster I showed co-expression of *PDX1* and *NKX6-1*, to which PP protocols are generally optimized (**Figure 20a,b**). With a similar transcriptional profile to cluster I, cluster II was identified as a temporally downstream cluster. Upon transferring the cells from 2D to 3D onto the microwell chip, increased expression of *GP2* and *PTF1A* was detected in this

cluster (**Figure 20a,c**). The cell clusters were named 2D and 3D multipotent progenitors (MPP), based on the common expression of these markers, indicating a multipotent cell type that gives rise to both endocrine and exocrine cells in mice[204,205].

However, increased expression levels of ductal marker genes, such as *KRT8*, were detected in cluster III (**Figure 20a,d**). Moreover, the expression of *NKX6-1*, later exclusive in endocrine cells, was decreased in cluster III, suggesting ductal priming at the end of 2D PP differentiation[206,207]. Similar to the MPPs, a transcriptionally related cluster was found after transfer to the microwell chip. The cluster IV also showed an enrichment of ductal markers such as hes family bHLH transcription factor 1 (*HES1*) and S100 calcium-binding protein A10 (*S100A10*) (**Figure 20a,e**). On the basis of this enhancement of early ductal-related gene expression in clusters III and IV, they were designated as 2D and 3D unipotent ductal progenitor (UDP) cells, respectively.[1]

Toward the end of differentiation, three duct-like cell clusters could be identified, all characterized by high *KRT19*, *SOX9* and intermediate *CA2* expression (**Figure 20a,g**). In contrast to *KRT19* and *SOX9,* the *CA2* enzyme is only found in mature ductal cells in the primary pancreas[208]. Calculation of the top 300 DEGs for a combined cluster of the three duct-like subtypes revealed significant upregulation of ductal epithelial markers such as *CLDN1* and S100 calcium-binding protein A14 (*S100A14)* (**Figure 20a,h**). Within the three duct-like cell clusters, an enrichment of *CFTR*, a protein specifically related to HCO_3^- secretion, was found in cluster V (**Figure 20a,i**). In contrast, upregulation of mucin-related genes, such as mucin-13 (*MUC13*) and trefoil factor 1 (*TFF1*)[4], was found in duct-like cells 2 (**Figure 20a,j**). The remaining duct-like cells 3 cluster showed significantly upregulated expression of claudin-4 (*CLDN4*) and interstitial collagenase (*MMP1*) (**Figure 20a,k**). However, it contained only 134 cells, showed similarities to duct-like cells 2 cluster, and also fell into cluster 2 in other clustering approaches (data not shown), so subsequent analyses focused on the first two subtypes.[1]

A small fraction of pancreatic endocrine-like cells expressing *CHGA*, insulin (*INS*), and somatostatin (*SST*) were resolved in all samples (**Figure 20a,f**). Only a few non-pancreatic cells were present and could be identified as platelet endothelial cell adhesion molecule (*PECAM1)* and endothelial cell-specific molecule 1 (*ESM1)* expressing

endothelial-like cells. The scRNA-seq data validated the successful and reproducible differentiation of PDLOs containing two duct-like subclusters within the microwell chip.[1]

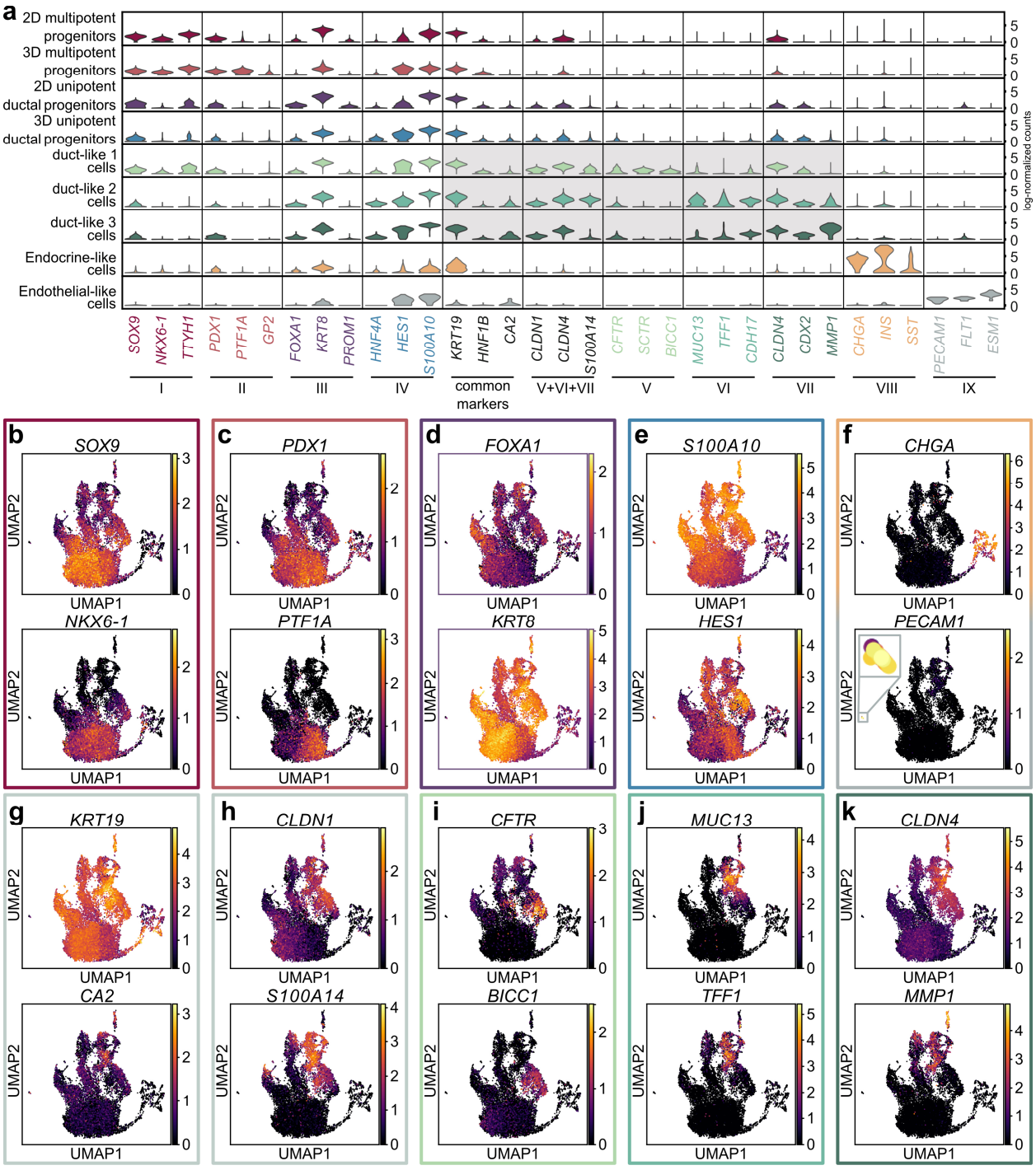

Figure 20 | DEG analysis of the nine different Louvain cell clusters.

a, The violin plot shows a selection of three significant DEGs for each of the nine cell clusters (labeld with their Roman numerals). In addition, three significant DEGs for the combined duct-

like cell clusters (labeld with V+VI+VII) and three common ductal marker genes (labeld with common markers). **b-k,** UMAP plot of expression patterns of marker genes used for pancreatic cluster annotation. Legends scale denote the log-normalized counts. UMAP plots for DEGs of **b**, 2D multipotent progenitors; **c**, 3D multipotent progenitors; **d**, 2D unipotent ductal progenitors; **e**, 3D unipotent ductal progenitors; **f**, endocrine-like and endothelial-like cells; **g**, common ductal markers; **h**, all three duct-like cell clusters; **i**, duct-like cells 1; **j**, duct-like cells 2; **k**, duct-like cells 3 are shown.[1] *The figures are adapted from Wiedenmann, et al. [1] and used with "author permission rights" from Nature.*

3.4 Identification of duct-like subpopulations at the protein level *in vitro* and *in vivo*

Aiming to determine the duct-like subpopulation cell types at the protein level, PDLOs and the appropriate controls were immunofluorescently labeled with specific antibodies for the respective cluster proteins. Thus, CFTR and MUC13 were subjected to immunostaining in PDLOs differentiated through days 23, 27, and 31 on the microwell chip. Within PDLOs, CFTR was expressed earlier than MUC13, consistent with the transcriptomic data (**Figure 21a,b**). Toward the end of differentiation, CFTR was found expressed only in cells of the multi-layered epithelial PDLOs. In contrast, MUC13 was found on the outside of the cells in the outermost layer of the multi-layered epithelial PDLOs and the cystic organoid type. In general, CFTR and MUC13 were expressed in different cells. Baron, et al. [4] previously found two distinct expression patterns of mucin-rich (*MUC1*$^{+}$/*TFF1*$^{+}$) and *CFTR*-rich ductal subtypes within the primary human pancreas at the single-cell transcriptome level. Although *MUC1* expression was not found in the PDLOs at the transcriptome level, *TFF1* was also expressed in duct-like cells 2. However, the ductal marker MUC1 was detected at the protein level by mass spectrometry and immunostaining (**Figure 21b**: first three rows**; Figure 22a**: last row; **Supplementary Data 4)**. Both MUC1 and CFTR were also found in different cells of the organoids, although in rare cases, in the same cells.[1]

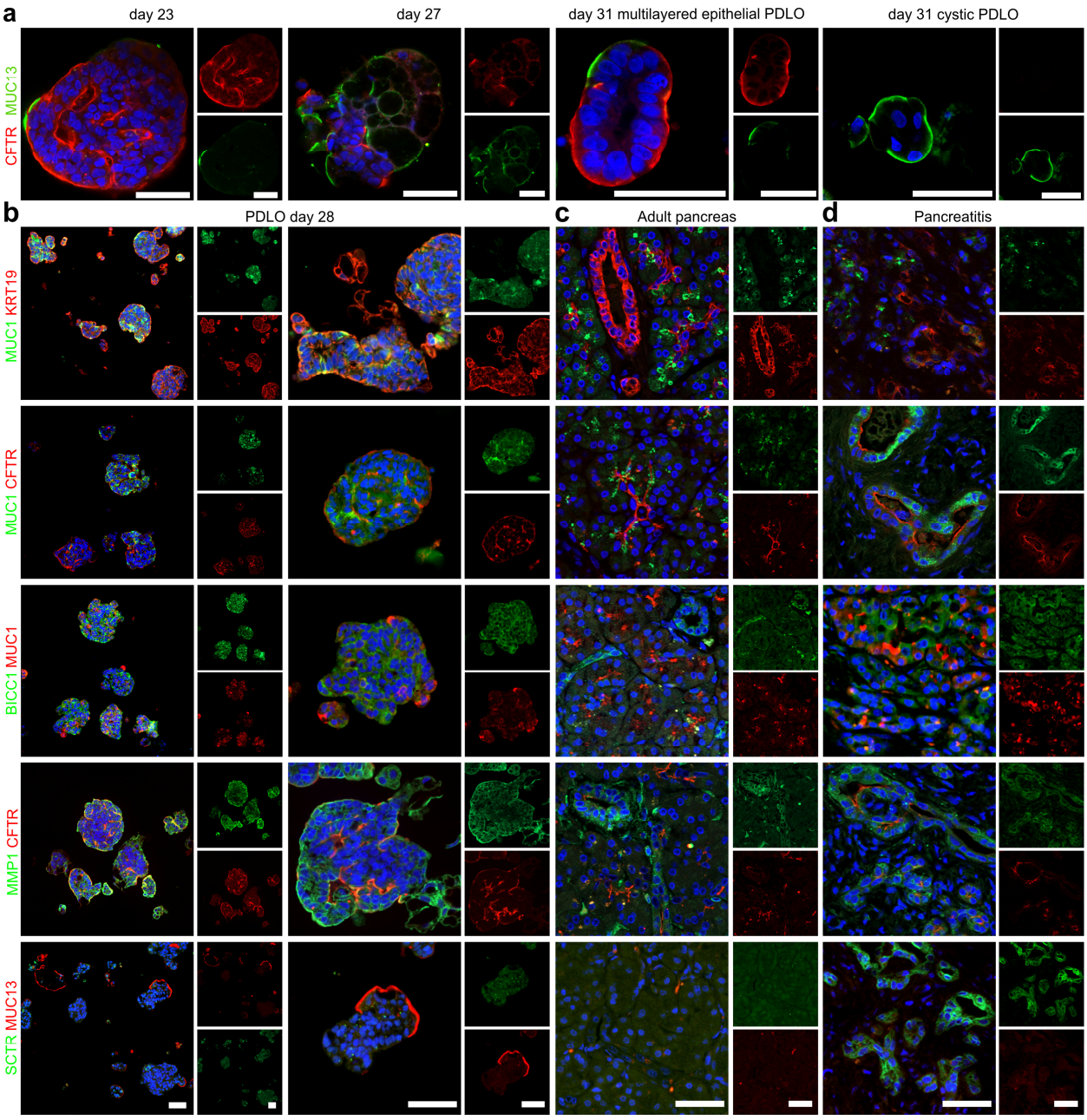

Figure 21 | Duct-like subcluster-specific genes stained within PLDOs and primary pancreatic tissue - part 1

a, The PDLOs after 23, 27, and 31 days DOD were stained for CFTR and MUC13, respectively. **b**, 28-days differentiated PDLOs were stained for duct-like subtype cell markers identified by the scRNA-seq analysis. **c, d**, Identical protein markers were used to detect the *in-vitro*-generated ductal cell subtypes in primary human pancreatic tissue, either (**c**) healthy or (**d**) pancreatitis tissue. The figure is continued in **Figure 22**. All scale bars denote 50 µm.[1] *The figures are adapted from Wiedenmann, et al. [1] and used with "author permission rights" from Nature.*

Subsequently, other duct-like subcluster markers were stained in combination and compared to each other. Indeed, different expression patterns were detected in the multi-layered epithelial PDLOs. For example, BICC1 (a marker for duct-like cells 1) was often weaker expressed in MUC1-positive cells (**Figure 21b**: third row). Whereas TFF1 (a marker for duct-like cells 2) was found weakly expressed in some cells, it was mostly in other cells than CFTR (**Figure 22a**: second row). Within larger PDLOs, MMP1 (a marker for duct-like cells 3) was present in the peripheral layers, whereas CFTR was localized in luminal structures of the organoid in other cells (**Figure 21b**: forth row). The luminal expression is in agreement with the functional response to forskolin and the hypothesis that organoids exhibit partial apical-in polarity. Furthermore, MUC1 was found in common cells with MMP1, although in fewer cells (**Figure 22a**: last row). In general, all three duct-like subcluster markers CFTR, MUC1, and MMP1 were found in ductal KRT19-expressing cells (**Figure 21b**: first row; **Figure 22a**: first and third row). This observation was consistent with the scRNA-seq data, in which small amounts of both cluster marker genes were also expressed in the other cluster (**Figure 19e,f**).[1]

To investigate whether the same expression patterns also occur *in vivo*, the previously mentioned ductal subcluster-specific markers were additionally stained in human primary healthy pancreas and pancreatitis tissue. Immunostainings of KRT19 with the subcluster markers MUC1, CFTR, and MMP1 showed ductal localization of all three proteins (**Figure 21c,d**: first and third row; **Figure 22b,c**: first row). Expression of MUC1 was found in acinar structures, centroacinar cells, and the connected intercalated ducts (**Figure 21c,d**: first to third row; **Figure 22b,c**: last row). CFTR could also be stained in the intercalated ducts (**Figure 21c,d**: second row). Beyond that, CFTR expression changed depending on the size of the branching ducts. Expression decreased in intralobular ducts and was almost absent in larger ducts (**Figure 21c,d**: fourth row; **Figure 22b,c**: first and second row).[1]

In contrast, BICC1 was increasingly expressed in the latter but barely detected near MUC1-positive cells (**Figure 21c:** third row). MMP1 could not be detected in common cells with either CFTR or MUC1, thus practically absent in the intercalated ducts (**Figure 21c,d**: fourth row; **Figure 22b,c**: last row). In contrast, MMP1 was detected in larger ductal structures with a different staining intensity (**Figure 21c,d**: fourth row; **Figure**

22b,c: last two rows). None of the markers MUC13, TFF1, and secretin receptor (SCTR) could be detected in healthy ducts (**Figure 21c**: last row; **Figure 22b**: second row). Solely SCTR, a known ductal marker[190], could be stained in the metaplastic ductal epithelium of chronic pancreatitis tissue (**Figure 21d**: last row).[1]

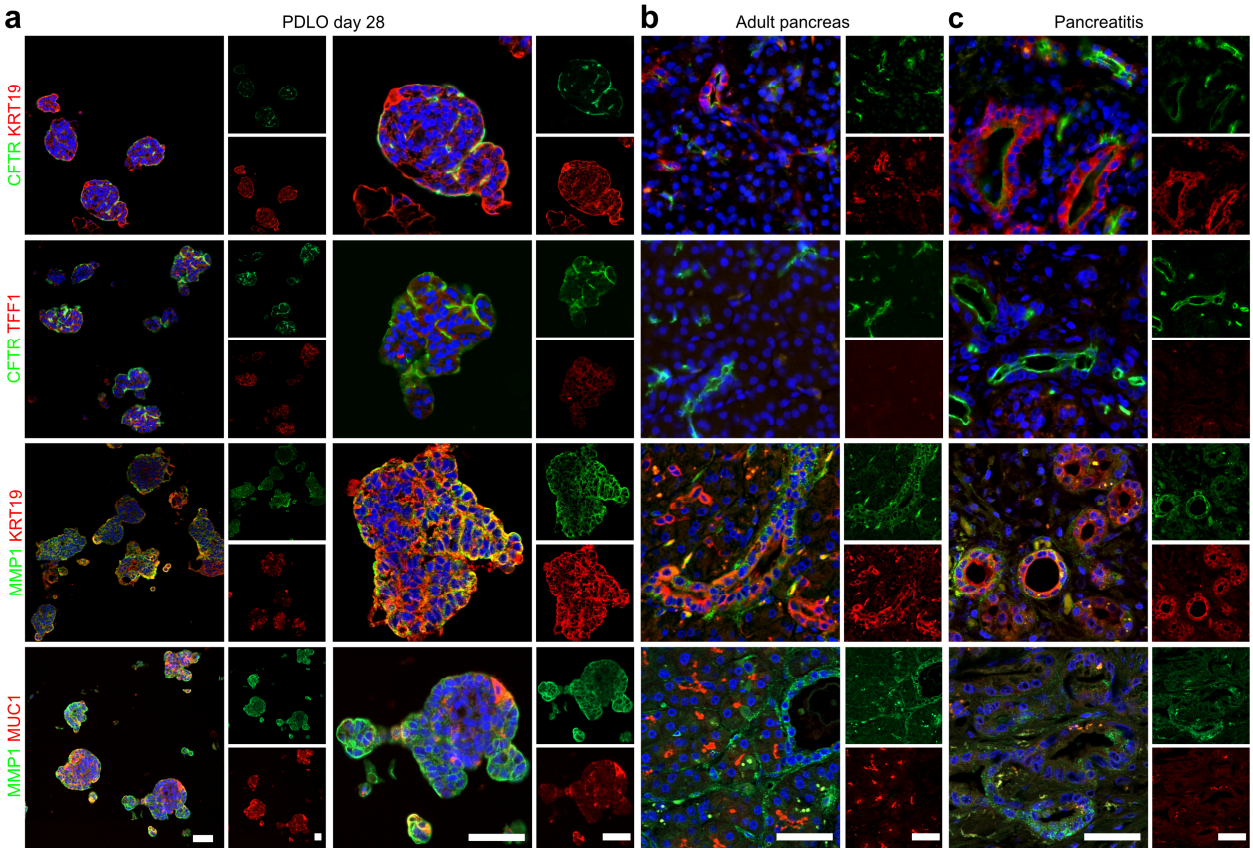

Figure 22 | Duct-like subcluster-specific genes stained within PLDOs and primary pancreatic tissue - part 2

a, 28-days-differentiated PDLOs were stained for cell subtype markers and pan-ductal marker KRT19. **b**, **c**, Identical protein markers were used to detect the *in-vitro*-generated ductal cell subtypes in primary human pancreatic tissue, either (**c**) healthy or (**d**) pancreatitis tissue. The figure is the extension of **Figure 21**. All scale bars denote 50 µm.[1] *The figures are adapted from Wiedenmann, et al. [1] and used with "author permission rights" from Nature.*

Overall, the results of the subtype staining revealed spatially alternating expression of the duct-like cell type markers at the protein level in PDLOs and primary human tissues. However, the protein-level expression states are more dynamic and complex than

implied by the PDLO transcriptomic subdivision, suggesting possible additional ductal cell types.[1]

3.5 Dynamic gene expression reveals *in vitro* PDLO differentiation trajectories

In an attempt to elucidate time-dependent developmental relationships during PDLO differentiation, a dynamic RNA velocity model[187,209] was calculated. First, a latent time was calculated based on the balance of unspliced (early) and spliced (later) RNA transcripts, whereby a cell with more unspliced RNA transcripts is temporally classified prior to a cell with similar RNA transcripts in the spliced state (**Figure 23a**). Thus, the calculated latent time matched the actual chronological differentiation time for the PDLOs (compared to **Figure 19b**). Consequently, the model provided a realistic model for further analysis of dynamic changes along the differentiation time.[1]

Accompanying streamlines of RNA velocity obtained from the model revealed two theoretical differentiation trajectories to duct-like cells (**Figure 23b**). The duct-like cells 1 originated from the 2D MPPs, which then developed from the 3D MPPs and subsequently into duct-like cells 1. The second differentiation route led from the second PP subpopulation, the UDPs, to duct-like cells 2. Additionally, some streamlines were directed from duct-like cells 1 to duct-like cells 2, suggesting a relevant level of plasticity within duct-like cells, also known from the primary human pancreas[20]. Similar to duct-like cells 1, endocrine-like cells originated from the 3D MPPs, although without a common trunk domain. Moreover, all three differentiation routes could be bifurcated using partition-based graph abstraction (PAGA) analysis, which reveals connectivity (edges) between clusters (dots) (**Figure 23c**). In particular, the correspondence along the differentiation route from UDPs to duct-like cells 2 was strong.[1]

The assignment of the single cells to the cell cycle stages showed a maturation of the duct-like cells additionally by the decrease of the cell numbers in the G2- and S-phase (**Figure 23d**). Subsequently, cells were arranged along latent time to resolve ductal differentiation temporally. This also demonstrated maturation as the expression of progenitor markers such as *GP2*, tweety family member 1 (*TTYH1*), *PDX1* and *PTF1A*

decreased over the theoretically calculated time, and more mature ductal markers such as *S100A14*, *CFTR*, *TFF1* and *CA2* increased (**Figure 23e**).[1]

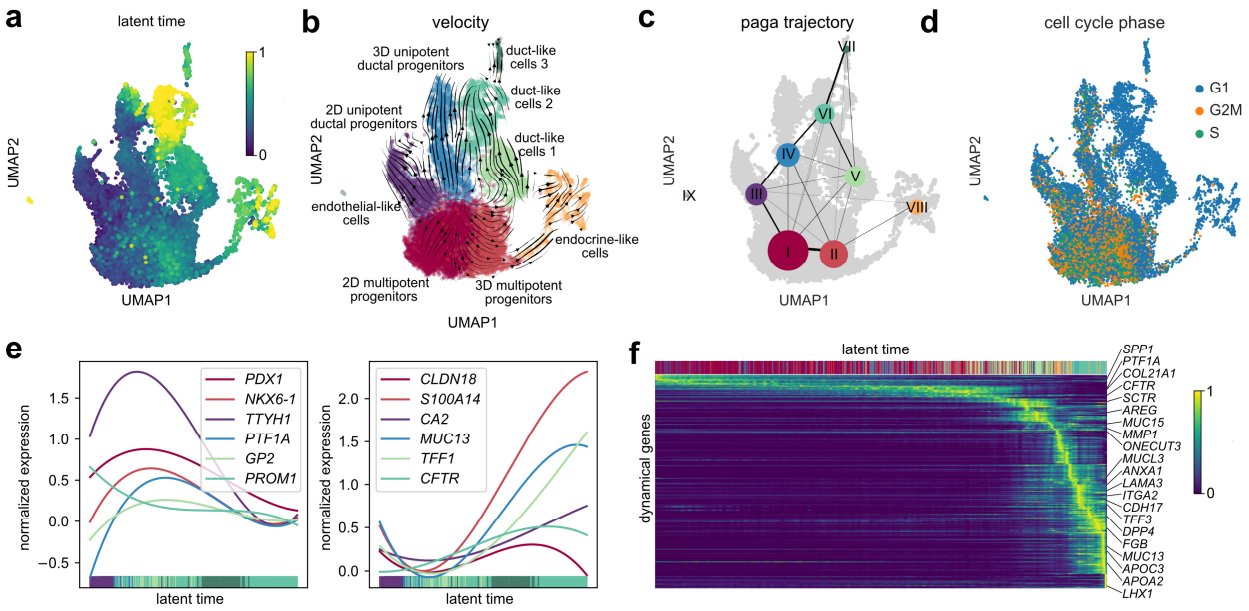

Figure 23 | Reconstruction of transcriptome dynamics allowed a prediction of the *in vitro* differentiation routes of the PDLO cell types.

a, Shading of the UMAP cluster plot by latent time calculated from dynamic RNA analysis. **b,** UMAP plot of velocity streamlines shows the theoretical temporal trajectories of the cells. **c,** UMAP plot with PAGA map shows the weighted connectivity between each cell cluster. **d,** UMAP plot displaying the cell cycle state of the cells during the differentiation. **e,** Polyfit of the expression levels of different progenitor or ductal marker genes against the latent time. **f,** the top 300 of the dynamically expressed genes sorted by their likelihood score and cells sorted by their latent time.[1] *The figures are adapted from Wiedenmann, et al.* [1] *and used with "author permission rights" from Nature.*

The arrangement of the cells along their latent time further revealed interesting dynamic expressions during ductal differentiation. For example, during the differentiation process, there was not only a concordance in the transcriptional dynamics of MPP markers but also a decrease in the levels of genes that are important during mitosis (topoisomerase 2 (*TOP2*) and cyclin B2 (*CCNB2*)) (**Figure 23f**). A listing of the top 300 dynamically expressed genes is provided in **Supplementary Data 2**. After specification of ductal cell fate, gene expression of *CFTR* and *SCTR*, hallmarks of pancreatic secretion, was temporarily induced (**Figure 23f**). This induction was accompanied by a gradual increase

in the expression of genes known to be involved in mineral absorption, such as metallothionein 1E (*MT1E*). Furthermore, the upregulation of *MUC13* rendered a temporal expression profile similar to that of genes associated with lipid transport/metabolism (apolipoprotein B (*APOB*)). In addition, these analyses revealed dynamic gene expression of genes less common and studied in the pancreatic duct, such as trefoil factor 3 (*TFF3)* or macrophage-stimulating 1 (*MST1*). Thus, *MST1* was recently reported to be critical for maintaining exocrine differentiation status and tissue integrity[210]. In conclusion, the velocity analysis delivered insights into the *in vitro* differentiation process toward the two ductal subtypes and the time-dependent dynamics of the expression profiles.[1]

3.5.1 Dynamical expression of extracellular matrix genes

The last section revealed a dynamic expression of several ECM-related genes (**Figure 23f**). There was an interest in analyzing the scRNA-seq data in more detail, particularly concerning the changes of ECM components during PDLO maturation. The presence of duct-like cells was associated with an increased expression of laminin α3 and α5 subunits (**Figure 24a**). At the same time, the expression of laminin-binding integrins is indicative of ECM formation along the differentiation course. Furthermore, duct-like cells featured a suppression of basal matrix collagens concomitant to the upregulation of the collagenases *MMP1* and stromelysin-2 (*MMP10*) (**Figure 24b**). During physiological development, the pancreatic mesenchyme secretes basement membrane laminin-1 and the α6-containing integrin receptor, which are necessary for pancreatic tubulogenesis[200-202]. Consistently, the progenitor cells and the duct-like cells 1 expressed α1-laminin, while the duct-like cells 2 and 3 expressed α3- and α5-laminin, respectively (**Figure 24a**). Notably, central components for β-cell formation[125], such as α4-laminin[211] and α5-integrin, were not expressed in PDLOs or the progenitor cells. Conversely, consistent with previous results[212], an upregulation of αVβ5-integrins was found in ductal cells (**Figure 24b**).

Thus, these analyses indicate that PDLOs secrete soluble ECMs and corresponding binding proteins similar to those secreted under *in vivo* conditions. However, due to the open format of the microwell culture, the ECM proteins are probably dissolved by the

media. This might explain the observed polarity reversal of microwell chip-derived PDLOs upon transplantation into mice or 3D Matrigel cultures (**Figure 17d**).[1]

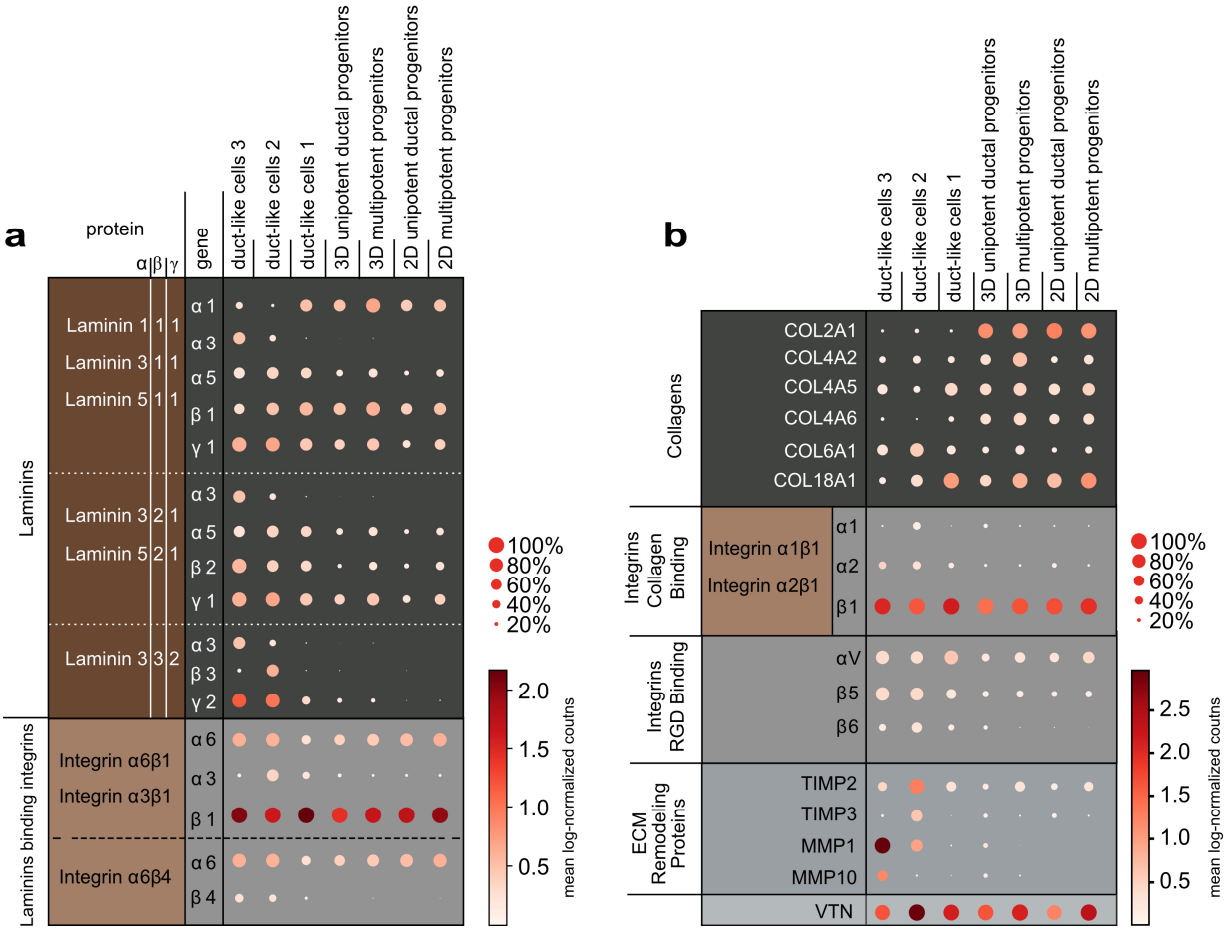

Figure 24 | Dynamic expression of extracellular matrix (ECM)-associated genes during the differentiation of PDLOs.

a, Dot plot of the changing laminin and laminin-binding integrin gene expression within the cells related to different clusters. **b**, Dot plot of the changing collagen, collagen-binding integrins, RGD binding integrins, and ECM remodeling gene expression within the cells related to different clusters.[1] *The figures are from Wiedenmann, et al. [1] and used with "author permission rights" from Nature.*

3.5.2 Pathway enrichments along the differentiation route

As the ECM gene analysis indicated, signaling pathways involved in epithelial cell organization like cell adhesion molecules and different junction types (adherens, focal, and tight junction) were also activated within the duct-like cells (**Figure 25a**). Thus, the

pancreatic ductal identity could be further confirmed by revealing the upregulation of functional pathways specific for pancreatic secretion, carbohydrate digestion and absorption, mucin type O-glycan biosynthesis, bile secretion, fat digestion and absorption, and collecting duct acid secretion within the duct-like cell clusters (**Figure 25b,c**). Moreover, the integration of a set of signaling pathways related to the applied growth factor stimuli demonstrated *EGF*/*FGF10*-mediated *MAPK*/*ERK activation*. It augmented ErbB signaling in the duct-like clusters 1 and 2 (**Figure 25c**)[1].

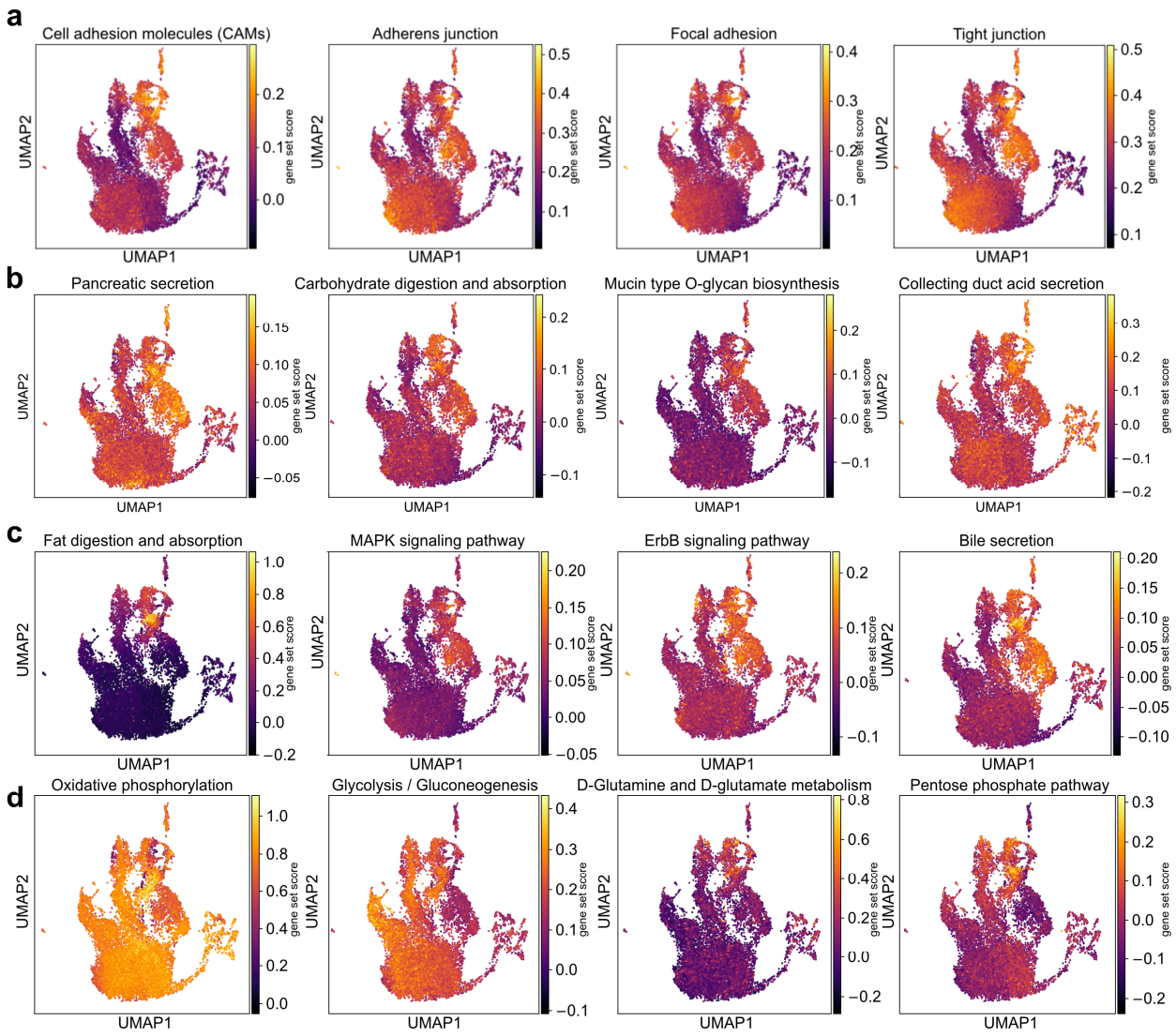

Figure 25 | Pathway activation within the PDLO kinetics.

Pathway activation scores for **a,** epithelial cell organization, **b,** ductal function, **c,** pancreas function and signaling, and **d,** metabolic energy conversion.[1] *The figures are adapted from Wiedenmann, et al. [1] and used with "author permission rights" from Nature.*

Furthermore, duct-like cells 2 showed a metabolic energy conversion compared to duct-like cells 1 within pathways like oxidative phosphorylation, glycolysis/gluconeogenesis, D-glutamine and D-glutamate metabolism, and pentose phosphate pathway (**Figure 25d**).

The pathway analysis could show increased ductal function and signaling, cell organization processes, and metabolic energy differences within the PDLOs.

3.5.3 PDLOs exhibit a more advanced maturity than the human fetal pancreas at seven to ten weeks post-conception

Due to the lack of human fetal data, the development of ductal differentiation protocols is mainly based on murine comparative data. Just recently, Gonçalves, et al. [213] acquired a single-cell dataset of human fetal pancreas seven to ten weeks post-conception (WPC). Gonçalves, et al. [213] obtained eight cell clusters at this developmental stage of the human pancreas: a proliferative, a trunk, a tip, an endocrine, a mesenchymal, an erythroblast, a neural, and one unknown cell cluster. To compare the PDLO developmental route, the top 50 DEGs of these clusters were scored on the PDLO scRNA-seq dataset.

Indeed, the proliferative top 50 DEGs were enriched in all progenitor cells and decreased in duct-like and endocrine cells, indicating further maturation (**Figure 26a**). Moreover, the trunk gene set score was highest between 3D MPPs and duct-like cells cluster (**Figure 26b**). Indicating a possible trunk-like stage between them on the one hand, which might be obtained with deeper time-resolved sampling as suggested before. On the other hand, it shows the high similarity of duct-like cells 1 with the closest but preceding stage to ductal cells in the human fetal pancreas (**Figure 26b**). The tip progenitor markers were also enriched in the 3D MPP cells, further supporting the previous hypothesis of a multipotent cell type (**Figure 26c**). Fetal endocrine markers were increased in expression in the endocrine-like cells (**Figure 26d**). The gene set scores for mesenchymal, erythroblast, neuronal, and unknown cell markers, present in the fetal pancreas, were not found at high levels (**Figure 26e-f**).

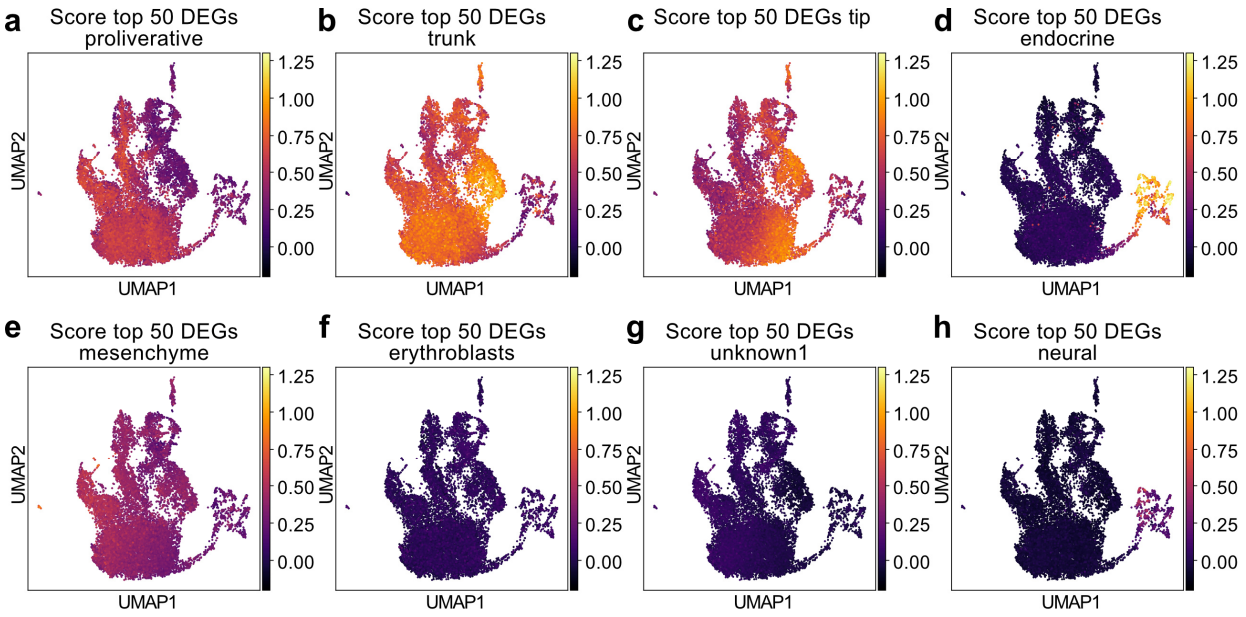

Figure 26 | Scoring top 50 DEGs of a fetal single-cell dataset clusters[213] onto the PDLO transcriptome.

Enriched expression of the marker genes for the **a**, proliferative, **b**, trunk, **c**, tip, **d**, endocrine, **e,** mesenchyme, **f**, erythroblast, **g**, neural, and **h**, unknown cell clusters of a fetal single-cell dataset acquired by Gonçalves, et al. [213] at seven to ten WPC. Legends show the calculated gene set score.

In summary, the comparison of the PDLO transcriptome with the human fetal pancreas showed similarities of proliferating cells to progenitors, and subsequent trunk cells more resembled the transition to duct-like cells 1. In the absence of ductal cells in the data set, further maturation of the duct-like cells can not be demonstrated but assumed.

3.6 The *CFTR*$^{+}$ and mucin^{+} duct-like subpopulations found in primary human ductal tissue

3.6.1 Data integration of the PDLO transcriptome into three primary data sets

A requirement and an advantage of PDLOs derived from microwell chips are that the duct-like cell types closely resemble human tissue. In order to demonstrate this, the PDLO differentiation kinetics were integrated into three scRNA-seq datasets from primary human pancreatic tissue[4-6] (**Figure 27a i),iii)**). In the combined, re-clustered

dataset, the duct-like cells from the PDLOs clustered together with the primary ductal cells to form the same cluster. In addition, the ten Louvain clusters were grouped into two ductal clusters.[1]

Baron, et al. [4] previously described two ductal cell types in primary ducts: The first one with *MUC1 and TFF1* and the second with *CFTR* as cluster marker genes. Detection of *CFTR* and *TFF1* expression in the combined data set re-confirmed the existence of ductal cell subtypes within the PDLOs (**Figure 27a ii)**,**vi)**; **Supplementary Data 3**). While *CFTR*-positive PDLO cells indeed clustered with the primary *CFTR*$^{+}$ ductal cell type, *MUC13*- and *TFF1*-positive PDLOs clustered with primary *MUC1*$^{+}$/*TFF1*$^{+}$-ductal cells. *In vitro* differentiated UDPs and MPPs clustered separately (**Figure 27a ii)**,**v)**). The few endocrine-like cells clustered with the primary cells of the islets of Langerhans (α-, β-, δ-, γ-, and ε- cells) and homogenously expressed *CHGA* (**Figure 27a ii)**,**viii)**). Similarly, the endothelial-like cells assembled with the primary PECAM1 expressing endothelial cells (**Figure 27a ii)**,**iv)**). At the same time, the primary acinar cells clustered and expressed *CTRC* separately as expected (**Figure 27a ii)**,**vii)**).[1]

Analysis of the original cell type assignments by matching the cluster position in the combined dataset provided additional evidence for the integration approach (**Figure 27b**). Moreover, the enrichment score of the top 100 DEGs of the primary *CFTR*$^{+}$ and *MUC1*$^{+}$/*TFF1*$^{+}$ ductal subpopulations[4] was calculated for PDLO differentiation kinetics.[1]

Thus, *CFTR*$^{+}$ and *MUC13*$^{+}$ PDLO cells indeed correlated with their respective primary ductal subpopulations (**Figure 27c**). The data integration supported imaging and transcriptomic analysis results with the evidence of transcriptomic similarities to primary ductal cells.[1]

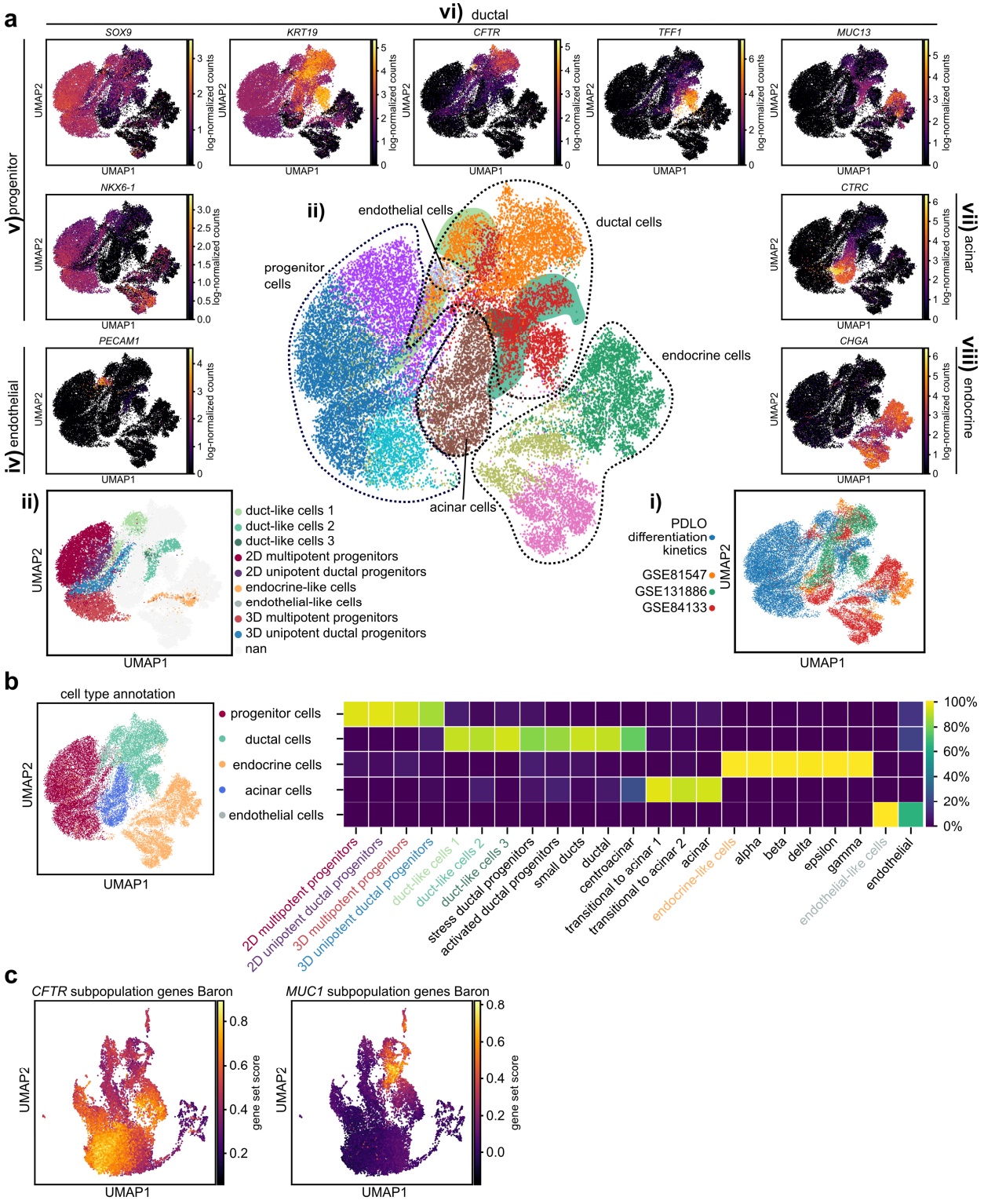

Figure 27 | The duct-like cells cluster together with primary human *CFTR*⁺ and mucin⁺ ductal subcell types.

a, UMAP plots from the integration of three primary human pancreas scRNA-seq datasets[4-6] into the PDLO cell differentiation dataset show in **i)** the localization of the different datasets; **ii)** the

ten recovered Louvain clusters, with the three duct-like clusters highlighted in their cluster color; **iii)** the cells of each cluster of the PDLO differentiation kinetics; **iv)** endothelial marker expression; **v)** progenitor marker expression; **vi)** ductal marker expression; **vii)** acinar marker expression; and **viii)** endocrine marker expression. **b,** UMAP plot of annotated cell clusters with the percentile distribution of the original cluster annotation of each dataset. **c,** UMAP plot of the enrichment score for the DEGs obtained from the data set of Baron, et al. [4] for the *CFTR*$^{+}$/*MUC1*$^{-}$/*TFF1*$^{-}$ and *CFTR*$^{-}$/*MUC1*$^{+}$/*TFF1*$^{+}$ subpopulations for the PDLO differentiation transcriptome data.[1] *The figures are adapted from Wiedenmann, et al. [1] and used with "author permission rights" from Nature.*

3.6.2 Re-clustering of primary ductal scRNA-seq data[5]

Data integration can lead to unintended over-interpretation of cell type[1]. To strengthen the analysis of ductal cell subpopulations without data integration, the primary human single-cell dataset[5] containing the most ductal cells was reclustered, and ductal cluster markers were searched for (**Figure 28a**)[1]. The Louvain re-clustering revealed four clusters. These could be assigned as: transitional-to-acinar related (cluster 1), immune cells (cluster 3) and two ductal clusters (clusters 0 and 2) (**Figure 28a**). The two ductal clusters were associated with a high expression of common ductal markers *KRT19* and *CLDN4* (**Figure 28b**).

Investigation of expression levels of duct-like cells 1 cluster markers *CFTR*, *BICC1,* and *SCTR* ductal cluster 0 revealed an increased expression indeed (**Figure 28d**). Furthermore, the duct-like cells 2 and 3 cluster markers *MUC1*, *TFF1,* and *MMP1* were upregulated in ductal cluster 2 (**Figure 28e**). At the same time, *MUC13* was in both clusters weakly expressed (**Figure 28e**). In summary, according to the *in vitro* PDLOs on microwell duct-on-chip technology, the two primary ductal cell subtypes demonstrated a similar scRNA-seq expression pattern[1].

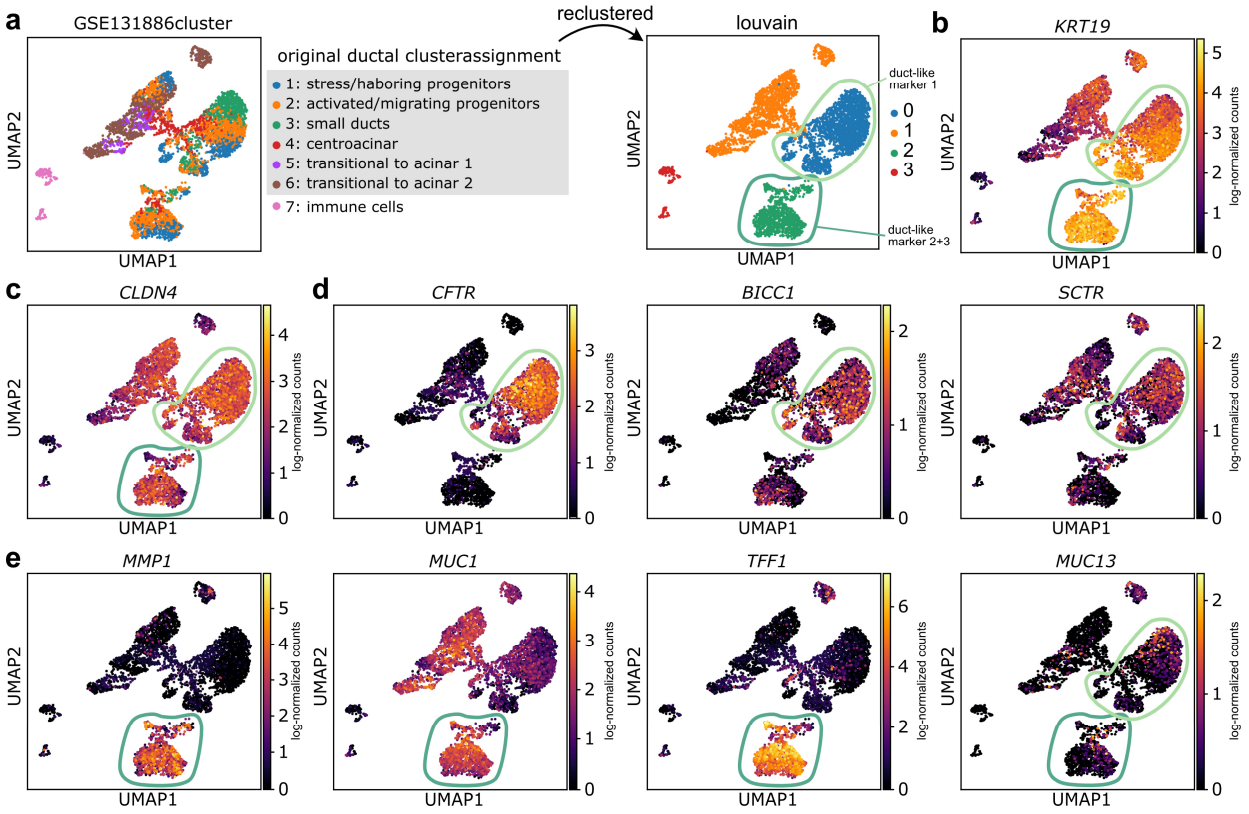

Figure 28 | Significant DEGs for the *CFTR*⁺ and mucin⁺ duct-like clusters can be recovered in cell clusters from the primary human pancreas[5].

a, UMAP plot of the single-cell transcriptome data reanalysis from a primary human ductal dataset[5]. **b-e**, UMAP plots of the expression patterns in the reprocessed scRNA-seq data[5]. The clusters similar to the respective duct-like clusters are circled with the corresponding color. Expression is shown for **b**, common ductal *KRT19*; **c**, common ductal *CLDN4*; **d**, duct-like cells 1 cluster marker *CFTR*, *BICC1*, and *SCTR*; and **e**, duct-like cells 3 cluster marker *MMP1* and duct-like cells 2 cluster marker *MUC1*, *TFF1*, and *MUC13*.[1] *The figures are adapted from Wiedenmann, et al. [1] and used with "author permission rights" from Nature.*

3.7 Application possibilities of the microwell duct-on-chip technology

3.7.1 Co-culturing PDLOs with human pancreatic stellate cells

The microwell duct-on-chip technology has several other potential applications beyond organoid differentiation, live-cell imaging, stimulation, or on-chip staining. For instance, the cell-cell communication between the pancreatic ducts and different stromal cells can be investigated. To execute such an experiment, the four separately fillable hexagonal

arrays were seeded with PDLOs and human pancreatic stellate cells (HPaSteC) to establish a cross-contamination-free co-culture (**Figure 29a**). The HPaSteCs closely resemble quiescent stromal cells within the pancreas. HPaSteCs can undergo a transition to a metabolically active state as a result of auto- and paracrine signals released during inflammation, injury, and cancer development[214]. Such metabolically activated stromal cells contribute crucially to the pathogenesis of pancreatic disorders[214].[1]

The individual organoid types from the co-culture and the monoculture controls were analyzed with bulk proteome measurements to investigate the cellular changes upon co-culturing. The quantitative proteomic composition analysis clearly separated the PDLOs and HPaSteCs from the co-cultures from their mono-cultured controls (**Figure 29b**). To ensure that no cross-contamination had occurred, it was examined whether the top 10% of the highest expressed proteins of the single cultures were found in the upregulated proteins co-culture in the other cell type. No HPaSteCs proteins were found in the PDLOs of the co-cultures and only 2% in the HPaSteCs (**Figure 29c**). This illustrated that only negligible cross-contamination occurred.[1]

The comparison of the upregulated genes in the co-culture showed protein interactions in the PDLOs with various transcription factors such as signal transducer and activator of transcription 1 and 3 (STAT1, STAT3) or transcription factor AP-1 (JUN), STAT1, NF- κB in the HPaSteCs. Gene Ontology (GO) term analysis revealed the enrichment of related proteins. More specifically, in the PDLOs, signaling pathways associated with energy metabolisms were activated, such as respiratory electron transport, respiratory chain complex, ATP synthesis, or oxidative phosphorylation. In contrast, pathways in HPaSteCs were actually activated by co-culture, indicating activation of the cell type. Proteins related to autocrine and paracrine signaling pathways (membrane-bound organelle, extracellular vesicle, vesicle-mediated transport) were upregulated. The hypothesis of metabolic activation was further supported by protein network analysis, which showed a mitogenic pattern of cells[214] (**Figure 29d**).[1]

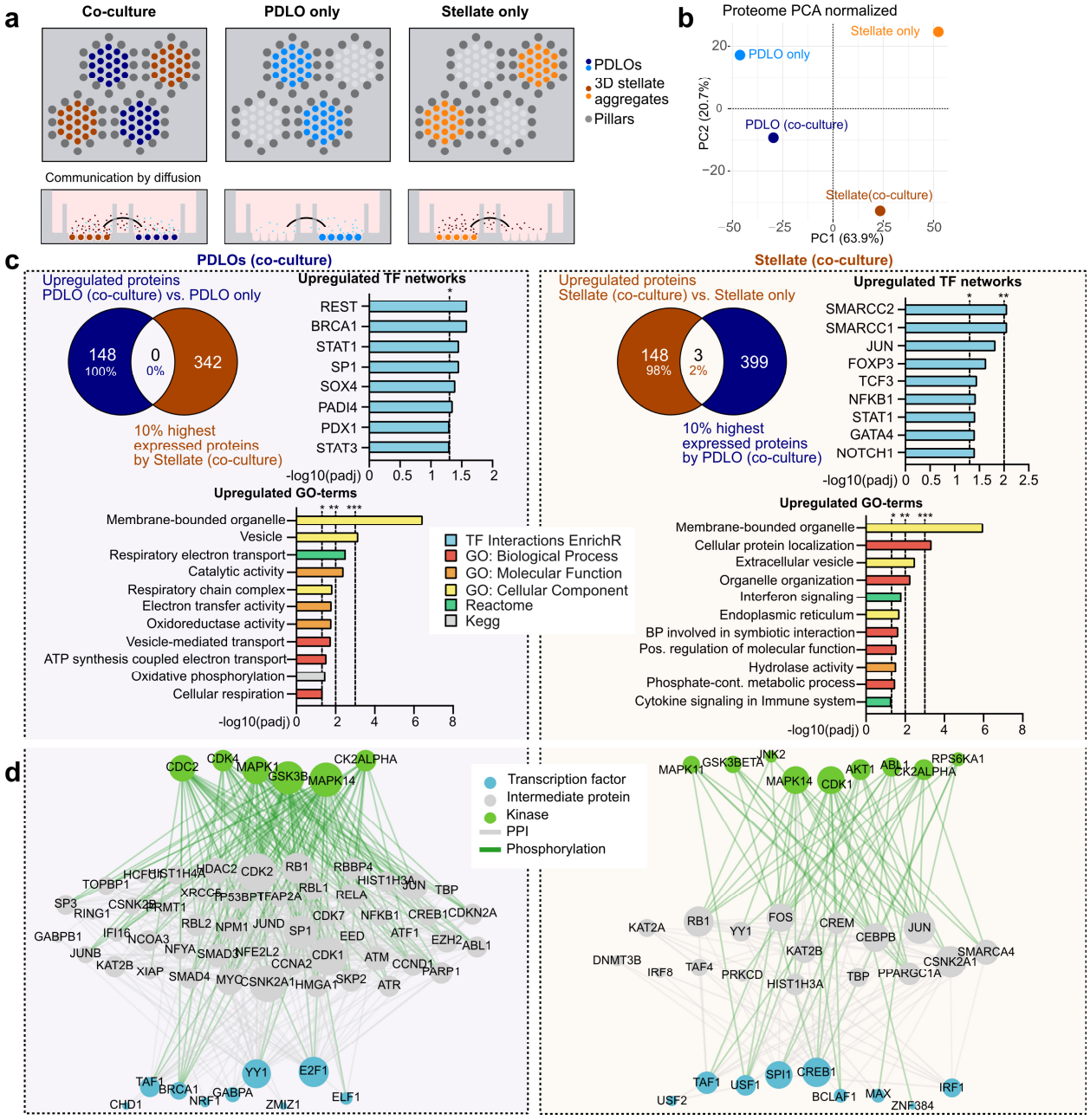

Figure 29 | Co-cultivation of PDLOs and HPaSteC aggregates on the microwell chip.

a, Co-cultivation of PDLOs and 3D HPaSteC aggregates using the microwell chip. The four separately fillable hexagonal arrays facilitated co-culture while avoiding the mixing of cell types. Protein levels of the co-culture and individually-cultured controls were determined after three days by label-free mass spectrometry (n=1). **b**, The graph shows a principal component analysis (PCA) analysis separating the co-culture from their single culture controls. **c**, Analyses of the proteome from the co-culture are shown on the left for the PDLOs and on the right for stellate

cells. Venn diagrams show the test for cross-contamination based on the overlap of the top 10% of the highest expressed proteins within the individual cultures in each of the opposing cell types in the co-culture. Further shown are the highly regulated proteins from a transcription factor (TF) and GO-term analysis. The corresponding significance levels are as follows: *: $p < 0.05$; **: $p < 0.01$; ***: $p < 0.001$. **d**, The analysis of protein networks[215] among the upregulated protein sets found in co-cultured PDLOs and HPaSteCs indicated reciprocal signal transduction.[1] *The figures are adapted from Wiedenmann, et al. [1] and used with "author permission rights" from Nature.*

3.7.2 Secretome studies for the discovery of biomarkers

A second microwell chip application aimed to discover prognosticators or biomarkers for early-stage PDAC. Given the mainly apical-out polarity, the PDLOs provide the opportunity to measure protein content, which is usually secreted to the luminal side of organoids. The secretomes of healthy or genetically modified PDLOs could be a promising tool for discovering a biomarker set applicable in liquid biopsy. Open access to the microwell-encaptured organoids allows the characterization of their secretome in a hydrogel-free environment by measuring the supernatant.[1]

To ensure that adequate protein material could be obtained, the microwell chip was scaled up to 1 196 PDLOs, and label-free mass spectrometry (LS-MS/MS) was used (**Figure 30a**). After eight hours of incubation in media without supplements, measurement of the secretome resulted in detecting 2,789 proteins within the supernatant (**Figure 30b**). 2,528 secreted proteins were identified with a high confidence level during quality filtration and 167 contained a peptide for active secretion into the extracellular space (**Figure 30b**, **Supplementary Data 4**)[191]. The performed GO term analysis of the filtered secretome highlighted the enrichment of enzymes with hydrolytic and lipid-binding functions (**Figure 30b**). Furthermore, a comparison with all human tissue types revealed significant concordance for "pancreas, glandular cell" (**Figure 30b**).[1]

Subsequently, both secretome and scRNA-seq data were employed to determine potential prognostic markers for PDAC, obtained using microwell duct-on-chip technology. Thirty unfavorable markers for pancreatic cancer[216] were found within the top 200 DEGs of the duct-like clusters. Within the filtered PDLO secretome, the 2,528

proteins revealed 186 unfavorable prognostic markers[216] (**Figure 30c**). Eleven proteins identified in the transcriptome and 38 identified in the secretome were expressed mainly in the ductal cells of the pancreas. Only three unfavorable marker proteins were exclusively found in the top 200 DEGs (**Figure 30c**).

To note, secretome studies confirmed once again the ductal identity. Furthermore, they indicate the possibility to measure cancer-related proteins expressed in the healthy pancreas or increased in PDAC. [1]

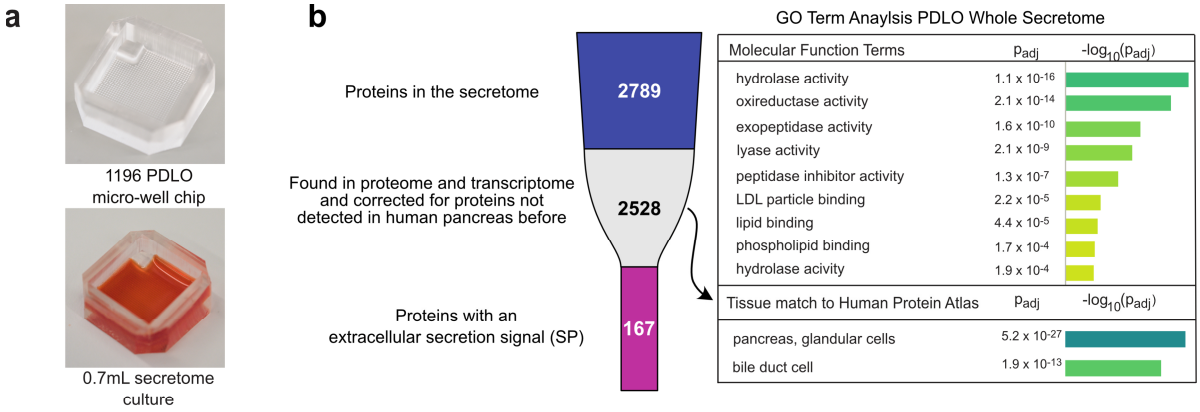

Figure 30 | Screening for potential PDAC biomarkers within the PDLO secretome and transcriptome with the microwell chip.

a, Design of a microwell chip for LC-MS/MS-based measurement of the PDLO secretome in three biological replicates and one, two, and five technical replicates, respectively. **b**, The process of secretome filtering is shown on the left. GO terms relevant for ductal function enriched in the filtered PDLO secretome are shown on the right side. **c**, Illustration of prognostic markers for PDAC in the 200 DEGs of the combined ductal clusters and proteins identified in the PDLO secretome. Stainings obtained from the human protein atlas[190] were used to study expression in pancreatic ductal tissue. Overlaps between the unfavorable prognostic markers for pancreatic cancer found in both approaches are shown in a Venn diagram.[1] *The figures are adapted from Wiedenmann, et al. [1] and used with "author permission rights" from Nature.*

3.7.2.1 Expression of the potential biomarker filamin b in pancreatic cancer patients

Literature research revealed that only 17[217-236] of the unfavorable markers are established PDAC markers, twelve[237-251] were found before but not further validated, and twelve were not mentioned in relation to PDAC before (**Figure 31a**). An unfavorable PDAC marker found in the secretome, lysate proteome, as well as in the top 200 DEG of the transcriptome was filamin b (FLNB) (**Figure 30c**). Previously, a secretome screen of pancreatic cancer cell lines identified FLNB without further confirmation in PDAC patients[252] (**Figure 31a**). The functions of FLNB are tissue- and context-dependent in different cancer types. Function-promoting, as well as function-loss, have been shown to enhance cancerous properties[253,254]. The expression of FLNB in pancreatic carcinogenesis[255] was examined using IHC stainings of an independent cohort of resected PDACs[177-179] (**Figure 31b**). While normal pancreatic ductal ducts and some acinar glands showed rather low FLNB immunoreactivity at their luminal surface, FLNB expression was much higher in the precursor lesions and cancerous tissues (**Figure 31b**). The latter showed strong FLNB expression in the cytoplasm and on the cell surface, consistent with a loss of polarity in cancer cells. PDLOs derived from the microwell chips were also FLNB-positive, coherent with the expectations (**Figure 31c**).[1]

The IHC stains were further statistically analyzed using the semiquantitative H-score method[180,181]. Thus, the significant increase of FLNB levels in PDAC and PanIN lesions compared with healthy ductal tissue was substantiated (**Figure 31d**). However, it was not observed that decreased survival correlated with increased FLNB expression, as previously shown in the Human Protein Atlas[190] (**Figure 31e**). In contrast and interestingly, a higher FLNB expression in PanINs even had a favorable effect on the probability of survival (**Figure 31e**). PanINs, the precursor lesions of PDAC, are frequently detected in the proximity of PDAC, and their presence has considerable prognostic importance. Along with prognostic potential, FLNB expression levels in PanINs were shown to have prognostic potential as they significantly correlated with higher patient survival (median overall survival (mOS); p=0.0019).[1]

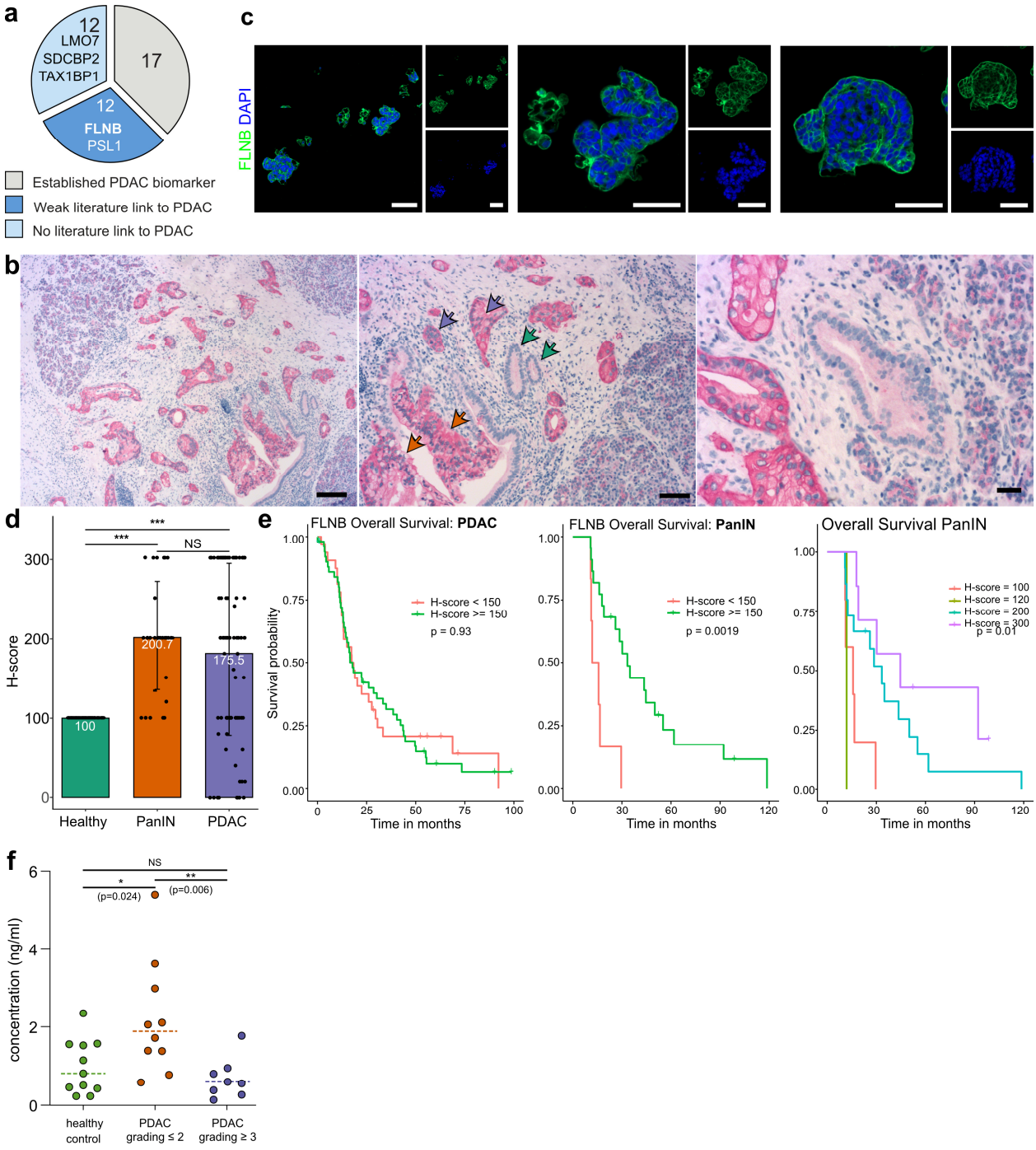

Figure 31 | Analysis of expression patterns of FLNB in PDLOs and PDAC patients.

a, Reviewing related literature for the identified unfavorable prognostic markers in the table of **Figure 30c**. **b**, Staining of FLNB in PDAC tissue by IHC (purple arrows: PDAC, orange arrows: PanINs, green arrows: healthy ducts). Scale bar denotes 100 µm on the left side, 50 µm in the middle, and 20 µm on the right side. **c,** PDLO staining for FLNB visualized via fluorescence

imaging. Scale bar denotes 100 µm and 50 µm for the magnifications. **d**, Bar plot showing the mean H-scores of FLNB in healthy, PanIN, and PDAC tissues with sample sizes of n=86, n=28, and n=84, respectively. The error bars indicate the standard deviation. Statistical significance was tested using a Mann-Whitney U-rank test with significance levels as follows: *: $p < 0.05$; **: $p < 0.01$; ***: $p < 0.001$. **e**, Visualization of overall survival curves of patients with high and low FNLB H-score. It was found that the favorable prognosis of patients with high FNLB H scores correlated with PanINs. The statistical significance of the correlation was tested with a log-rank test. **f**, Analysis of median FLNB level within peripheral blood of a healthy control group with n=11 patients and two comparison groups with PDAC grade ≤2 (n=10) and PDAC grade ≤3 (n=7). Statistical significance was tested with a Mann-Whitney U-rank test and the same significance levels as in **d**.[1] *The figures are adapted from Wiedenmann, et al. [1] and used with "author permission rights" from Nature.*

A similar effect of increased expression in preneoplastic lesions has been found in other cancers. For example, higher expression of the epigenetic silencer Enhancer of Zeste Homolog 2 (EZH2) appeared to be linked to a better prognosis, although only in established cancers[256]. Alternative splicing may result in different or shorter FLNB isoforms, which have been reported to be strongly associated with EMT gene signatures in biopsies of basal-like breast cancer[257]. Similarly, various FLNB isoforms might be present in the PanIN lesions of pancreatic cancer, having different biological effects.[1]

Last, it was tested whether FLNB could be applicable as a liquid biomarker. Therefore, FLNB levels were determined in the peripheral blood (PB) of human metastatic PDAC patients from an independent cohort and a volunteer healthy control group. Initially, no obvious increase was detected when FLNB levels were compared between the control and PDAC groups. However, a difference was observed after separating the samples according to tumor stage. Thereby, the clinical and histological characteristics of the PDAC patients were included, and interestingly, differentiated tumors (≤G2) had significantly higher FLNB levels than less differentiated tumors (≥G3) or healthy donors (**Figure 31f**). Actually, the FLNB levels of the less differentiated tumors (≥G3) were comparable with those in healthy donors.[1]

The results suggest that FLNB is a biomarker for biopsies and may be a suitable blood biomarker for differentiated PDACs and complement biomarker panels. FLNB levels

could indicate early PDAC formation and, in combination with other biomarkers, the differentiation stage of PDACs.[1]

4 Discussion

In this thesis, different microsystem tools have been used to generate a highly controllable model for pancreatic cancer. Therefore, a microwell duct-on-chip technology was designed as an open microwell array chip with the possibility of seeding up to four cell types or analyzing four conditions for the same cell type. HiPSC-derived pancreatic duct-like organoids were generated on the chip before charting their differentiation trajectories to two main duct-like subtypes with time-resolved scRNA-seq sampling. A *CFTR*$^{+}$- and *mucin*$^{+}$-expressing subtype was found in the transcriptome and proteome in the PDLOs and *in vivo*. The applicability and the potential of this microwell duct-on-chip technology were investigated, and the secretome was extensively analyzed to determine putative PDAC prognostic and diagnostic biomarkers.[1]

The microwell duct-on-chip technology extends the existing PDAC engineering models from a poorly studied perspective to date. The deployment of microwell duct-on-chip technology in a screening of early biomarkers renders as promising. It provides the opportunity to develop a screening test for highly lethal pancreatic cancer with further studies.

4.1 Design of a microwell duct-on-chip technology to acquire secreted proteins from PDLOs

The microwell duct-on-chip technology was designed to differentiate 3D PP aggregates to PDLOs and subsequently measure the secreted proteins. In addition, the chip was tailored to the application with various capabilities. The prototyping with a 3D DLA printer allowed the generation of complex negative chip molds subjectable to further modification and refinement. While the chip can be adapted individually to additional applications or cell types, it can also be modified within the individual arrays. The work has also successfully demonstrated fast adaptability with the up-scaling of the chip to 1196 microwells. Another advantage of the chip, besides its low-cost production, is the reduced consumption of expensive media and the use of elaborately differentiated cells. The design represented by the hexagonal arrangement of the microwells, the roundings between them, and the pillars on the outside of the wells allowed the formation of

homogeneous 3D aggregates within a few hours by employing a defined cell number per well and surface tension.[1]

The open chip design allows simple and controlled seeding of cells. Further, it is possible to retrieve organoids for various experiments or downstream analyses with minimal perturbation. This is usually only possible on closed chips by dissolving the organoids or applying high shear stress and thus losing the integrity of the organoid[162]. Furthermore, the design featuring a 180 µm thin bottom enables several analyses to be performed directly on the chip. Thereby, the chip was successfully used for live imaging over a couple of days. In addition, the individual arrays with the surrounding pillars allowed up to four different simultaneous IF stainings to be carried out on the whole organoids and imaged at high resolution within the chip. Moreover, the 61 microwells per array simultaneously delivered an adequate number of technical organoid replicates.[1]

The 3D aggregates generated in this process were cultured and differentiated in the chip with high reproducibility over a period of up to 19 days[1]. Whether this long-term culture can be extended has not been examined yet. In the study of Breunig, et al. [2], the PDLOs were cultured and passaged for a prolonged period of up to 59 days. In this study, PDLOs continued proliferating upon being embedded in Matrigel[2]. While no substantial cell death and no growth were observed in the microwell chip, the restructuring of the organoids could be documented[1]. This may suggest a potential for long-term cultivation of the organoids. However, under given culture conditions, cultivation organoids should be regarded only for a limited time in order to avoid potential experimental artifacts.

In addition, the four different arrays allowed the establishment of co-cultures and the detection of a response to the secreted proteins of each of the other cell types in the lysate of organoids[1]. Thus, the chip allows more detailed studies of secretion-driven communication between cell types. An interesting aspect for further studies would be to measure the secretome of the 3D aggregates and organoids in the co-cultures. This would enable the analysis of the secretory proteins responsible for the cellular changes and PDAC-related cell types communication. However, this study involved only measurements of the secretome of the 1196-organoid chip with mono-culture of PDLOs. Just 1-3% of the supernatant was subjected to LC-MS/MS for high-quality analysis during the secretome measurement. This indicated that secretome measurement within a

smaller chip is, at least theoretically, feasible. At the same time, the number of organoids per array or the number of arrays could be increased for higher material yield.

Similar chips have already been used for automated seeding and culturing of PSC-derived intestinal organoids and subsequent high-throughput drug screening in collateral cancer organoids[258]. Cell culture automation on the microwell chip should also be feasible by employing dedicated pipetting robots. However, materials featuring no small-molecule absorption or release should be involved in differentiation protocols starting at the stem cell stage and drug studies. Whether the response of cultured cancer organoids reflects the *in vivo* scenario is another question to be addressed. Organoids' drug responses become significantly and physiologically closer when the drugs are delivered and cleared through an artificial blood vessel and cancer-related cell co-cultures[94].

4.2 Pancreatic duct-like organoid differentiation on-chip

In 2021, the first protocols describing the generation of stem cell-derived pancreatic duct organoids were published[2,136]. Breunig, et al. [2] and Huang, et al. [136] transferred PPs into a 3D Matrigel culture as single cells and differentiated them into PDLOs in a multi-phase protocol. These studies aimed to achieve the organoids' accurate physiological form and expression pattern. These cystic PDLOs exhibited apical-in polarity and showed functional CFTR activity when stimulated with forskolin. Different stages of pancreatic cancer could also be mimicked within these organoids by the inducible oncogenes $KRAS^{G12D}$ and $GNAS^{R201H/C}$.

The work presented in this thesis was carried out in parallel to the study of Breunig, et al. [2] as an alternative approach for pancreatic cancer diagnostics. The best option to diagnose pancreatic cancer earlier is to find a set of early secreted biomarkers. The advantage of this thesis compared to the Matrigel-based organoid culture of Breunig was the possibility to examine the secretome of PDLOs on the chip due to the matrix-free microenvironment and the resulting reversed polarity. Therefore confirmation of whether ductal organoids could be generated on a microwell chip with the protocol of Breunig, et al. [2] was mandatory.

4.2.1 Morphological changes to two distinct pancreatic duct-like organoid types

The on-chip formed 3D PP aggregates underwent major morphological changes during differentiation toward organoid structures. Initially, the PPs formed uniformly round-shaped aggregates within a few hours. Upon employing time-resolved IF staining for nuclei, epithelial and junction markers, the reorganization of the cells could be closely monitored. Initially, small lumens were formed, and the cells arranged themselves in a multi-layered epithelial structure, which is comparable to micro-lumen forming murine developmental stage E11.5[259]. In the second differentiation phase, outgrowths were paralleled by a decreased number of epithelial layers. Two different organoid types were observed at this stage: i) a multi-layered epithelial PDLO type with apical-out polarity and ii) the cystic PDLO type originating from the former.[1] None of the two morphologic types showed a different phenotype than PDLOs differentiated in Matrigel. However, upon orthotopic transplantation or Matrigel embedding, the PDLOs restructured to cystic epithelial organoids like described before[2,136].

Since the two different cell types could be detected in the transcriptome analysis, the next question was whether these different types are reflected in the morphological organoid types as well. The findings indicated that cystic organoid type expressed mucin exclusively. However, consistent with the transcriptome data, multi-layered epithelial PDLO type expressed CFTR in the early stages, although both CFTR and mucin in the later stages. Thus, neither the markers nor the bright field images could conclusively demonstrate that the transcriptome types reflect the distinct morphological types.

The majority of the stainings for organoid characterization were performed on day 28. Both morphological types could be observed within the same organoid at this time. Further, the multi-layered epithelial PDLOs with reduced layers could be observed more frequently on day 31. Therefore it is conceivable that prolonged cultivation of multi-layered organoids may restructure them into bi-layered epithelial structures. On day 28, two layers were often separated from other two-layered structures by expressing apically localized markers in between. In addition, with extended cultivation, the separation of the cystic organoids from the multi-layered structures may divide the cell and organoid types. These hypotheses need to be addressed in future studies upon employing prolonged

cultivation and staining of the organoids. However, as the dynamic velocity analyses emphasized, a dynamic transition from CFTR^{+}-cells to mucin^{+}-cells could occur alternatively within the multi-layered epithelial organoids.

In conclusion, while the two morphological types do not match PDLOs cultured in hydrogel or *in vivo*, they can develop into organoids similar to Breunig, et al. [2] and Huang, et al. [136] by providing ECM. Further, the morphological subtypes did not split the duct-like subtypes but may do upon prolonged cultivation.

4.2.2 Predominant apical-out polarity supports secretome studies and is switchable upon ECM contact

In vivo ducts and primary or hPSC-derived PDOs/PCOs cultured in a hydrogel exhibit an apical-in, basal-out polarity[2,35,60,136,165]. Thus, secretion is directed from the apical side of the ductal cells toward the lumen and trapped inside the organoid or the hydrogel. On the contrary, PDLOs generated on microwell duct-on-chip technology showed a predominantly, but not completely, apical-out polarity[1]. The IF stainings and the swelling of cystic PDLOs, when stimulated with forskolin, indicate a relevant amount of functional luminal CFTR at the inner membrane of the PDLOs.[1]

Upon transplantation into immunosuppressed mice, PDLOs formed ductal structures exhibiting the apical side toward the lumen[1]. An identical transition to an apical-in polarity was observed after the transfer of PDLOs from the microwell chip to a Matrigel hydrogel culture enriched in laminin[1]. The apical-in to apical-out conversion of cell polarity for organoids transferred from hydrogel to suspension cultures has been reported previously for epithelial intestinal organoids[166,260]. Additionally, intestinal organoids cultured on microstructured chip formats exhibit an apical-in polarity with the addition of only 2% of Matrigel supplemented in the media[258]. This suggests that ECM components participate in inducing the ductal epithelial polarity.

However, organoids with apical-out polarity can become advantageous in certain applications, where organoids with apical-in polarity cannot be used, e.g., secretome analysis or stimulation of the apical cell membrane. It promotes the accessibility of the apical membrane for various studies, such as the investigation of membrane barrier functions or pathogen infections. Furthermore, the predominant apical-out polarity of the

PDLOs facilitates the exposure to external stimuli and enables swift access to the secretome of the organoids.

4.2.3 Limited functional swelling upon forskolin stimulation

One of the main functions of pancreatic ductal cells is the secretion of bicarbonate and water through the apical-localized CFTR channel upon contact with acinar-secreted enzymes. To test this function *in vitro*, organoids were stimulated with forskolin and the subsequent swelling event was monitored. The findings revealed only sporadic swelling after forskolin stimulation of PDLOs on the microwell chip, consistent with the main external CFTR expression. The swelling was only observed in the multi-layered epithelial duct-like organoids, which can be explained by the lack of connection of cystic organoids to the multi-layered counterparts and their free migration through the well. At the same time, CFTR expression was not detected in the cystic organoids. Whether the PDLOs show functional swelling in the hydrogel after the polarity switch, comparable to PDOs, remains to be determined.

To summarize, the PDLOs show limited functionality due to the minimal apical-in polarity. However, the main secretion from the organoids is likely to occur in the medium through the expression of CFTR on the outer surface of the PDLOs. Consequently, the inversed polarity is supporting the development of secretion studies.

4.2.4 PDLOs exhibit a maturation level comparable to a human fetus

The differentiation of PDLOs in the microwell chip also allows examining the synchronous human ductal development in a two-stage protocol. The entire cell development from the PP to the duct-like cell stage was characterized using time-resolved single-cell transcriptomics and IF stainings. It revealed four progenitor clusters, a few endocrine-like and endothelial-like cells, and three duct-like cell clusters. Various commonly known progenitor markers were used to verify in detail that differentiation had begun with the correct starting cell type.

Based on analysis of various protein and transcriptome markers, maturation to ductal organoids could be detected. However, this maturation process did not entirely resemble theirs in the adult pancreas. Within the PDLOs, ductal markers such as SOX9, HNF1B, KRT8, CDH1, and KRT19 were widely documented. However, their expression is

detectable already in the early stages. Further, progenitor markers, only present in other late-stage pancreas cell types, like NKX6-1, GP2, and PTF1A, decreased over time. More mature markers such as CFTR, MUC1, AQP5, CA2, and KRT7 could also be revealed by IF stainings in many but not all cells. The transcriptome data showed end-stage *CA2* and *CFTR* expression, whereas *MUC1*, *AQP5*, and *KRT7* could only be found in a few cells, further indicating an incomplete maturation of the PDLOs.[1]

The maturation of progenitor cells into ductal cells similar to a fetal stage was further demonstrated with data integration into three primary single-cell data sets[1,4-6]. Thereby, the duct-like cells clustered together with the ductal cells of the adult primary pancreas[1]. This is also evident from the common expression of ductal markers, where the expression of progenitor cell markers was still elevated, and the more mature markers were decreased compared with adult ductal cells.

Human comparative data from fetal to adult pancreas development does not reveal the precise degree of maturation. The current knowledge on pancreas development is based almost exclusively on murine data, which does not share the same level of similarity for pancreas development as it does for other organs. A single-cell transcriptome dataset for the human fetal pancreas has only recently been obtained from seven to ten WPC[213]. Gonçalves, et al. [213] showed similarities to murine development among the top 50 DEGs in the tip/trunk development. At the same time, the study also revealed major differences in the number and intensity of cell expression. Importantly to mention, the dataset was acquired before the development of ductal cells in the tip/trunk patterning stage. Scoring the top 50 DEGs from this data set[213] showed that trunk cells, representing the latest stage toward ductal cells, were most similar at the transition from 3D MPP to duct-like cells 1. In general, expression was mostly uniform across clusters except for the endocrine-like and endothelial-like cells. This suggests that the progenitor cells were less mature, and the duct-like cells were more mature than fetal cells from seven to ten WPC. Just recently, Sean, et al. [261] published a preprint of a single-cell roadmap of human fetal pancreatic development with samples from eight to 19 WPC. Sean, et al. [261] found tip/trunk pattering and three ductal clusters. However, the preprint focused on endocrine development, and the data is not accessible yet. Nevertheless, this data provided

essential information on human exocrine development and might allow further optimization of differentiation protocols.

In conclusion, PDLO maturity corresponds to a fetal maturation level more advanced than seven to ten WPC but lower than the adult pancreas at this point.

4.2.5 Two differential routes into *CFTR*- and mucin-rich ductal subtypes

For the first time, the differentiation of hiPSCs to PDLOs on-chip was performed. For detailed characterization of differentiation to PDLOs, seven time points were recorded as single-cell transcriptomics, starting at the PP stage. Initially, two different progenitor clusters were found: unipotent and multipotent progenitors. These already matured during transfer in 3D within one day, supporting the thesis that 3D cultivation enhances maturation. During differentiation, sporadic endocrine-like and endothelial-like cells were observed. In the end, three different duct-like clusters belonging to two functional subtypes could be identified. These two groups resembled the transcriptome profile of mucosal restitution (*MUC1*) and HCO_3^- secretion (*CFTR*) previously identified in a primary data set at the scRNA-seq level[4].[1]

In addition to ductal heterogeneity in the final stage, the emerging intermediate stages revealed important information about the specification of duct-like cell types. Previously, endocrine progenitor cells and later ductal cells were thought to segregate from a common trunk domain[205]. This arises in mice around E12.5 and subsequently undergoes tubular morphogenesis to form the ductal network[205]. While the timing of expression of certain markers is slightly different, evidence of similar markers indicates the presence of a trunk domain and a tip domain during human pancreatic development[139,205].[1]

4.2.5.1 Two differentiation routes from the pancreatic progenitor stage

Velocity analysis suggested different potency of the microwell chip-derived ductal cell types that arose from distinct, temporarily coexisting progenitor populations. *CFTR*$^+$ duct-like cells 1 have evolved from 3D MPPs, such as the few endocrine cells. These MPPs arose from the classical *PDX1*$^+$/*NKX6*-1$^+$ cell type (2D MPPs), to which PP protocols are optimized. However, while *GP2* and *PTF1A*, indicative of classical tripotency, were not yet expressed in 2D MPPs, their expression was detected upon transfer in 3D setting.[1]

An unexpected outcome of the analysis was the absence of a common trunk domain subcluster for the endocrine- and duct-like cells[1]. A separate *PTF1A*$^{-}$/*NKX6-1*$^{+}$ cell cluster was not detected in close proximity to endocrine and ductal cells, representing an intermediate population that gives rise to both lineages[1]. However, such a population was detected upon crossing 3D MPP and duct-like cells 1, which also maximized the score for a gene expression pattern resembling the human fetal trunk region. These findings may suggest that a deeper scRNA-seq sampling interval with more cells would show a distinct trunk cluster between MPPs and duct-like cells 1. However, a common trunk domain emerging in the endocrine cells as described in mouse development cannot be envisaged[138].

Velocity analyses showed an additional developmental route to duct-like cells *in vitro*, originating from UDPs and, to a small extent, from *CFTR*$^{+}$ cells in *MUC13*$^{+}$ cells. Such a developmental route to ductal cells was not described in mice yet. However, velocity analysis, ductal identity at the end of differentiation, and expression of diverse early ductal markers in the 2D and 3D UDPs strengthened the hypothesis of an alternative differentiation trajectory in the PDLOs. It is possible that the chemical induction protocol does not accurately reflect the *in vivo* development and that artificial variations from the trunk pattern were induced. *In vitro* and *in vivo* progenitor cell differences have been observed previously during endocrine development, in which a distinct trunk-like stage was also not detected[262-264]. Using *in vivo* scRNA-seq data from mice, additional developmental routes of PPs were hypothesized[265]. Further *in vivo* lineage tracing experiments directly demonstrated the progression of a ductal subpopulation of Pdx1^{+}/Ptf1a^{-} PP cells[266,267].[1]

The recently published fetal single-cell transcriptome dataset contained some endocrine cells but no ductal counterparts, thus not allowing to screen for a common trunk domain[213]. In this study, PP cells of several differentiations were sequenced additionally with a few co-evolving *CFTR*$^{+}$ cells[213]. However, also in this approach, no common origin of these small number of endocrine and *CFTR*$^{+}$ ductal cells was demonstrated, suggesting the early ductal priming of PDLOs by the chemical induction *in vitro*[1]. The integration of different PP protocols into the human fetal dataset further showed differences *in vivo* and *in vitro*, with the 3D clusters most closely resembling the *in vivo*

cells[213]. However, the protocol used here was not included. The human dataset requires clustering at a higher resolution in order to investigate minute differences in the progenitor populations. Additional early and late sampling is mandatory for a highly informative charting of the human development trajectories. Conversely, the samples from the advanced-developed fetal pancreas[261] would teach us more about the potential absence of a common trunk domain in the human pancreas.

Altogether, the *in vivo* development of PPs into pancreatic duct-like organoids is rather heterogeneous. Further investigations within the human fetal datasets are required to draw differences and similarities to *in vitro* differentiation approaches.

4.2.5.2 CFTR$^+$ and mucin$^+$ cell types in the PDLOs and adult pancreas

To investigate whether *CFTR*$^+$ and mucin$^+$ duct-like cell types could also be recovered *in vivo*, primary IF stainings and single-cell transcriptomes were examined. Baron, et al. [4] first detected the two ductal subtypes in a single-cell dataset. The scoring of the DEGs of the primary subtypes in the PDLO data showed a high concordance with the respective duct-like clusters. Moreover, integration of the PDLO transcriptomes into primary datasets demonstrated a dichotomy between the two ductal subtypes. Since such data integration can lead to overcorrection, the dataset containing the most ductal cells was re-clustered. Several of the duct-like cell cluster markers were consistently found in distinct clusters. Thereby, it is possible to find the two clusters in other primary datasets with and without integration.[1]

To identify these cell clusters on protein level, some of the differentially and jointly expressed markers were subjected to IF analysis in PDLOs and the adult pancreas[1]. The stainings showed indeed a different, but not exclusive, level of marker expression in distinct cells[1]. These findings were in agreement with the scRNA-seq data since an enrichment of the markers could also be seen, although their expression was not necessarily exclusive[1]. Also, Breunig, et al. [2] observed the development of CFTR$^+$ and MUC1$^+$ positive cell types in the hydrogel cultures and hPSC-derived PDLOs.

The two cell types were detected in primary tissue sections. However, the differences were more widespread than in the PDLOs. Consistent with staining data from Baron, et al. [4], the MUC1 positive ductal cells were in close proximity to acinar cells, namely in

the centroacinar and intercalated ducts. On the other hand, CFTR expression was observed in the intercalated ducts and branching ducts. Moreover, other markers of the individual clusters were found in other ductal cells (BICC1, MMP1) or not found in the healthy pancreas (SCTR, TFF1 or MUC13). This suggests additional ductal cell types in the adult pancreas and incomplete maturation of PDLOs. Furthermore, the plasticity indicates that the ductal cells have a possible common progenitor stage.

The comparison and retrieval of $CFTR^+$ and $mucin^+$ ductal cell types in primary tissue indicated that PDLOs have a high potential for model diseases of the pancreatic ductal compartment, particularly pancreatic cancer[1].

4.3 Identification of potential diagnostic and prognostic biomarkers within the PDLO secretome

Unfortunately, no efficient screening approach for early PDAC detection has been established to date. In addition, personalized treatment is still in its infancy, and predictive biomarkers are widely lacking for pancreatic cancer. Secreted biomarker proteins from early neoplastic ducts may consequently address this unsolved issue. Considering the aspects above, the microwell duct-on-chip technology can provide a central tool for analytical methods such as mass spectrometry. Indeed, oncogenic driver gene-expressing PDLOs subjected to screening on the microwell chip may render a major advance for the analysis of oncogene-specific secretomes. This thesis' data delivers a proof-of-concept by determining the secretome of genetically unmodified hiPSC-derived PDLOs and the subsequent implementation of a systematic biomarker classification approach.[1]

Within the secretome and transcriptome, several unfavorable and favorable markers specifically expressed in pancreatic ductal cells were revealed. Among the unfavorable markers, less than half are established biomarkers for PDAC. For the proof-of-concept investigations, filamin B, detected in both the secretome and transcriptome, was further studied in cancer patients. Indeed, FLNB was found to be significantly elevated in PDAC in biopsies. Interestingly, a significant expression increase was additionally observed in PanIN lesions. Contrary to the data from Human Protein Atlas[190], no unfavorable effect could be observed in the cohort of cancer patients examined in this study. Conversely,

higher FLNB expression was found to be associated with better mean overall survival. In addition, FLNB levels were measured in healthy and PDAC patient blood to interrogate the feasibility as a liquid biopsy marker. Indeed, the PDAC patient's FLNB blood level concentrations were associated with a marked increase in FLNB levels, although exclusively in early cancer stages.[1]

Thus, the data indicate that FLNB is an (early) PDAC biomarker. However, FLNB is unsuitable as a liquid biopsy marker given its rather low levels in peripheral patient blood samples in later pancreatic cancer stages, which their hypovascularization may reason. In order to establish a specific set of biomarkers for liquid biopsies in a follow-up study, a broad screening approach needs to be addressed. In this regard, the involvement of several markers featuring significantly elevated levels in the blood at early and later stages is mandatory in order to prevent patients from being misdiagnosed at a more advanced stage.

All the secreted markers identified in this study and not further evaluated might be tested for their potential as liquid biopsy markers to screen for better biomarkers. However, a more straightforward approach should consider the use of either primary cancer organoids or hPSC-derived PDLOs with inducible oncogenes, as published by Breunig, et al. [2] and Huang, et al. [136]. The systematic measurement of the secretome might reveal secretion at the earliest possible stages through a controlled activation of oncogenes. The employment of PDLOs with inducible oncogenes circumvents to some extent the sole use of databases for identification of the secretome and may ultimately provide potential early biomarkers and therefore offer deep insights into oncogene-specific secretion changes.

Taken together, microwell duct-on-chip technology is applicable for secretome analysis and identification of potential diagnostic and prognostic biomarkers. In a follow-up study, (inducible) cancer organoids can be screened for additional early biomarkers within the chip.

5 Conclusion

The exocrine function of the pancreas is central to the human digestive system. The destruction of exocrine cell types and tissues by chronic pancreatitis leads to pancreatic insufficiency and increased risk of pancreatic cancer[268,269] - one of the most devastating cancers to date[19]. In the past decades, the main research was based on 2D cell culture and later 3D Matrigel culture involving cell lines, primary mouse or human tumor cell material and *in vivo* experimental settings. Substantial knowledge about the genetic components and key regulators has been gained through these studies. However, the progress in developing pharmaceutical therapies and preventive medical testing for human pancreatic cancer remained rather limited. Previous studies lack the complex TME, cell composition, and characterization of the early stages of tumors. The inaccessibility of the human pancreas and the shortage of healthy or early disease-prone ductal material further hampered the discovery of biomarkers for diagnostic purposes or drug development.

Therefore, human stem cell-derived organoids of the exocrine pancreas hold tremendous potential for engineering *in vitro* disease models and to advance human pancreas development knowledge. Newly established differentiation protocols toward pure exocrine pancreatic organoids represent a major step toward the design of an artificial pancreas[2,136]. Rebuilding the healthy pancreas from the earliest possible stage – stem cells allows the study of developmental routes and the control and reconstruction of different genetic perturbations of pancreatic cancer. Inducing and investigating pancreatic cancer from the healthy cell type origin can give substantial insights into cancer development, driver pathways and key regulators. However, since these organoids are cultured in hydrogel and have apical-in polarity, they may not be used to measure the altered secretion upon oncogene induction.

During my doctoral study, I designed a matrix-free microwell duct-on-chip technology to extend the current research with the enablement of secretome studies within apical-out organoids. The benefits of the microwell chip are represented by i) the reduced amount of cells and material, ii) controlled and homogeneous 3D aggregate size, iii) capability of long-term 3D cell culture with live-imaging, iv) sampling for downstream analysis with minimal perturbation, and v) the opportunity to initiate co-cultures.[1]

In the microwell chip, I differentiated hiPSC-derived 3D PP aggregates into PDLOs to establish a healthy model of the ductal pancreas, which can later be used to measure secretion changes in pancreatic cancer progression[1]. To validate this novel and first PDLO on-chip model, I first analyzed in detail the organoids and their differentiation route with time-resolved IF and scRNA-seq analysis[1]. The single-cell transcriptomics revealed two and so-far only partially known differentiation routes toward two duct-like cell types[1]. It provides a new opportunity to trace and understand the ductal *in vitro* differentiation route. The main ductal subtypes expressing *mucin*$^+$ or *CFTR*$^+$ have also been identified in primary scRNA-seq datasets[1,4] and IF stainings of the PDLOs, adult pancreas, and pancreatitis tissue sections[1]. The duct-like cells of the organoids resembled a fetal maturity, which was more advanced than after ten weeks post-conception in a human fetus. Thereby, the system supplements the current research with a novel exocrine ductal pancreas on-chip model, which reflects the pancreatic development to a certain degree.

Due to the apical-out polarity, PDLOs showed only a limited functional swelling upon forskolin stimulation. However, it proved the functionality of the CFTR channel and enabled the establishment of secretome studies, as the proteins are secreted to the measurable media. Several hundreds of favorable and unfavorable PDAC markers could be identified within the secretome analysis. One marker present in secretome and transcriptome was FLNB, which was also increased in cancer biopsies and early cancer stages in patient blood.[1]

The combination of microwell duct-on-chip technology with the cell engineering approach[2,136] may allow monitoring of the earliest possible changes within the secretome of the organoids upon induction of the oncogene expression. Comparing these early mutation-specific changes will help uncover early biomarkers that might be detected in patient blood and a combination of them to establish medical prevention testing.

6 Outlook

Pancreatic ductal cells are organized in a tubular system meant to transport the digestive enzymes produced by the acinar cells to the intestine. Currently, a tubular lumen from pancreatic epithelium has only been used by Nguyen, et al. [103]. The rebuilding of a healthy pancreatic duct in the form of a tube within a system connected to the acinar cells resembles, to a certain extent, the functional unit of the exocrine pancreas, which offers insights into the development and disease origins. One could even envisage that both cell types may be differentiated on the chip using a cytokine gradient. A simpler, faster, and in practice, more feasible alternative is the differentiation and seeding of the hPSC-derived PAOs next to an on-chip formed ductal tube. Testing the optimal time to seed the ductal progenitors into the tube is compulsory to engineer such an hPSC-derived duct-like tube. In mice, branching starts around E9.5 but only at E11.5 forms micro-lumens as observed in the PDLOs around day 20[1,259]. Therefore, a good starting cell type for the transition into the tubular structure might be represented by the cells that underwent 20 days of differentiation and were subjected to close testing. Furthermore, the shear stress inflicted by perfusion can support and even enhance the maturation of *in vitro* differentiated epithelial cells, e.g., by realignment, cytokeratin deposition and development of polarity[270-274]. The model may thus improve the *in vit*ro maturation of the currently fetal-stage-like hPSC-derived PDLOs to mirror closer to the adult pancreas.

One limitation within this model is the Matrigel-based hydrogel, which is batch-dependent, mouse- and tumor-derived. Replacement of Matrigel with the recently developed, fully synthetic hydrogel ECM described by Below, et al. [81] resembles a completely controllable TME. Furthermore, close monitoring of oncogene-specific changes within the hPSC-derived organoids featuring inducible oncogenes, as described by Breunig, et al. [2] and Huang, et al. [136], may advance the PDAC on-chip approach to a more accurately controllable model. Further customization of the model upon integration of artificial vessels or with endothelial cells derived from the same hPSCs[3,275,276] can boost the relevance of drug response, vascularization or hypovascularization studies[94,103]. Additionally, changes in cell communication or stiffness in PDAC changes can be studied by seeding different cells like HPaSteC, hFBs or other tumor-related cell types into the synthetic hydrogel[1,81,94,103]. While such a model requires substantial development and refinement time, it could significantly advance

pancreas and PDAC modeling. A combination of these engineering techniques may render the exocrine pancreas to model PADC in a small, controllable system, easily adaptable according to aims and the experimental setting.

The first milestones for translating *in vitro* exocrine models into disease models have been set in the current phase. However, complex factors of pancreatic cancer have not been addressed yet. Mutations and combinations[277] other than *KRAS*^{G12D} and *GNAS*$^{R201C/H}$ have yet to be regarded, and their contribution to the complex pancreatic cancer investigated. Furthermore, the different cancer-related cell types are not studied in a combined setting. The process of developing an immunosuppressive TME, reflecting a combination of desmoplastic stroma, hypovascularity, myeloid cells, and macrophages[278], remains to be modeled. Further, the distinct types of cell differentiation and transdifferentiation, such as ADM[279] or EMT[280], need to be considered in future studies. Also, the metastatic processes of PDAC require more attention. Previous studies from Nguyen, et al. [103] and Lai, et al. [94] may represent here a valid start. In the same line, extravasation and the metastatic invasion of other organs requires further investigations. In addition, several aspects like perineuronal invasion[281], circulating free DNA and RNA[282], pancreatitis[268] or pancreatic insufficiency[269] must be simulated and studied *in vitro*.

7 Literature

[1] Wiedenmann, S., Breunig, M., Merkle, J., von Toerne, C., Georgiev, T., Moussus, M., Schulte, L., Seufferlein, T., Sterr, M., Lickert, H., Weissinger, S. E., Möller, P., Hauck, S. M., Hohwieler, M., Kleger, A. & Meier, M. Single-cell-resolved differentiation of human induced pluripotent stem cells into pancreatic duct-like organoids on a microwell chip. *Nature Biomedical Engineering* **2021**, *5*, 897-913, doi:10.1038/s41551-021-00757-2.

[2] Breunig, M., Merkle, J., Wagner, M., Melzer, M. K., Barth, T. F. E., Engleitner, T., Krumm, J., Wiedenmann, S., Cohrs, C. M., Perkhofer, L., Jain, G., Kruger, J., Hermann, P. C., Schmid, M., Madacsy, T., Varga, A., Griger, J., Azoitei, N., Muller, M., Wessely, O., Robey, P. G., Heller, S., Dantes, Z., Reichert, M., Gunes, C., Bolenz, C., Kuhn, F., Maleth, J., Speier, S., Liebau, S., Sipos, B., Kuster, B., Seufferlein, T., Rad, R., Meier, M., Hohwieler, M. & Kleger, A. Modeling plasticity and dysplasia of pancreatic ductal organoids derived from human pluripotent stem cells. *Cell Stem Cell* **2021**, *28*, 1105-1124 e1119, doi:10.1016/j.stem.2021.03.005.

[3] Rosowski, S., Brähler, C., Marder, M., Akishiba, M., Platen, A., Ussar, S., Theis, F., Wiedenmann, S. & Meier, M. Single-cell characterization of neovascularization using hiPSC-derived endothelial cells in a 3D microenvironment. *bioRxiv* **2022**, 2022.2002.2015.480506, doi:10.1101/2022.02.15.480506.

[4] Baron, M., Veres, A., Wolock, S. L., Faust, A. L., Gaujoux, R., Vetere, A., Ryu, J. H., Wagner, B. K., Shen-Orr, S. S., Klein, A. M., Melton, D. A. & Yanai, I. A Single-Cell Transcriptomic Map of the Human and Mouse Pancreas Reveals Inter- and Intra-cell Population Structure. *Cell Systems* **2016**, *3*, 346-360 e344, doi:10.1016/j.cels.2016.08.011.

[5] Qadir, M. M. F., Álvarez-Cubela, S., Klein, D., van Dijk, J., Muñiz-Anquela, R., Moreno-Hernández, Y. B., Lanzoni, G., Sadiq, S., Navarro-Rubio, B., García, M. T., Díaz, Á., Johnson, K., Sant, D., Ricordi, C., Griswold, A., Pastori, R. L. & Domínguez-Bendala, J. Single-cell resolution analysis of the human pancreatic ductal progenitor cell niche. *Proceedings of the National Academy of Sciences* **2020**, *117*, 10876-10887, doi:10.1073/pnas.1918314117.

[6] Enge, M., Arda, H. E., Mignardi, M., Beausang, J., Bottino, R., Kim, S. K. & Quake, S. R. Single-Cell Analysis of Human Pancreas Reveals Transcriptional Signatures of Aging and Somatic Mutation Patterns. *Cell* **2017**, *171*, 321-330 e314, doi:10.1016/j.cell.2017.09.004.

[7] Da Silva Xavier, G. The Cells of the Islets of Langerhans. *Journal of Clinical Medicine* **2018**, *7*, doi:10.3390/jcm7030054.

[8] Rahier, J., Wallon, J. & Henquin, J. C. Cell populations in the endocrine pancreas of human neonates and infants. *Diabetologia* **1981**, *20*, 540-546, doi:10.1007/BF00252762.

[9] Leung, P. S. & Ip, S. P. Pancreatic acinar cell: Its role in acute pancreatitis. *The International Journal of Biochemistry & Cell Biology* **2006**, *38*, 1024-1030, doi:10.1016/j.biocel.2005.12.001.

[10] Logsdon, C. D. & Ji, B. The role of protein synthesis and digestive enzymes in acinar cell injury. *Nature Reviews Gastroenterology & Hepatology* **2013**, *10*, 362-370, doi:10.1038/nrgastro.2013.36.

[11] Lee, M. G., Ohana, E., Park, H. W., Yang, D. & Muallem, S. Molecular mechanism of pancreatic and salivary gland fluid and HCO3 secretion. *Physiological Reviews* **2012**, *92*, 39-74, doi:10.1152/physrev.00011.2011.

[12] Bayliss, W. M. & Starling, E. H. The mechanism of pancreatic secretion. *Jorunal of Physiology* **1902**, *28*, 325-353, doi:10.1113/jphysiol.1902.sp000920.

[13] Whitcomb, D. C. & Lowe, M. E. Human pancreatic digestive enzymes. *Digestive Diseases and Sciences* **2007**, *52*, 1-17, doi:10.1007/s10620-006-9589-z.

[14] DeFronzo, R. A., Ferrannini, E., Groop, L., Henry, R. R., Herman, W. H., Holst, J. J., Hu, F. B., Kahn, C. R., Raz, I., Shulman, G. I., Simonson, D. C., Testa, M. A. & Weiss, R. Type 2 diabetes mellitus. *Nature Reviews Disease Primers* **2015**, *1*, 15019, doi:10.1038/nrdp.2015.19.

[15] Wilcox, N. S., Rui, J., Hebrok, M. & Herold, K. C. Life and death of β cells in Type 1 diabetes: A comprehensive review. *Journal of Autoimmunity* **2016**, *71*, 51-58, doi:10.1016/j.jaut.2016.02.001.

[16] Capurso, G., Traini, M., Piciucchi, M., Signoretti, M. & Arcidiacono, P. G. Exocrine pancreatic insufficiency: prevalence, diagnosis, and management. *Clinical and Experimental Gastroenterology* **2019**, *12*, 129-139, doi:10.2147/CEG.S168266.

[17] Mitchell, R. M. S., Byrne, M. F. & Baillie, J. Pancreatitis. *The Lancet* **2003**, *361*, 1447-1455, doi:10.1016/S0140-6736(03)13139-X.

[18] Nousia-Arvanitakis, S. Cystic Fibrosis and the Pancreas: Recent Scientific Advances. *Journal of Clinical Gastroenterology* **1999**, *29*.

[19] Kleeff, J., Korc, M., Apte, M., La Vecchia, C., Johnson, C. D., Biankin, A. V., Neale, R. E., Tempero, M., Tuveson, D. A., Hruban, R. H. & Neoptolemos, J. P. Pancreatic cancer. *Nature Reviews Disease Primers* **2016**, *2*, 16022, doi:10.1038/nrdp.2016.22.

[20] Puri, S., Folias, A. E. & Hebrok, M. Plasticity and dedifferentiation within the pancreas: development, homeostasis, and disease. *Cell Stem Cell* **2015**, *16*, 18-31, doi:10.1016/j.stem.2014.11.001.

[21] Siegel, R. L., Miller, K. D. & Jemal, A. Cancer statistics, 2018. *CA Cancer Journal for Clinicans* **2018**, *68*, 7-30, doi:10.3322/caac.21442.

[22] Ansari, D., Gustafsson, A. & Andersson, R. Update on the management of pancreatic cancer: surgery is not enough. *World Journal of Gastroenterology* **2015**, *21*, 3157-3165, doi:10.3748/wjg.v21.i11.3157.

[23] Zhou, B., Xu, J. W., Cheng, Y. G., Gao, J. Y., Hu, S. Y., Wang, L. & Zhan, H. X. Early detection of pancreatic cancer: Where are we now and where are we going? *International Journal of Cancer* **2017**, *141*, 231-241, doi:10.1002/ijc.30670.

[24] Hingorani, S. R., Wang, L., Multani, A. S., Combs, C., Deramaudt, T. B., Hruban, R. H., Rustgi, A. K., Chang, S. & Tuveson, D. A. Trp53R172H and KrasG12D cooperate to promote chromosomal instability and widely metastatic pancreatic ductal adenocarcinoma in mice. *Cancer Cell* **2005**, *7*, 469-483, doi:10.1016/j.ccr.2005.04.023.

[25] Waddell, N., Pajic, M., Patch, A.-M., Chang, D. K., Kassahn, K. S., Bailey, P., Johns, A. L., Miller, D., Nones, K., Quek, K., Quinn, M. C. J., Robertson, A. J., Fadlullah, M. Z. H., Bruxner, T. J. C., Christ, A. N., Harliwong, I., Idrisoglu, S., Manning, S., Nourse, C., Nourbakhsh, E., Wani, S., Wilson, P. J., Markham, E., Cloonan, N., Anderson, M. J., Fink, J. L., Holmes, O., Kazakoff, S. H., Leonard, C., Newell, F., Poudel, B., Song, S., Taylor, D., Waddell, N., Wood, S., Xu, Q., Wu, J., Pinese, M., Cowley, M. J., Lee, H. C., Jones, M. D., Nagrial, A. M., Humphris, J., Chantrill, L. A., Chin, V., Steinmann, A. M., Mawson, A., Humphrey, E. S., Colvin, E. K., Chou, A., Scarlett, C. J., Pinho, A. V., Giry-Laterriere, M., Rooman, I., Samra, J. S., Kench, J. G., Pettitt, J. A., Merrett, N. D., Toon, C., Epari, K., Nguyen, N. Q., Barbour, A., Zeps, N., Jamieson, N. B., Graham, J. S., Niclou, S. P., Bjerkvig, R., Grützmann, R., Aust, D., Hruban, R. H., Maitra, A., Iacobuzio-Donahue, C. A., Wolfgang, C. L., Morgan, R. A., Lawlor, R. T., Corbo, V., Bassi, C., Falconi, M., Zamboni, G., Tortora, G., Tempero, M. A., Biankin, A. V., Johns, A. L., Mawson, A., Chang, D. K., Scarlett, C. J., Brancato, M.-A. L., Rowe, S. J., Simpson, S. H., Martyn-Smith, M., Thomas, M. T., Chantrill, L. A., Chin, V. T., Chou, A., Cowley, M. J., Humphris, J. L., Jones, M. D., Scott Mead, R., Nagrial, A. M., Pajic, M. et al. Whole genomes redefine the mutational landscape of pancreatic cancer. *Nature* **2015**, *518*, 495-501, doi:10.1038/nature14169.

[26] Rhim, A. D., Mirek, E. T., Aiello, N. M., Maitra, A., Bailey, J. M., McAllister, F., Reichert, M., Beatty, G. L., Rustgi, A. K., Vonderheide, R. H., Leach, S. D. & Stanger, B. Z. EMT

and dissemination precede pancreatic tumor formation. *Cell* **2012**, *148*, 349-361, doi:10.1016/j.cell.2011.11.025.
[27] Storz, P. Acinar cell plasticity and development of pancreatic ductal adenocarcinoma. *Nature Reviews Gastroenterology & Hepatology* **2017**, *14*, 296-304.
[28] Samandari, M., Julia, M. G., Rice, A., Chronopoulos, A. & del Rio Hernandez, A. E. Liquid biopsies for management of pancreatic cancer. *Translational Research* **2018**, *201*, 98-127, doi:10.1016/j.trsl.2018.07.008.
[29] Cooper, C. L., O'Toole, S. A. & Kench, J. G. Classification, morphology and molecular pathology of premalignant lesions of the pancreas. *Pathology* **2013**, *45*, 286-304.
[30] Hruban, R. H. & Fukushima, N. Pancreatic adenocarcinoma: update on the surgical pathology of carcinomas of ductal origin and PanINs. *Modern Pathology* **2007**, *20*, S61-S70.
[31] Hruban, R. H., Goggins, M., Parsons, J. & Kern, S. E. Progression model for pancreatic cancer. *Clinical cancer research* **2000**, *6*, 2969-2972.
[32] Hezel, A. F., Kimmelman, A. C., Stanger, B. Z., Bardeesy, N. & Depinho, R. A. Genetics and biology of pancreatic ductal adenocarcinoma. *Genes & Development* **2006**, *20*, 1218-1249, doi:10.1101/gad.1415606.
[33] Zhu, L., Shi, G., Schmidt, C. M., Hruban, R. H. & Konieczny, S. F. Acinar cells contribute to the molecular heterogeneity of pancreatic intraepithelial neoplasia. *American Journal of Pathology* **2007**, *171*, 263-273, doi:10.2353/ajpath.2007.061176.
[34] Kopp, J. L., von Figura, G., Mayes, E., Liu, F. F., Dubois, C. L., Morris, J. P. t., Pan, F. C., Akiyama, H., Wright, C. V., Jensen, K., Hebrok, M. & Sander, M. Identification of Sox9-dependent acinar-to-ductal reprogramming as the principal mechanism for initiation of pancreatic ductal adenocarcinoma. *Cancer Cell* **2012**, *22*, 737-750, doi:10.1016/j.ccr.2012.10.025.
[35] Boj, S. F., Hwang, C. I., Baker, L. A., Chio, II, Engle, D. D., Corbo, V., Jager, M., Ponz-Sarvise, M., Tiriac, H., Spector, M. S., Gracanin, A., Oni, T., Yu, K. H., van Boxtel, R., Huch, M., Rivera, K. D., Wilson, J. P., Feigin, M. E., Ohlund, D., Handly-Santana, A., Ardito-Abraham, C. M., Ludwig, M., Elyada, E., Alagesan, B., Biffi, G., Yordanov, G. N., Delcuze, B., Creighton, B., Wright, K., Park, Y., Morsink, F. H., Molenaar, I. Q., Borel Rinkes, I. H., Cuppen, E., Hao, Y., Jin, Y., Nijman, I. J., Iacobuzio-Donahue, C., Leach, S. D., Pappin, D. J., Hammell, M., Klimstra, D. S., Basturk, O., Hruban, R. H., Offerhaus, G. J., Vries, R. G., Clevers, H. & Tuveson, D. A. Organoid models of human and mouse ductal pancreatic cancer. *Cell* **2015**, *160*, 324-338, doi:10.1016/j.cell.2014.12.021.
[36] DeNardo, D. G. & Ruffell, B. Macrophages as regulators of tumour immunity and immunotherapy. *Nature Reviews Immunology* **2019**, *19*, 369-382, doi:10.1038/s41577-019-0127-6.
[37] Sahai, E., Astsaturov, I., Cukierman, E., DeNardo, D. G., Egeblad, M., Evans, R. M., Fearon, D., Greten, F. R., Hingorani, S. R., Hunter, T., Hynes, R. O., Jain, R. K., Janowitz, T., Jorgensen, C., Kimmelman, A. C., Kolonin, M. G., Maki, R. G., Powers, R. S., Puré, E., Ramirez, D. C., Scherz-Shouval, R., Sherman, M. H., Stewart, S., Tlsty, T. D., Tuveson, D. A., Watt, F. M., Weaver, V., Weeraratna, A. T. & Werb, Z. A framework for advancing our understanding of cancer-associated fibroblasts. *Nature Reviews Cancer* **2020**, *20*, 174-186, doi:10.1038/s41568-019-0238-1.
[38] Waghray, M., Yalamanchili, M., di Magliano, M. P. & Simeone, D. M. Deciphering the role of stroma in pancreatic cancer. *Current Opinion in Gastroenterology* **2013**, *29*, 537-543, doi:10.1097/MOG.0b013e328363affe.
[39] Hingorani, S. R., Petricoin, E. F., Maitra, A., Rajapakse, V., King, C., Jacobetz, M. A., Ross, S., Conrads, T. P., Veenstra, T. D., Hitt, B. A., Kawaguchi, Y., Johann, D., Liotta, L. A., Crawford, H. C., Putt, M. E., Jacks, T., Wright, C. V., Hruban, R. H., Lowy, A. M. & Tuveson, D. A. Preinvasive and invasive ductal pancreatic cancer and its early detection in the mouse. *Cancer Cell* **2003**, *4*, 437-450, doi:10.1016/s1535-6108(03)00309-x.

[40] Gao, H., Korn, J. M., Ferretti, S., Monahan, J. E., Wang, Y., Singh, M., Zhang, C., Schnell, C., Yang, G., Zhang, Y., Balbin, O. A., Barbe, S., Cai, H., Casey, F., Chatterjee, S., Chiang, D. Y., Chuai, S., Cogan, S. M., Collins, S. D., Dammassa, E., Ebel, N., Embry, M., Green, J., Kauffmann, A., Kowal, C., Leary, R. J., Lehar, J., Liang, Y., Loo, A., Lorenzana, E., Robert McDonald, E., McLaughlin, M. E., Merkin, J., Meyer, R., Naylor, T. L., Patawaran, M., Reddy, A., Röelli, C., Ruddy, D. A., Salangsang, F., Santacroce, F., Singh, A. P., Tang, Y., Tinetto, W., Tobler, S., Velazquez, R., Venkatesan, K., Von Arx, F., Wang, H. Q., Wang, Z., Wiesmann, M., Wyss, D., Xu, F., Bitter, H., Atadja, P., Lees, E., Hofmann, F., Li, E., Keen, N., Cozens, R., Jensen, M. R., Pryer, N. K., Williams, J. A. & Sellers, W. R. High-throughput screening using patient-derived tumor xenografts to predict clinical trial drug response. *Nature Medicine* **2015**, *21*, 1318-1325, doi:10.1038/nm.3954.

[41] Shi, Y., Gao, W., Lytle, N. K., Huang, P., Yuan, X., Dann, A. M., Ridinger-Saison, M., DelGiorno, K. E., Antal, C. E., Liang, G., Atkins, A. R., Erikson, G., Sun, H., Meisenhelder, J., Terenziani, E., Woo, G., Fang, L., Santisakultarm, T. P., Manor, U., Xu, R., Becerra, C. R., Borazanci, E., Von Hoff, D. D., Grandgenett, P. M., Hollingsworth, M. A., Leblanc, M., Umetsu, S. E., Collisson, E. A., Scadeng, M., Lowy, A. M., Donahue, T. R., Reya, T., Downes, M., Evans, R. M., Wahl, G. M., Pawson, T., Tian, R. & Hunter, T. Targeting LIF-mediated paracrine interaction for pancreatic cancer therapy and monitoring. *Nature* **2019**, *569*, 131-135, doi:10.1038/s41586-019-1130-6.

[42] Martinez-Garcia, R., Juan, D., Rausell, A., Muñoz, M., Baños, N., Menéndez, C., Lopez-Casas, P. P., Rico, D., Valencia, A. & Hidalgo, M. Transcriptional dissection of pancreatic tumors engrafted in mice. *Genome Medicine* **2014**, *6*, 27, doi:10.1186/gm544.

[43] Sipos, B., Möser, S., Kalthoff, H., Török, V., Löhr, M. & Klöppel, G. A comprehensive characterization of pancreatic ductal carcinoma cell lines: towards the establishment of an in vitro research platform. *Virchows Archiv* **2003**, *442*, 444-452, doi:10.1007/s00428-003-0784-4.

[44] Deer, E. L., González-Hernández, J., Coursen, J. D., Shea, J. E., Ngatia, J., Scaife, C. L., Firpo, M. A. & Mulvihill, S. J. Phenotype and genotype of pancreatic cancer cell lines. *Pancreas* **2010**, *39*, 425.

[45] Gadaleta, E., Cutts, R. J., Kelly, G. P., Crnogorac-Jurcevic, T., Kocher, H. M., Lemoine, N. R. & Chelala, C. A global insight into a cancer transcriptional space using pancreatic data: importance, findings and flaws. *Nucleic Acids Research* **2011**, *39*, 7900-7907, doi:10.1093/nar/gkr533.

[46] Frappart, P.-O. & Hofmann, T. G. Pancreatic ductal adenocarcinoma (Pdac) organoids: The shining light at the end of the tunnel for drug response prediction and personalized medicine. *Cancers* **2020**, *12*, 2750.

[47] Hofer, M. & Lutolf, M. P. Engineering organoids. *Nature Reviews Materials* **2021**, 1-19, doi:10.1038/s41578-021-00279-y.

[48] Moreira, L., Bakir, B., Chatterji, P., Dantes, Z., Reichert, M. & Rustgi, A. K. Pancreas 3D Organoids: Current and Future Aspects as a Research Platform for Personalized Medicine in Pancreatic Cancer. *Cellular and Molecular Gastroenterology and Hepatology* **2018**, *5*, 289-298, doi:10.1016/j.jcmgh.2017.12.004.

[49] Huch, M., Gehart, H., Van Boxtel, R., Hamer, K., Blokzijl, F., Verstegen, M. M., Ellis, E., Van Wenum, M., Fuchs, S. A. & de Ligt, J. Long-term culture of genome-stable bipotent stem cells from adult human liver. *Cell* **2015**, *160*, 299-312.

[50] Blokzijl, F., de Ligt, J., Jager, M., Sasselli, V., Roerink, S., Sasaki, N., Huch, M., Boymans, S., Kuijk, E., Prins, P., Nijman, I. J., Martincorena, I., Mokry, M., Wiegerinck, C. L., Middendorp, S., Sato, T., Schwank, G., Nieuwenhuis, E. E. S., Verstegen, M. M. A., van der Laan, L. J. W., de Jonge, J., Ijzermans, J. N. M., Vries, R. G., van de Wetering, M., Stratton, M. R., Clevers, H., Cuppen, E. & van Boxtel, R. Tissue-specific mutation

accumulation in human adult stem cells during life. *Nature* **2016**, *538*, 260-264, doi:10.1038/nature19768.
[51] Sato, T., Vries, R. G., Snippert, H. J., van de Wetering, M., Barker, N., Stange, D. E., van Es, J. H., Abo, A., Kujala, P., Peters, P. J. & Clevers, H. Single Lgr5 stem cells build crypt-villus structures in vitro without a mesenchymal niche. *Nature* **2009**, *459*, 262-265, doi:10.1038/nature07935.
[52] Barker, N., Huch, M., Kujala, P., van de Wetering, M., Snippert, H. J., van Es, J. H., Sato, T., Stange, D. E., Begthel, H. & van den Born, M. Lgr5+ ve stem cells drive self-renewal in the stomach and build long-lived gastric units in vitro. *Cell Stem Cell* **2010**, *6*, 25-36.
[53] Sato, T., Stange, D. E., Ferrante, M., Vries, R. G., Van Es, J. H., Van Den Brink, S., Van Houdt, W. J., Pronk, A., Van Gorp, J. & Siersema, P. D. Long-term expansion of epithelial organoids from human colon, adenoma, adenocarcinoma, and Barrett's epithelium. *Gastroenterology* **2011**, *141*, 1762-1772.
[54] Sato, T. & Clevers, H. Growing self-organizing mini-guts from a single intestinal stem cell: mechanism and applications. *Science* **2013**, *340*, 1190-1194.
[55] Huch, M., Bonfanti, P., Boj, S. F., Sato, T., Loomans, C. J., van de Wetering, M., Sojoodi, M., Li, V. S., Schuijers, J., Gracanin, A., Ringnalda, F., Begthel, H., Hamer, K., Mulder, J., van Es, J. H., de Koning, E., Vries, R. G., Heimberg, H. & Clevers, H. Unlimited in vitro expansion of adult bi-potent pancreas progenitors through the Lgr5/R-spondin axis. *Embo Journal* **2013**, *32*, 2708-2721, doi:10.1038/emboj.2013.204.
[56] Bhushan, A., Itoh, N., Kato, S., Thiery, J. P., Czernichow, P., Bellusci, S. & Scharfmann, R. Fgf10 is essential for maintaining the proliferative capacity of epithelial progenitor cells during early pancreatic organogenesis. *Development* **2001**, *128*, 5109-5117.
[57] Cras-Méneur, C., Elghazi, L., Czernichow, P. & Scharfmann, R. Epidermal growth factor increases undifferentiated pancreatic embryonic cells in vitro: a balance between proliferation and differentiation. *Diabetes* **2001**, *50*, 1571-1579, doi:10.2337/diabetes.50.7.1571.
[58] Broutier, L., Andersson-Rolf, A., Hindley, C. J., Boj, S. F., Clevers, H., Koo, B. K. & Huch, M. Culture and establishment of self-renewing human and mouse adult liver and pancreas 3D organoids and their genetic manipulation. *Nature Protocols* **2016**, *11*, 1724-1743, doi:10.1038/nprot.2016.097.
[59] Loomans, C. J. M., Williams Giuliani, N., Balak, J., Ringnalda, F., van Gurp, L., Huch, M., Boj, S. F., Sato, T., Kester, L., de Sousa Lopes, S. M. C., Roost, M. S., Bonner-Weir, S., Engelse, M. A., Rabelink, T. J., Heimberg, H., Vries, R. G. J., van Oudenaarden, A., Carlotti, F., Clevers, H. & de Koning, E. J. P. Expansion of Adult Human Pancreatic Tissue Yields Organoids Harboring Progenitor Cells with Endocrine Differentiation Potential. *Stem Cell Reports* **2018**, *10*, 712-724, doi:10.1016/j.stemcr.2018.02.005.
[60] Georgakopoulos, N., Prior, N., Angres, B., Mastrogiovanni, G., Cagan, A., Harrison, D., Hindley, C. J., Arnes-Benito, R., Liau, S. S., Curd, A., Ivory, N., Simons, B. D., Martincorena, I., Wurst, H., Saeb-Parsy, K. & Huch, M. Long-term expansion, genomic stability and in vivo safety of adult human pancreas organoids. *BMC Developmental Biology* **2020**, *20*, 4, doi:10.1186/s12861-020-0209-5.
[61] Krieger, T. G., Le Blanc, S., Jabs, J., Ten, F. W., Ishaque, N., Jechow, K., Debnath, O., Leonhardt, C.-S., Giri, A. & Eils, R. Single-cell analysis of patient-derived PDAC organoids reveals cell state heterogeneity and a conserved developmental hierarchy. *Nature Communications* **2021**, *12*, 1-13.
[62] Driehuis, E., van Hoeck, A., Moore, K., Kolders, S., Francies, H. E., Gulersonmez, M. C., Stigter, E. C. A., Burgering, B., Geurts, V., Gracanin, A., Bounova, G., Morsink, F. H., Vries, R., Boj, S., van Es, J., Offerhaus, G. J. A., Kranenburg, O., Garnett, M. J., Wessels, L., Cuppen, E., Brosens, L. A. A. & Clevers, H. Pancreatic cancer organoids recapitulate disease and allow personalized drug screening. *Proceedings of the National Academy of Sciences* **2019**, *116*, 26580-26590, doi:10.1073/pnas.1911273116.

[63] Tiriac, H., Belleau, P., Engle, D. D., Plenker, D., Deschênes, A., Somerville, T. D., Froeling, F. E., Burkhart, R. A., Denroche, R. E. & Jang, G.-H. Organoid profiling identifies common responders to chemotherapy in pancreatic cancer. *Cancer Discovery* **2018**, *8*, 1112-1129, doi:10.1158/2159-8290.CD-18-0349.

[64] Tian, C., Huang, Y., Clauser, K. R., Rickelt, S., Lau, A. N., Carr, S. A., Vander Heiden, M. G. & Hynes, R. O. Suppression of pancreatic ductal adenocarcinoma growth and metastasis by fibrillar collagens produced selectively by tumor cells. *Nature Communications* **2021**, *12*, 1-16.

[65] Seino, T., Kawasaki, S., Shimokawa, M., Tamagawa, H., Toshimitsu, K., Fujii, M., Ohta, Y., Matano, M., Nanki, K. & Kawasaki, K. Human pancreatic tumor organoids reveal loss of stem cell niche factor dependence during disease progression. *Cell Stem Cell* **2018**, *22*, 454-467. e456.

[66] Pinho, A. V., Rooman, I., Reichert, M., De Medts, N., Bouwens, L., Rustgi, A. K. & Real, F. X. Adult pancreatic acinar cells dedifferentiate to an embryonic progenitor phenotype with concomitant activation of a senescence programme that is present in chronic pancreatitis. *Gut* **2011**, *60*, 958-966, doi:10.1136/gut.2010.225920.

[67] Murtaugh, L. C. & Keefe, M. D. Regeneration and repair of the exocrine pancreas. *Annual Review of Physiology* **2015**, *77*, 229-249.

[68] Houbracken, I., de Waele, E., Lardon, J., Ling, Z., Heimberg, H., Rooman, I. & Bouwens, L. Lineage tracing evidence for transdifferentiation of acinar to duct cells and plasticity of human pancreas. *Gastroenterology* **2011**, *141*, 731-741, 741.e731-734, doi:10.1053/j.gastro.2011.04.050.

[69] Liou, G. Y., Döppler, H., Necela, B., Krishna, M., Crawford, H. C., Raimondo, M. & Storz, P. Macrophage-secreted cytokines drive pancreatic acinar-to-ductal metaplasia through NF-κB and MMPs. *Journal of Cell Biology* **2013**, *202*, 563-577, doi:10.1083/jcb.201301001.

[70] Shi, G., DiRenzo, D., Qu, C., Barney, D., Miley, D. & Konieczny, S. F. Maintenance of acinar cell organization is critical to preventing Kras-induced acinar-ductal metaplasia. *Oncogene* **2013**, *32*, 1950-1958.

[71] Wollny, D., Zhao, S., Everlien, I., Lun, X., Brunken, J., Brüne, D., Ziebell, F., Tabansky, I., Weichert, W., Marciniak-Czochra, A. & Martin-Villalba, A. Single-Cell Analysis Uncovers Clonal Acinar Cell Heterogeneity in the Adult Pancreas. *Developmental Cell* **2016**, *39*, 289-301, doi:10.1016/j.devcel.2016.10.002.

[72] Baldan, J., Houbracken, I., Rooman, I. & Bouwens, L. Adult human pancreatic acinar cells dedifferentiate into an embryonic progenitor-like state in 3D suspension culture. *Scientific Reports* **2019**, *9*, 4040, doi:10.1038/s41598-019-40481-1.

[73] De Waele, E., Wauters, E., Ling, Z. & Bouwens, L. Conversion of human pancreatic acinar cells toward a ductal-mesenchymal phenotype and the role of transforming growth factor β and activin signaling. *Pancreas* **2014**, *43*, 1083-1092, doi:10.1097/mpa.0000000000000154.

[74] Houbracken, I., De Waele, E., Lardon, J., Ling, Z., Heimberg, H., Rooman, I. & Bouwens, L. Lineage tracing evidence for transdifferentiation of acinar to duct cells and plasticity of human pancreas. *Gastroenterology* **2011**, *141*, 731-741. e734.

[75] Pinho, A. V., Rooman, I., Reichert, M., De Medts, N., Bouwens, L., Rustgi, A. K. & Real, F. X. Adult pancreatic acinar cells dedifferentiate to an embryonic progenitor phenotype with concomitant activation of a senescence programme that is present in chronic pancreatitis. *Gut* **2011**, *60*, 958-966.

[76] Rooman, I., Heremans, Y., Heimberg, H. & Bouwens, L. Modulation of rat pancreatic acinoductal transdifferentiation and expression of PDX-1 in vitro. *Diabetologia* **2000**, *43*, 907-914.

[77] Jennings, R. E., Berry, A. A., Strutt, J. P., Gerrard, D. T. & Hanley, N. A. Human pancreas development. *Development* **2015**, *142*, 3126-3137, doi:10.1242/dev.120063.

[78] Gaertner, B., Carrano, A. C. & Sander, M. Human stem cell models: lessons for pancreatic development and disease. *Genes & Development* **2019**, *33*, 1475-1490, doi:10.1101/gad.331397.119.
[79] Rezakhani, S., Gjorevski, N. & Lutolf, M. P. Extracellular matrix requirements for gastrointestinal organoid cultures. *Biomaterials* **2021**, *276*, 121020, doi:10.1016/j.biomaterials.2021.121020.
[80] Aisenbrey, E. A. & Murphy, W. L. Synthetic alternatives to Matrigel. *Nature Reviews Materials* **2020**, *5*, 539-551, doi:10.1038/s41578-020-0199-8.
[81] Below, C. R., Kelly, J., Brown, A., Humphries, J. D., Hutton, C., Xu, J., Lee, B. Y., Cintas, C., Zhang, X., Hernandez-Gordillo, V., Stockdale, L., Goldsworthy, M. A., Geraghty, J., Foster, L., O'Reilly, D. A., Schedding, B., Askari, J., Burns, J., Hodson, N., Smith, D. L., Lally, C., Ashton, G., Knight, D., Mironov, A., Banyard, A., Eble, J. A., Morton, J. P., Humphries, M. J., Griffith, L. G. & Jorgensen, C. A microenvironment-inspired synthetic three-dimensional model for pancreatic ductal adenocarcinoma organoids. *Nature Materials* **2021**, doi:10.1038/s41563-021-01085-1.
[82] Gjorevski, N., Sachs, N., Manfrin, A., Giger, S., Bragina, M. E., Ordonez-Moran, P., Clevers, H. & Lutolf, M. P. Designer matrices for intestinal stem cell and organoid culture. *Nature* **2016**, *539*, 560-564, doi:10.1038/nature20168.
[83] Cruz-Acuña, R., Quirós, M., Farkas, A. E., Dedhia, P. H., Huang, S., Siuda, D., García-Hernández, V., Miller, A. J., Spence, J. R. & Nusrat, A. Synthetic hydrogels for human intestinal organoid generation and colonic wound repair. *Nature Cell Biology* **2017**, *19*, 1326-1335.
[84] Hernandez-Gordillo, V., Kassis, T., Lampejo, A., Choi, G., Gamboa, M. E., Gnecco, J. S., Brown, A., Breault, D. T., Carrier, R. & Griffith, L. G. Fully synthetic matrices for in vitro culture of primary human intestinal enteroids and endometrial organoids. *Biomaterials* **2020**, *254*, 120125.
[85] Tian, C., Clauser, K. R., Öhlund, D., Rickelt, S., Huang, Y., Gupta, M., Mani, D. R., Carr, S. A., Tuveson, D. A. & Hynes, R. O. Proteomic analyses of ECM during pancreatic ductal adenocarcinoma progression reveal different contributions by tumor and stromal cells. *Proceedings of the National Academy of Sciences* **2019**, *116*, 19609-19618, doi:10.1073/pnas.1908626116.
[86] Naba, A., Clauser, K. R., Hoersch, S., Liu, H., Carr, S. A. & Hynes, R. O. The matrisome: in silico definition and in vivo characterization by proteomics of normal and tumor extracellular matrices. *Molecular & Cellular Proteomics* **2012**, *11*, M111.014647, doi:10.1074/mcp.M111.014647.
[87] Martins Cavaco, A. C., Rezaei, M., Caliandro, M. F., Martins Lima, A., Stehling, M., Dhayat, S. A., Haier, J., Brakebusch, C. & Eble, J. A. The Interaction between Laminin-332 and α3β1 Integrin Determines Differentiation and Maintenance of CAFs, and Supports Invasion of Pancreatic Duct Adenocarcinoma Cells. *Cancers* **2019**, *11*, 14.
[88] Burris3rd, H. A., Moore, M. J., Andersen, J., Green, M. R., Rothenberg, M. L., Modiano, M. R., Cripps, M. C., Portenoy, R. K., Storniolo, A. M., Tarassoff, P., Nelson, R., Dorr, F. A., Stephens, C. D. & Hoff, D. D. V. Improvements in survival and clinical benefit with gemcitabine as first-line therapy for patients with advanced pancreas cancer: a randomized trial. *Journal of Clinical Oncology* **1997**, *15*, 2403-2413, doi:10.1200/jco.1997.15.6.2403.
[89] Quinonero, F., Mesas, C., Doello, K., Cabeza, L., Perazzoli, G., Jimenez-Luna, C., Rama, A. R., Melguizo, C. & Prados, J. The challenge of drug resistance in pancreatic ductal adenocarcinoma: a current overview. *Cancer Biology & Medicine* **2019**, *16*, 688-699, doi:10.20892/j.issn.2095-3941.2019.0252.
[90] Lamichhane, S. P., Arya, N., Kohler, E., Xiang, S., Christensen, J. & Shastri, V. P. Recapitulating epithelial tumor microenvironment in vitro using three dimensional tri-

culture of human epithelial, endothelial, and mesenchymal cells. *BMC Cancer* **2016**, *16*, 581, doi:10.1186/s12885-016-2634-1.

[91] Amann, A., Zwierzina, M., Koeck, S., Gamerith, G., Pechriggl, E., Huber, J. M., Lorenz, E., Kelm, J. M., Hilbe, W., Zwierzina, H. & Kern, J. Development of a 3D angiogenesis model to study tumour - endothelial cell interactions and the effects of anti-angiogenic drugs. *Scientific Reports* **2017**, *7*, 2963, doi:10.1038/s41598-017-03010-6.

[92] Weigelt, B., Ghajar, C. M. & Bissell, M. J. The need for complex 3D culture models to unravel novel pathways and identify accurate biomarkers in breast cancer. *Advanced Drug Delivery Reviews* **2014**, *69-70*, 42-51, doi:10.1016/j.addr.2014.01.001.

[93] Lai, B. F. L., Huyer, L. D., Lu, R. X. Z., Drecun, S., Radisic, M. & Zhang, B. InVADE: Integrated Vasculature for Assessing Dynamic Events. *Advanced Functional Materials* **2017**, *27*, 1703524, doi:10.1002/adfm.201703524.

[94] Lai, B. F. L., Lu Rick, X., Hu, Y., Davenport, H. L., Dou, W., Wang, E. Y., Radulovich, N., Tsao, M. S., Sun, Y. & Radisic, M. Recapitulating pancreatic tumor microenvironment through synergistic use of patient organoids and organ-on-a-chip vasculature. *Advanced Functional Materials* **2020**, *30*, doi:10.1002/adfm.202000545.

[95] Levental, K. R., Yu, H., Kass, L., Lakins, J. N., Egeblad, M., Erler, J. T., Fong, S. F., Csiszar, K., Giaccia, A., Weninger, W., Yamauchi, M., Gasser, D. L. & Weaver, V. M. Matrix crosslinking forces tumor progression by enhancing integrin signaling. *Cell* **2009**, *139*, 891-906, doi:10.1016/j.cell.2009.10.027.

[96] Craven, K. E., Gore, J. & Korc, M. Overview of pre-clinical and clinical studies targeting angiogenesis in pancreatic ductal adenocarcinoma. **2016**, *381*, 201-210.

[97] Du, J., Gu, J. & Li, J. Mechanisms of drug resistance of pancreatic ductal adenocarcinoma at different levels. *Bioscience Reports* **2020**, *40*, doi:10.1042/bsr20200401.

[98] Tuveson, D. A. & Neoptolemos, J. P. Understanding metastasis in pancreatic cancer: a call for new clinical approaches. *Cell* **2012**, *148*, 21-23, doi:10.1016/j.cell.2011.12.021.

[99] Rhim, A. D., Thege, F. I., Santana, S. M., Lannin, T. B., Saha, T. N., Tsai, S., Maggs, L. R., Kochman, M. L., Ginsberg, G. G., Lieb, J. G., Chandrasekhara, V., Drebin, J. A., Ahmad, N., Yang, Y. X., Kirby, B. J. & Stanger, B. Z. Detection of circulating pancreas epithelial cells in patients with pancreatic cystic lesions. *Gastroenterology* **2014**, *146*, 647-651, doi:10.1053/j.gastro.2013.12.007.

[100] Lee, H., Park, W., Ryu, H. & Jeon, N. L. A microfluidic platform for quantitative analysis of cancer angiogenesis and intravasation. *Biomicrofluidics* **2014**, *8*, 054102, doi:10.1063/1.4894595.

[101] Zervantonakis, I. K., Hughes-Alford, S. K., Charest, J. L., Condeelis, J. S., Gertler, F. B. & Kamm, R. D. Three-dimensional microfluidic model for tumor cell intravasation and endothelial barrier function. *Proceedings of the National Academy of Sciences* **2012**, *109*, 13515-13520, doi:10.1073/pnas.1210182109.

[102] Sobrino, A., Phan, D. T., Datta, R., Wang, X., Hachey, S. J., Romero-López, M., Gratton, E., Lee, A. P., George, S. C. & Hughes, C. C. 3D microtumors in vitro supported by perfused vascular networks. *Scientific Reports* **2016**, *6*, 31589, doi:10.1038/srep31589.

[103] Nguyen, D.-H. T., Lee, E., Alimperti, S., Norgard, R. J., Wong, A., Lee, J. J.-K., Eyckmans, J., Stanger, B. Z. & Chen, C. S. A biomimetic pancreatic cancer on-chip reveals endothelial ablation via ALK7 signaling. *Science Advances* **2019**, *5*, eaav6789.

[104] Hong, S. M., Goggins, M., Wolfgang, C. L., Schulick, R. D., Edil, B. H., Cameron, J. L., Handra-Luca, A., Herman, J. M. & Hruban, R. H. Vascular invasion in infiltrating ductal adenocarcinoma of the pancreas can mimic pancreatic intraepithelial neoplasia: a histopathologic study of 209 cases. *The American Journal of Surgical Pathology* **2012**, *36*, 235-241, doi:10.1097/PAS.0b013e3182376e36.

[105] Tuveson, D. & Clevers, H. Cancer modeling meets human organoid technology. *Science* **2019**, *364*, 952-955, doi:10.1126/science.aaw6985.

[106] Frappart, P. O., Walter, K., Gout, J., Beutel, A. K., Morawe, M., Arnold, F., Breunig, M., Barth, T. F., Marienfeld, R., Schulte, L., Ettrich, T., Hackert, T., Svinarenko, M., Rosler, R., Wiese, S., Wiese, H., Perkhofer, L., Muller, M., Lechel, A., Sainz, B., Jr., Hermann, P. C., Seufferlein, T. & Kleger, A. Pancreatic cancer-derived organoids - a disease modeling tool to predict drug response. *United European Gastroenterol Journal* **2020**, 2050640620905183, doi:10.1177/2050640620905183.

[107] Tiriac, H., Belleau, P., Engle, D. D., Plenker, D., Deschenes, A., Somerville, T. D. D., Froeling, F. E. M., Burkhart, R. A., Denroche, R. E., Jang, G. H., Miyabayashi, K., Young, C. M., Patel, H., Ma, M., LaComb, J. F., Palmaira, R. L. D., Javed, A. A., Huynh, J. C., Johnson, M., Arora, K., Robine, N., Shah, M., Sanghvi, R., Goetz, A. B., Lowder, C. Y., Martello, L., Driehuis, E., LeComte, N., Askan, G., Iacobuzio-Donahue, C. A., Clevers, H., Wood, L. D., Hruban, R. H., Thompson, E., Aguirre, A. J., Wolpin, B. M., Sasson, A., Kim, J., Wu, M., Bucobo, J. C., Allen, P., Sejpal, D. V., Nealon, W., Sullivan, J. D., Winter, J. M., Gimotty, P. A., Grem, J. L., DiMaio, D. J., Buscaglia, J. M., Grandgenett, P. M., Brody, J. R., Hollingsworth, M. A., O'Kane, G. M., Notta, F., Kim, E., Crawford, J. M., Devoe, C., Ocean, A., Wolfgang, C. L., Yu, K. H., Li, E., Vakoc, C. R., Hubert, B., Fischer, S. E., Wilson, J. M., Moffitt, R., Knox, J., Krasnitz, A., Gallinger, S. & Tuveson, D. A. Organoid Profiling Identifies Common Responders to Chemotherapy in Pancreatic Cancer. *Cancer Discovery* **2018**, *8*, 1112-1129, doi:10.1158/2159-8290.CD-18-0349.

[108] Boj, S. F., Hwang, C. I., Baker, L. A., Engle, D. D., Tuveson, D. A. & Clevers, H. Model organoids provide new research opportunities for ductal pancreatic cancer. *Molcular & Cellular Oncolology* **2016**, *3*, e1014757, doi:10.1080/23723556.2015.1014757.

[109] Hohwieler, M., Illing, A., Hermann, P. C., Mayer, T., Stockmann, M., Perkhofer, L., Eiseler, T., Antony, J. S., Müller, M., Renz, S., Kuo, C. C., Lin, Q., Sendler, M., Breunig, M., Kleiderman, S. M., Lechel, A., Zenker, M., Leichsenring, M., Rosendahl, J., Zenke, M., Sainz, B., Jr., Mayerle, J., Costa, I. G., Seufferlein, T., Kormann, M., Wagner, M., Liebau, S. & Kleger, A. Human pluripotent stem cell-derived acinar/ductal organoids generate human pancreas upon orthotopic transplantation and allow disease modelling. *Gut* **2017**, *66*, 473-486, doi:10.1136/gutjnl-2016-312423.

[110] Huang, L., Holtzinger, A., Jagan, I., BeGora, M., Lohse, I., Ngai, N., Nostro, C., Wang, R., Muthuswamy, L. B., Crawford, H. C., Arrowsmith, C., Kalloger, S. E., Renouf, D. J., Connor, A. A., Cleary, S., Schaeffer, D. F., Roehrl, M., Tsao, M. S., Gallinger, S., Keller, G. & Muthuswamy, S. K. Ductal pancreatic cancer modeling and drug screening using human pluripotent stem cell- and patient-derived tumor organoids. *Nature Medicine* **2015**, doi:10.1038/nm.3973.

[111] Liu, G., David, B. T., Trawczynski, M. & Fessler, R. G. Advances in Pluripotent Stem Cells: History, Mechanisms, Technologies, and Applications. *Stem Cell Reviews and Reports* **2020**, *16*, 3-32, doi:10.1007/s12015-019-09935-x.

[112] Takahashi, K. & Yamanaka, S. Induction of pluripotent stem cells from mouse embryonic and adult fibroblast cultures by defined factors. *Cell* **2006**, *126*, 663-676, doi:10.1016/j.cell.2006.07.024.

[113] Takahashi, K., Tanabe, K., Ohnuki, M., Narita, M., Ichisaka, T., Tomoda, K. & Yamanaka, S. Induction of pluripotent stem cells from adult human fibroblasts by defined factors. *Cell* **2007**, *131*, 861-872, doi:10.1016/j.cell.2007.11.019.

[114] Zhou, Q., Law, A. C., Rajagopal, J., Anderson, W. J., Gray, P. A. & Melton, D. A. A multipotent progenitor domain guides pancreatic organogenesis. *Developmental Cell* **2007**, *13*, 103-114, doi:10.1016/j.devcel.2007.06.001.

[115] McCracken, K. W., Catá, E. M., Crawford, C. M., Sinagoga, K. L., Schumacher, M., Rockich, B. E., Tsai, Y. H., Mayhew, C. N., Spence, J. R., Zavros, Y. & Wells, J. M. Modelling human development and disease in pluripotent stem-cell-derived gastric organoids. *Nature* **2014**, *516*, 400-404, doi:10.1038/nature13863.

[116] Spence, J. R., Mayhew, C. N., Rankin, S. A., Kuhar, M. F., Vallance, J. E., Tolle, K., Hoskins, E. E., Kalinichenko, V. V., Wells, S. I., Zorn, A. M., Shroyer, N. F. & Wells, J. M. Directed differentiation of human pluripotent stem cells into intestinal tissue in vitro. *Nature* **2011**, *470*, 105-109, doi:10.1038/nature09691.

[117] D'Amour, K. A., Bang, A. G., Eliazer, S., Kelly, O. G., Agulnick, A. D., Smart, N. G., Moorman, M. A., Kroon, E., Carpenter, M. K. & Baetge, E. E. Production of pancreatic hormone–expressing endocrine cells from human embryonic stem cells. *Nature Biotechnology* **2006**, *24*, 1392-1401.

[118] Nostro, M. C., Sarangi, F., Ogawa, S., Holtzinger, A., Corneo, B., Li, X., Micallef, S. J., Park, I.-H., Basford, C. & Wheeler, M. B. Stage-specific signaling through TGFβ family members and WNT regulates patterning and pancreatic specification of human pluripotent stem cells. *Development* **2011**, *138*, 861-871.

[119] Loh, Kyle M., Ang, Lay T., Zhang, J., Kumar, V., Ang, J., Auyeong, Jun Q., Lee, Kian L., Choo, Siew H., Lim, Christina Y. Y., Nichane, M., Tan, J., Noghabi, Monireh S., Azzola, L., Ng, Elizabeth S., Durruthy-Durruthy, J., Sebastiano, V., Poellinger, L., Elefanty, Andrew G., Stanley, Edouard G., Chen, Q., Prabhakar, S., Weissman, Irving L. & Lim, B. Efficient Endoderm Induction from Human Pluripotent Stem Cells by Logically Directing Signals Controlling Lineage Bifurcations. *Cell Stem Cell* **2014**, *14*, 237-252, doi:10.1016/j.stem.2013.12.007.

[120] Teo, A. K., Ali, Y., Wong, K. Y., Chipperfield, H., Sadasivam, A., Poobalan, Y., Tan, E. K., Wang, S. T., Abraham, S. & Tsuneyoshi, N. Activin and BMP4 synergistically promote formation of definitive endoderm in human embryonic stem cells. *Stem Cells* **2012**, *30*, 631-642.

[121] Gouon-Evans, V., Boussemart, L., Gadue, P., Nierhoff, D., Koehler, C. I., Kubo, A., Shafritz, D. A. & Keller, G. BMP-4 is required for hepatic specification of mouse embryonic stem cell–derived definitive endoderm. *Nature biotechnology* **2006**, *24*, 1402-1411.

[122] Grapin-Botton, A. & Melton, D. A. Endoderm development: from patterning to organogenesis. *Trends in Genetics* **2000**, *16*, 124-130.

[123] Offield, M. F., Jetton, T. L., Labosky, P. A., Ray, M., Stein, R. W., Magnuson, M. A., Hogan, B. & Wright, C. PDX-1 is required for pancreatic outgrowth and differentiation of the rostral duodenum. *Development* **1996**, *122*, 983-995.

[124] Sander, M., Sussel, L., Conners, J., Scheel, D., Kalamaras, J., Dela Cruz, F., Schwitzgebel, V., Hayes-Jordan, A. & German, M. Homeobox gene Nkx6. 1 lies downstream of Nkx2. 2 in the major pathway of beta-cell formation in the pancreas. *Development* **2000**, *127*, 5533-5540.

[125] Mamidi, A., Prawiro, C., Seymour, P. A., de Lichtenberg, K. H., Jackson, A., Serup, P. & Semb, H. Mechanosignalling via integrins directs fate decisions of pancreatic progenitors. *Nature* **2018**, *564*, 114-118, doi:10.1038/s41586-018-0762-2.

[126] Rezania, A., Bruin, J. E., Arora, P., Rubin, A., Batushansky, I., Asadi, A., O'dwyer, S., Quiskamp, N., Mojibian, M. & Albrecht, T. Reversal of diabetes with insulin-producing cells derived in vitro from human pluripotent stem cells. *Nature Biotechnology* **2014**, *32*, 1121-1133.

[127] Veres, A., Faust, A. L., Bushnell, H. L., Engquist, E. N., Kenty, J. H.-R., Harb, G., Poh, Y.-C., Sintov, E., Gürtler, M. & Pagliuca, F. W. Charting cellular identity during human in vitro β-cell differentiation. *Nature* **2019**, *569*, 368-373.

[128] Bakhti, M., Scheibner, K., Tritschler, S., Bastidas-Ponce, A., Tarquis-Medina, M., Theis, F. J. & Lickert, H. Establishment of a high-resolution 3D modeling system for studying pancreatic epithelial cell biology in vitro. *Molecular Metabolism* **2019**, *30*, 16-29.

[129] Hogrebe, N. J., Augsornworawat, P., Maxwell, K. G., Velazco-Cruz, L. & Millman, J. R. Targeting the cytoskeleton to direct pancreatic differentiation of human pluripotent stem cells. *Nature Biotechnology* **2020**, *38*, 460-470.

[130] Saber, N., Bruin, J. E., O'Dwyer, S., Schuster, H., Rezania, A. & Kieffer, T. J. Sex differences in maturation of human embryonic stem cell–derived β cells in mice. *Endocrinology* **2018**, *159*, 1827-1841.
[131] Chen, S., Borowiak, M., Fox, J. L., Maehr, R., Osafune, K., Davidow, L., Lam, K., Peng, L. F., Schreiber, S. L. & Rubin, L. L. A small molecule that directs differentiation of human ESCs into the pancreatic lineage. *Nature chemical biology* **2009**, *5*, 258-265.
[132] Brennan, J., Lu, C. C., Norris, D. P., Rodriguez, T. A., Beddington, R. S. & Robertson, E. J. Nodal signalling in the epiblast patterns the early mouse embryo. *Nature* **2001**, *411*, 965-969.
[133] Engert, S., Burtscher, I., Liao, W. P., Dulev, S., Schotta, G. & Lickert, H. Wnt/β-catenin signalling regulates Sox17 expression and is essential for organizer and endoderm formation in the mouse. *Development* **2013**, *140*, 3128-3138.
[134] D'Amour, K. A., Agulnick, A. D., Eliazer, S., Kelly, O. G., Kroon, E. & Baetge, E. E. Efficient differentiation of human embryonic stem cells to definitive endoderm. *Nature Biotechnology* **2005**, *23*, 1534-1541.
[135] Chen, A. E., Borowiak, M., Sherwood, R. I., Kweudjeu, A. & Melton, D. A. Functional evaluation of ES cell-derived endodermal populations reveals differences between Nodal and Activin A-guided differentiation. *Development* **2013**, *140*, 675-686.
[136] Huang, L., Desai, R., Conrad, D. N., Leite, N. C., Akshinthala, D., Lim, C. M., Gonzalez, R., Muthuswamy, L. B., Gartner, Z. & Muthuswamy, S. K. Commitment and oncogene-induced plasticity of human stem cell-derived pancreatic acinar and ductal organoids. *Cell Stem Cell* **2021**, *28*, 1090-1104 e1096, doi:10.1016/j.stem.2021.03.022.
[137] Villani, V., Thornton, M. E., Zook, H. N., Crook, C. J., Grubbs, B. H., Orlando, G., De Filippo, R., Ku, H. T. & Perin, L. SOX9+/PTF1A+ Cells Define the Tip Progenitor Cells of the Human Fetal Pancreas of the Second Trimester. *Stem Cells Translational Medicine* **2019**, *8*, 1249-1264, doi:10.1002/sctm.19-0231.
[138] Schaffer, A. E., Freude, K. K., Nelson, S. B. & Sander, M. Nkx6 transcription factors and Ptf1a function as antagonistic lineage determinants in multipotent pancreatic progenitors. *Developmental Cell* **2010**, *18*, 1022-1029, doi:10.1016/j.devcel.2010.05.015.
[139] Jennings, R. E., Berry, A. A., Kirkwood-Wilson, R., Roberts, N. A., Hearn, T., Salisbury, R. J., Blaylock, J., Piper Hanley, K. & Hanley, N. A. Development of the human pancreas from foregut to endocrine commitment. *Diabetes* **2013**, *62*, 3514-3522, doi:10.2337/db12-1479.
[140] Pagliuca, F. W., Millman, J. R., Gürtler, M., Segel, M., Van Dervort, A., Ryu, J. H., Peterson, Q. P., Greiner, D. & Melton, D. A. Generation of functional human pancreatic β cells in vitro. *Cell* **2014**, *159*, 428-439.
[141] Waters, A. M. & Der, C. J. KRAS: the critical driver and therapeutic target for pancreatic cancer. *Cold Spring Harbor Perspectives in Medicine* **2018**, *8*, a031435.
[142] Kanda, M., Matthaei, H., Wu, J., Hong, S. M., Yu, J., Borges, M., Hruban, R. H., Maitra, A., Kinzler, K. & Vogelstein, B. Presence of somatic mutations in most early-stage pancreatic intraepithelial neoplasia. *Gastroenterology* **2012**, *142*, 730-733. e739.
[143] Springer, S., Wang, Y., Dal Molin, M., Masica, D. L., Jiao, Y., Kinde, I., Blackford, A., Raman, S. P., Wolfgang, C. L. & Tomita, T. A combination of molecular markers and clinical features improve the classification of pancreatic cysts. *Gastroenterology* **2015**, *149*, 1501-1510.
[144] Wu, J., Matthaei, H., Maitra, A., Molin, M. D., Wood, L. D., Eshleman, J. R., Goggins, M., Canto, M. I., Schulick, R. D., Edil, B. H., Wolfgang, C. L., Klein, A. P., Diaz, L. A., Allen, P. J., Schmidt, C. M., Kinzler, K. W., Papadopoulos, N., Hruban, R. H. & Vogelstein, B. Recurrent GNAS Mutations Define an Unexpected Pathway for Pancreatic Cyst Development. *Science Translational Medicine* **2011**, *3*, 92ra66-92ra66, doi:10.1126/scitranslmed.3002543.

[145] Nostro, M. C., Sarangi, F., Yang, C., Holland, A., Elefanty, A. G., Stanley, E. G., Greiner, D. L. & Keller, G. Efficient generation of NKX6-1+ pancreatic progenitors from multiple human pluripotent stem cell lines. *Stem Cell Reports* **2015**, *4*, 591-604, doi:10.1016/j.stemcr.2015.02.017.
[146] Hohwieler, M., Perkhofer, L., Liebau, S., Seufferlein, T., Muller, M., Illing, A. & Kleger, A. Stem cell-derived organoids to model gastrointestinal facets of cystic fibrosis. *United European Gastroenterol Journal* **2017**, *5*, 609-624, doi:10.1177/2050640616670565.
[147] Patra, K. C., Kato, Y., Mizukami, Y., Widholz, S., Boukhali, M., Revenco, I., Grossman, E. A., Ji, F., Sadreyev, R. I. & Liss, A. S. Mutant GNAS drives pancreatic tumourigenesis by inducing PKA-mediated SIK suppression and reprogramming lipid metabolism. *Nature Cell Biology* **2018**, *20*, 811-822.
[148] Ideno, N., Yamaguchi, H., Ghosh, B., Gupta, S., Okumura, T., Steffen, D. J., Fisher, C. G., Wood, L. D., Singhi, A. D. & Nakamura, M. GNASR201C induces pancreatic cystic neoplasms in mice that express activated KRAS by inhibiting YAP1 signaling. *Gastroenterology* **2018**, *155*, 1593-1607. e1512.
[149] Low, L. A., Mummery, C., Berridge, B. R., Austin, C. P. & Tagle, D. A. Organs-on-chips: into the next decade. *Nature Reviews Drug Discovery* **2021**, *20*, 345-361, doi:10.1038/s41573-020-0079-3.
[150] Thomsen, A. R., Aldrian, C., Bronsert, P., Thomann, Y., Nanko, N., Melin, N., Rücker, G., Follo, M., Grosu, A. L., Niedermann, G., Layer, P. G., Heselich, A. & Lund, P. G. A deep conical agarose microwell array for adhesion independent three-dimensional cell culture and dynamic volume measurement. *Lab on a Chip* **2018**, *18*, 179-189, doi:10.1039/C7LC00832E.
[151] Miyamoto, Y., Ikeuchi, M., Noguchi, H., Yagi, T. & Hayashi, S. Spheroid Formation and Evaluation of Hepatic Cells in a Three-Dimensional Culture Device. *Cell Medicine* **2015**, *8*, 47-56, doi:10.3727/215517915x689056.
[152] Dahlmann, J., Kensah, G., Kempf, H., Skvorc, D., Gawol, A., Elliott, D. A., Dräger, G., Zweigerdt, R., Martin, U. & Gruh, I. The use of agarose microwells for scalable embryoid body formation and cardiac differentiation of human and murine pluripotent stem cells. *Biomaterials* **2013**, *34*, 2463-2471, doi:10.1016/j.biomaterials.2012.12.024.
[153] Hwang, Y. S., Chung, B. G., Ortmann, D., Hattori, N., Moeller, H. C. & Khademhosseini, A. Microwell-mediated control of embryoid body size regulates embryonic stem cell fate via differential expression of WNT5a and WNT11. *Proceedings of the National Academy of Sciences* **2009**, *106*, 16978-16983, doi:10.1073/pnas.0905550106 PMID - 19805103.
[154] Manzoor, A. A., Romita, L. & Hwang, D. K. A review on microwell and microfluidic geometric array fabrication techniques and its potential applications in cellular studies. *The Canadian Journal of Chemical Engineering* **2020**, *99*, 61-96, doi:10.1002/cjce.23875.
[155] Mosaad, E. O., Chambers, K. F., Futrega, K., Clements, J. A. & Doran, M. R. The Microwell-mesh: A high-throughput 3D prostate cancer spheroid and drug-testing platform. *Scientific Reports* **2018**, *8*, 253, doi:10.1038/s41598-017-18050-1.
[156] Pettinato, G., Wen, X. & Zhang, N. Formation of Well-defined Embryoid Bodies from Dissociated Human Induced Pluripotent Stem Cells using Microfabricated Cell-repellent Microwell Arrays. *Scientific Reports* **2014**, *4*, 7402, doi:10.1038/srep07402.
[157] Wolf, M. P., Salieb-Beugelaar, G. B. & Hunziker, P. PDMS with designer functionalities—Properties, modifications strategies, and applications. *Progress in Polymer Science* **2018**, *83*, 97-134, doi:10.1016/j.progpolymsci.2018.06.001.
[158] Kamei, K.-i., Mashimo, Y., Koyama, Y., Fockenberg, C., Nakashima, M., Nakajima, M., Li, J. & Chen, Y. 3D printing of soft lithography mold for rapid production of polydimethylsiloxane-based microfluidic devices for cell stimulation with concentration gradients. *Biomedical Microdevices* **2015**, *17*, 36, doi:10.1007/s10544-015-9928-y.

[159] Kuo, A. P., Bhattacharjee, N., Lee, Y. S., Castro, K., Kim, Y. T. & Folch, A. High-Precision Stereolithography of Biomicrofluidic Devices. *Advanced Material Technologies* **2019**, *4*, doi:10.1002/admt.201800395.
[160] Kamei, K., Mashimo, Y., Koyama, Y., Fockenberg, C., Nakashima, M., Nakajima, M., Li, J. & Chen, Y. 3D printing of soft lithography mold for rapid production of polydimethylsiloxane-based microfluidic devices for cell stimulation with concentration gradients. *Biomed Microdevices* **2015**, *17*, 36, doi:10.1007/s10544-015-9928-y.
[161] Razavi Bazaz, S., Kashaninejad, N., Azadi, S., Patel, K., Asadnia, M., Jin, D. & Ebrahimi Warkiani, M. Rapid Softlithography Using 3D-Printed Molds. *Advanced Materials Technologies* **2019**, *4*, doi:10.1002/admt.201900425.
[162] Compera, N., Atwell, S., Wirth, J., Wolfrum, B. & Meier, M. Upscaling of pneumatic membrane valves for the integration of 3D cell cultures on chip. *Lab Chip* **2021**, *21*, 2986-2996, doi:10.1039/d1lc00194a.
[163] Ghatnekar, O., Andersson, R., Svensson, M., Persson, U., Ringdahl, U., Zeilon, P. & Borrebaeck, C. A. Modelling the benefits of early diagnosis of pancreatic cancer using a biomarker signature. *International Journal of Cancer* **2013**, *133*, 2392-2397, doi:10.1002/ijc.28256.
[164] Kamyabi, N., Bernard, V. & Maitra, A. Liquid biopsies in pancreatic cancer. *Expert Review of Anticancer Therapy* **2019**, *19*, 869-878, doi:10.1080/14737140.2019.1670063.
[165] Driehuis, E., van Hoeck, A., Moore, K., Kolders, S., Francies, H. E., Gulersonmez, M. C., Stigter, E. C. A., Burgering, B., Geurts, V., Gracanin, A., Bounova, G., Morsink, F. H., Vries, R., Boj, S., van Es, J., Offerhaus, G. J. A., Kranenburg, O., Garnett, M. J., Wessels, L., Cuppen, E., Brosens, L. A. A. & Clevers, H. Pancreatic cancer organoids recapitulate disease and allow personalized drug screening. *Proc Natl Acad Sci U S A* **2019**, doi:10.1073/pnas.1911273116.
[166] Co, J. Y., Margalef-Català, M., Monack, D. M. & Amieva, M. R. Controlling the polarity of human gastrointestinal organoids to investigate epithelial biology and infectious diseases. *Nature Protocols* **2021**, *16*, 5171-5192, doi:10.1038/s41596-021-00607-0.
[167] Saliba, A.-E., Westermann, A. J., Gorski, S. A. & Vogel, J. Single-cell RNA-seq: advances and future challenges. *Nucleic Acids Research* **2014**, *42*, 8845-8860.
[168] Islam, S., Zeisel, A., Joost, S., La Manno, G., Zajac, P., Kasper, M., Lönnerberg, P. & Linnarsson, S. Quantitative single-cell RNA-seq with unique molecular identifiers. *Nature methods* **2014**, *11*, 163-166.
[169] Luecken, M. D. & Theis, F. J. Current best practices in single-cell RNA-seq analysis: a tutorial. *Molecular Systems Biology* **2019**, *15*, e8746, doi:10.15252/msb.20188746.
[170] Seger, C. & Salzmann, L. After another decade: LC–MS/MS became routine in clinical diagnostics. *Clinical biochemistry* **2020**, *82*, 2-11.
[171] Hathout, Y. Approaches to the study of the cell secretome. *Expert Review of Proteomics* **2007**, *4*, 239-248, doi:10.1586/14789450.4.2.239.
[172] Siegel, R., Ma, J., Zou, Z. & Jemal, A. Cancer statistics, 2014. *CA: A Cancer Journal for Clinicans* **2014**, *64*, 9-29, doi:10.3322/caac.21208.
[173] Kamisawa, T., Wood, L. D., Itoi, T. & Takaori, K. Pancreatic cancer. *The Lancet* **2016**, *388*, 73-85, doi:10.1016/s0140-6736(16)00141-0.
[174] Gitlin, L., Schulze, P. & Belder, D. Rapid replication of master structures by double casting with PDMS. *Lab Chip* **2009**, *9*, 3000-3002, doi:10.1039/b904684d.
[175] Jesnowski, R., Fürst, D., Ringel, J., Chen, Y., Schrödel, A., Kleeff, J., Kolb, A., Schareck, W. D. & Löhr, M. Immortalization of pancreatic stellate cells as an in vitro model of pancreatic fibrosis: deactivation is induced by matrigel and N-acetylcysteine. *Lab Invest* **2005**, *85*, 1276-1291, doi:10.1038/labinvest.3700329.
[176] Mohammad Rezazadeh, F., Saedi, S., Rahmanifar, F., Namavar, M. R., Dianatpour, M., Tanideh, N., Akhlaghi, A., Niazi, A., Arabi Monfared, A., Tsutsui, K., Jafarzadeh Shirazi, M. R. & Tamadon, A. Fast free of acrylamide clearing tissue (FACT) for clearing,

immunolabelling and three-dimensional imaging of partridge tissues. *Microscopy Resesearch & Technique* **2018**, *81*, 1374-1382, doi:10.1002/jemt.23078.
[177] Arnold, F., Gout, J., Wiese, H., Weissinger, S., Roger, E., Perkhofer, L., Walter, K., Scheible, J., Prelli-Bozzo, C., Lechel, A., Ettrich, T. J., Azoitei, N., Hao, L., Fuerstberger, A., Kaminska, E. K., Sparrer, K. M. J., Rasche, V., Wiese, S., Kestler, H. A., Möller, P., Seufferlein, T., Frappart, P. O. & Kleger, A. RINT1 regulates SUMOylation and the DNA damage response to preserve cellular homeostasis in pancreatic cancer. *Cancer Research* **2021**, doi:10.1158/0008-5472.Can-20-2633.
[178] Schmid, S. J., Glatzel, M. C., Welke, C., Kornmann, M., Kleger, A., Barth, T. F., Fulda, S., Lennerz, J. K. & Möller, P. Absence of FLICE-inhibitory protein is a novel independent prognostic marker for very short survival in pancreatic ductal adenocarcinoma. *Pancreas* **2013**, *42*, 1114-1119, doi:10.1097/MPA.0b013e31829655ed.
[179] Feld, F. M., Nagel, P. D., Weissinger, S. E., Welke, C., Stenzinger, A., Möller, P. & Lennerz, J. K. GOT1/AST1 expression status as a prognostic biomarker in pancreatic ductal adenocarcinoma. *Oncotarget* **2015**, *6*, 4516-4526, doi:10.18632/oncotarget.2799.
[180] Hirsch, F. R., Varella-Garcia, M., Bunn, P. A., Jr., Di Maria, M. V., Veve, R., Bremmes, R. M., Barón, A. E., Zeng, C. & Franklin, W. A. Epidermal growth factor receptor in non-small-cell lung carcinomas: correlation between gene copy number and protein expression and impact on prognosis. *Journal of Clinical Oncology* **2003**, *21*, 3798-3807, doi:10.1200/jco.2003.11.069.
[181] John, T., Liu, G. & Tsao, M. S. Overview of molecular testing in non-small-cell lung cancer: mutational analysis, gene copy number, protein expression and other biomarkers of EGFR for the prediction of response to tyrosine kinase inhibitors. *Oncogene* **2009**, *28 Suppl 1*, S14-23, doi:10.1038/onc.2009.197.
[182] Schindelin, J., Arganda-Carreras, I., Frise, E., Kaynig, V., Longair, M., Pietzsch, T., Preibisch, S., Rueden, C., Saalfeld, S., Schmid, B., Tinevez, J. Y., White, D. J., Hartenstein, V., Eliceiri, K., Tomancak, P. & Cardona, A. Fiji: an open-source platform for biological-image analysis. *Nature Methods* **2012**, *9*, 676-682, doi:10.1038/nmeth.2019.
[183] Guillaumet-Adkins, A., Rodriguez-Esteban, G., Mereu, E., Mendez-Lago, M., Jaitin, D. A., Villanueva, A., Vidal, A., Martinez-Marti, A., Felip, E., Vivancos, A., Keren-Shaul, H., Heath, S., Gut, M., Amit, I., Gut, I. & Heyn, H. Single-cell transcriptome conservation in cryopreserved cells and tissues. *Genome Biology* **2017**, *18*, 45, doi:10.1186/s13059-017-1171-9.
[184] Wolf, F. A., Angerer, P. & Theis, F. J. SCANPY: large-scale single-cell gene expression data analysis. *Genome Biology* **2018**, *19*, 15, doi:10.1186/s13059-017-1382-0.
[185] Blondel, V. D., Guillaume, J.-L., Lambiotte, R. & Lefebvre, E. Fast unfolding of communities in large networks. *Journal of Statistical Mechanics: Theory and Experiment* **2008**, *2008*, P10008, doi:10.1088/1742-5468/2008/10/p10008.
[186] McInnes, L., Healy, J. & Melville, J. UMAP: Uniform Manifold Approximation and Projection for Dimension Reduction. *ArXiv e-prints 1802.03426* **2018**.
[187] Bergen, V., Lange, M., Peidli, S., Wolf, F. A. & Theis, F. J. Generalizing RNA velocity to transient cell states through dynamical modeling. *Nature Biotechnology* **2020**, doi:10.1038/s41587-020-0591-3.
[188] Bastidas-Ponce, A., Tritschler, S., Dony, L., Scheibner, K., Tarquis-Medina, M., Salinno, C., Schirge, S., Burtscher, I., Bottcher, A., Theis, F. J., Lickert, H. & Bakhti, M. Comprehensive single cell mRNA profiling reveals a detailed roadmap for pancreatic endocrinogenesis. *Development* **2019**, *146*, doi:10.1242/dev.173849.
[189] Livnat-Levanon, N., Kevei, E., Kleifeld, O., Krutauz, D., Segref, A., Rinaldi, T., Erpapazoglou, Z., Cohen, M., Reis, N., Hoppe, T. & Glickman, M. H. Reversible 26S proteasome disassembly upon mitochondrial stress. *Cell Reports* **2014**, *7*, 1371-1380, doi:10.1016/j.celrep.2014.04.030.

[190] Uhlén, M., Fagerberg, L., Hallström, B. M., Lindskog, C., Oksvold, P., Mardinoglu, A., Sivertsson, Å., Kampf, C., Sjöstedt, E., Asplund, A., Olsson, I., Edlund, K., Lundberg, E., Navani, S., Szigyarto, C. A.-K., Odeberg, J., Djureinovic, D., Takanen, J. O., Hober, S., Alm, T., Edqvist, P.-H., Berling, H., Tegel, H., Mulder, J., Rockberg, J., Nilsson, P., Schwenk, J. M., Hamsten, M., Feilitzen, K. v., Forsberg, M., Persson, L., Johansson, F., Zwahlen, M., Heijne, G. v., Nielsen, J. & Pontén, F. Tissue-based map of the human proteome. *Science* **2015**, *347*, 1260419, doi:10.1126/science.1260419 PMID - 25613900.

[191] Uhlén, M., Karlsson, M. J., Hober, A., Svensson, A.-S., Scheffel, J., Kotol, D., Zhong, W., Tebani, A., Strandberg, L., Edfors, F., Sjöstedt, E., Mulder, J., Mardinoglu, A., Berling, A., Ekblad, S., Dannemeyer, M., Kanje, S., Rockberg, J., Lundqvist, M., Malm, M., Volk, A.-L., Nilsson, P., Månberg, A., Dodig-Crnkovic, T., Pin, E., Zwahlen, M., Oksvold, P., Feilitzen, K. v., Häussler, R. S., Hong, M.-G., Lindskog, C., Ponten, F., Katona, B., Vuu, J., Lindström, E., Nielsen, J., Robinson, J., Ayoglu, B., Mahdessian, D., Sullivan, D., Thul, P., Danielsson, F., Stadler, C., Lundberg, E., Bergström, G., Gummesson, A., Voldborg, B. G., Tegel, H., Hober, S., Forsström, B., Schwenk, J. M., Fagerberg, L. & Sivertsson, Å. The human secretome. *Science Signaling* **2019**, *12*, eaaz0274, doi:10.1126/scisignal.aaz0274 PMID - 31772123.

[192] Raudvere, U., Kolberg, L., Kuzmin, I., Arak, T., Adler, P., Peterson, H. & Vilo, J. g:Profiler: a web server for functional enrichment analysis and conversions of gene lists (2019 update). *Nucleic Acids Research* **2019**, *47*, W191-w198, doi:10.1093/nar/gkz369.

[193] Chen, E. Y., Tan, C. M., Kou, Y., Duan, Q., Wang, Z., Meirelles, G. V., Clark, N. R. & Ma'ayan, A. Enrichr: interactive and collaborative HTML5 gene list enrichment analysis tool. *BMC Bioinformatics* **2013**, *14*, 128, doi:10.1186/1471-2105-14-128.

[194] Kuleshov, M. V., Jones, M. R., Rouillard, A. D., Fernandez, N. F., Duan, Q., Wang, Z., Koplev, S., Jenkins, S. L., Jagodnik, K. M., Lachmann, A., McDermott, M. G., Monteiro, C. D., Gundersen, G. W. & Ma'ayan, A. Enrichr: a comprehensive gene set enrichment analysis web server 2016 update. *Nucleic Acids Research* **2016**, *44*, W90-97, doi:10.1093/nar/gkw377.

[195] Chen, E. Y., Xu, H., Gordonov, S., Lim, M. P., Perkins, M. H. & Ma'ayan, A. Expression2Kinases: mRNA profiling linked to multiple upstream regulatory layers. *Bioinformatics* **2012**, *28*, 105-111, doi:10.1093/bioinformatics/btr625.

[196] Single-cell-resolved differentiation of human induced pluripotent stem cells into pancreatic duct-like organoids on a microwell chip (Zenodo, 2021).

[197] Jeong, G. S., Jun, Y., Song, J. H., Shin, S. H. & Lee, S.-H. Meniscus induced self organization of multiple deep concave wells in a microchannel for embryoid bodies generation. *Lab on a Chip* **2012**, *12*, 159-166, doi:10.1039/C1LC20619B.

[198] Yeon, S.-E., No, D. Y., Lee, S.-H., Nam, S. W., Oh, I.-H., Lee, J. & Kuh, H.-J. Application of Concave Microwells to Pancreatic Tumor Spheroids Enabling Anticancer Drug Evaluation in a Clinically Relevant Drug Resistance Model. *PLOS ONE* **2013**, *8*, e73345, doi:10.1371/journal.pone.0073345.

[199] Freyer, J. P. Role of necrosis in regulating the growth saturation of multicellular spheroids. *Cancer Research* **1988**, *48*, 2432-2439.

[200] Crisera, C. A., Kadison, A. S., Breslow, G. D., Maldonado, T. S., Longaker, M. T. & Gittes, G. K. Expression and role of laminin-1 in mouse pancreatic organogenesis. *Diabetes* **2000**, *49*, 936-944.

[201] Miner, J. H. & Yurchenco, P. D. Laminin functions in tissue morphogenesis. *Annu Rev Cell Dev Biol* **2004**, *20*, 255-284, doi:10.1146/annurev.cellbio.20.010403.094555.

[202] Jiang, F. X., Cram, D. S., DeAizpurua, H. J. & Harrison, L. C. Laminin-1 promotes differentiation of fetal mouse pancreatic beta-cells. *Diabetes* **1999**, *48*, 722-730, doi:10.2337/diabetes.48.4.722.

[203] Angyal, D., Bijvelds, M. J. C., Bruno, M. J., Peppelenbosch, M. P. & de Jonge, H. R. Bicarbonate Transport in Cystic Fibrosis and Pancreatitis. *Cells* **2021**, *11*, doi:10.3390/cells11010054.
[204] Pan, F. C. & Wright, C. Pancreas organogenesis: from bud to plexus to gland. *Developmental Dynamics* **2011**, *240*, 530-565, doi:10.1002/dvdy.22584.
[205] Nair, G. & Hebrok, M. Islet formation in mice and men: lessons for the generation of functional insulin-producing beta-cells from human pluripotent stem cells. *Current Opinion in Genetics & Development* **2015**, *32*, 171-180, doi:10.1016/j.gde.2015.03.004.
[206] Kopp, J. L., Dubois, C. L., Hao, E., Thorel, F., Herrera, P. L. & Sander, M. Progenitor cell domains in the developing and adult pancreas. *Cell Cycle* **2011**, *10*, 1921-1927, doi:10.4161/cc.10.12.16010.
[207] Kopp, J. L., Dubois, C. L., Schaffer, A. E., Hao, E., Shih, H. P., Seymour, P. A., Ma, J. & Sander, M. Sox9+ ductal cells are multipotent progenitors throughout development but do not produce new endocrine cells in the normal or injured adult pancreas. *Development* **2011**, *138*, 653-665, doi:10.1242/dev.056499.
[208] Inada, A., Nienaber, C., Fonseca, S. & Bonner-Weir, S. Timing and expression pattern of carbonic anhydrase II in pancreas. *Developmental Dynamics* **2006**, *235*, 1571-1577, doi:10.1002/dvdy.20754.
[209] La Manno, G., Soldatov, R., Zeisel, A., Braun, E., Hochgerner, H., Petukhov, V., Lidschreiber, K., Kastriti, M. E., Lönnerberg, P., Furlan, A., Fan, J., Borm, L. E., Liu, Z., van Bruggen, D., Guo, J., He, X., Barker, R., Sundström, E., Castelo-Branco, G., Cramer, P., Adameyko, I., Linnarsson, S. & Kharchenko, P. V. RNA velocity of single cells. *Nature* **2018**, *560*, 494-498, doi:10.1038/s41586-018-0414-6.
[210] George, N. M., Day, C. E., Boerner, B. P., Johnson, R. L. & Sarvetnick, N. E. Hippo signaling regulates pancreas development through inactivation of Yap. *Molecular and Cellular Biolology* **2012**, *32*, 5116-5128, doi:10.1128/mcb.01034-12.
[211] Qu, H., Liu, X., Ni, Y., Jiang, Y., Feng, X., Xiao, J., Guo, Y., Kong, D., Li, A., Li, X., Zhuang, X., Wang, Z., Wang, Y., Chang, Y., Chen, S., Kong, F., Zhang, X., Zhao, S., Sun, Y., Xu, D., Wang, D. & Zheng, C. Laminin 411 acts as a potent inducer of umbilical cord mesenchymal stem cell differentiation into insulin-producing cells. *Journal of Translational Medicine* **2014**, *12*, 135, doi:10.1186/1479-5876-12-135.
[212] Cirulli, V., Beattie, G. M., Klier, G., Ellisman, M., Ricordi, C., Quaranta, V., Frasier, F., Ishii, J. K., Hayek, A. & Salomon, D. R. Expression and function of alpha(v)beta(3) and alpha(v)beta(5) integrins in the developing pancreas: roles in the adhesion and migration of putative endocrine progenitor cells. *Journal of Cell Biology* **2000**, *150*, 1445-1460, doi:10.1083/jcb.150.6.1445.
[213] Gonçalves, C. A., Larsen, M., Jung, S., Stratmann, J., Nakamura, A., Leuschner, M., Hersemann, L., Keshara, R., Perlman, S., Lundvall, L., Thuesen, L. L., Hare, K. J., Amit, I., Jørgensen, A., Kim, Y. H., del Sol, A. & Grapin-Botton, A. A 3D system to model human pancreas development and its reference single-cell transcriptome atlas identify signaling pathways required for progenitor expansion. *Nature Communications* **2021**, *12*, 3144, doi:10.1038/s41467-021-23295-6.
[214] Erkan, M., Adler, G., Apte, M. V., Bachem, M. G., Buchholz, M., Detlefsen, S., Esposito, I., Friess, H., Gress, T. M., Habisch, H. J., Hwang, R. F., Jaster, R., Kleeff, J., Kloppel, G., Kordes, C., Logsdon, C. D., Masamune, A., Michalski, C. W., Oh, J., Phillips, P. A., Pinzani, M., Reiser-Erkan, C., Tsukamoto, H. & Wilson, J. StellaTUM: current consensus and discussion on pancreatic stellate cell research. *Gut* **2012**, *61*, 172-178, doi:10.1136/gutjnl-2011-301220.
[215] Clarke, D. J. B., Kuleshov, M. V., Schilder, B. M., Torre, D., Duffy, M. E., Keenan, A. B., Lachmann, A., Feldmann, A. S., Gundersen, G. W., Silverstein, M. C., Wang, Z. & Ma'ayan, A. eXpression2Kinases (X2K) Web: linking expression signatures to upstream

cell signaling networks. *Nucleic Acids Research* **2018**, *46*, W171-w179, doi:10.1093/nar/gky458.
[216] Uhlen, M., Zhang, C., Lee, S., Sjöstedt, E., Fagerberg, L., Bidkhori, G., Benfeitas, R., Arif, M., Liu, Z., Edfors, F., Sanli, K., Feilitzen, K. v., Oksvold, P., Lundberg, E., Hober, S., Nilsson, P., Mattsson, J., Schwenk, J. M., Brunnström, H., Glimelius, B., Sjöblom, T., Edqvist, P.-H., Djureinovic, D., Micke, P., Lindskog, C., Mardinoglu, A. & Ponten, F. A pathology atlas of the human cancer transcriptome. *Science* **2017**, *357*, eaan2507, doi:10.1126/science.aan2507 PMID - 28818916.
[217] Zhang, Z., Liu, X., Huang, R., Liu, X., Liang, Z. & Liu, T. Upregulation of nucleoprotein AHNAK is associated with poor outcome of pancreatic ductal adenocarcinoma prognosis via mediating epithelial-mesenchymal transition. *Journal of Cancer* **2019**, *10*, 3860-3870, doi:10.7150/jca.31291.
[218] Vishwanatha, J. K., Chiang, Y., Kumble, K. D., Hollingsworth, M. A. & Pour, P. M. Enhanced expression of annexin II in human pancreatic carcinoma cells and primary pancreatic cancers. *Carcinogenesis* **1993**, *14*, 2575-2579, doi:10.1093/carcin/14.12.2575.
[219] Baine, M. J., Menning, M., Smith, L. M., Mallya, K., Kaur, S., Rachagani, S., Chakraborty, S., Sasson, A. R., Brand, R. E. & Batra, S. K. Differential gene expression analysis of peripheral blood mononuclear cells reveals novel test for early detection of pancreatic cancer. *Cancer Biomark* **2011**, *11*, 1-14, doi:10.3233/CBM-2012-0260.
[220] Wang, L., Wu, H., Wang, L., Lu, J., Duan, H., Liu, X. & Liang, Z. Expression of amphiregulin predicts poor outcome in patients with pancreatic ductal adenocarcinoma. *Diagnostic Pathology* **2016**, *11*, 60-60, doi:10.1186/s13000-016-0512-4.
[221] Murphy, S. J., Hart, S. N., Lima, J. F., Kipp, B. R., Klebig, M., Winters, J. L., Szabo, C., Zhang, L., Eckloff, B. W., Petersen, G. M., Scherer, S. E., Gibbs, R. A., McWilliams, R. R., Vasmatzis, G. & Couch, F. J. Genetic alterations associated with progression from pancreatic intraepithelial neoplasia to invasive pancreatic tumor. *Gastroenterology* **2013**, *145*, 1098-1109.e1091, doi:10.1053/j.gastro.2013.07.049.
[222] Zhang, R., Liu, Q., Peng, J., Wang, M., Gao, X., Liao, Q. & Zhao, Y. Pancreatic cancer-educated macrophages protect cancer cells from complement-dependent cytotoxicity by up-regulation of CD59. *Cell Death & Disease* **2019**, *10*, 836-836, doi:10.1038/s41419-019-2065-4.
[223] Liang, T., Sang, S., Shao, Q., Chen, C., Deng, Z., Wang, T. & Kang, Q. Abnormal expression and prognostic significance of EPB41L1 in kidney renal clear cell carcinoma based on data mining. *Cancer Cell International* **2020**, *20*, 356-356, doi:10.1186/s12935-020-01449-8.
[224] Chang, Y. T., Peng, H. Y., Hu, C. M., Huang, S. C., Tien, S. C. & Jeng, Y. M. Pancreatic cancer-derived small extracellular vesical Ezrin regulates macrophage polarization and promotes metastasis. *American Journal of Cancer Research* **2020**, *10*, 12-37.
[225] Xu, X., Yu, Y., Zong, K., Lv, P. & Gu, Y. Up-regulation of IGF2BP2 by multiple mechanisms in pancreatic cancer promotes cancer proliferation by activating the PI3K/Akt signaling pathway. *Journal of Experimental & Clinical Cancer Research* **2019**, *38*, 497-497, doi:10.1186/s13046-019-1470-y.
[226] Yao, H., Yang, Z., Liu, Z., Miao, X., Yang, L., Li, D., Zou, Q. & Yuan, Y. Glypican-3 and KRT19 are markers associating with metastasis and poor prognosis of pancreatic ductal adenocarcinoma. *Cancer Biomark* **2016**, *17*, 397-404, doi:10.3233/cbm-160655.
[227] Guillaumond, F., Bidaut, G., Ouaissi, M., Servais, S., Gouirand, V., Olivares, O., Lac, S., Borge, L., Roques, J., Gayet, O., Pinault, M., Guimaraes, C., Nigri, J., Loncle, C., Lavaut, M. N., Garcia, S., Tailleux, A., Staels, B., Calvo, E., Tomasini, R., Iovanna, J. L. & Vasseur, S. Cholesterol uptake disruption, in association with chemotherapy, is a promising combined metabolic therapy for pancreatic adenocarcinoma. *Proceedings of*

the National Academy of Sciences **2015**, *112*, 2473-2478, doi:10.1073/pnas.1421601112.

[228] Sitek, B., Sipos, B., Alkatout, I., Poschmann, G., Stephan, C., Schulenborg, T., Marcus, K., Lüttges, J., Dittert, D. D., Baretton, G., Schmiegel, W., Hahn, S. A., Klöppel, G., Meyer, H. E. & Stühler, K. Analysis of the pancreatic tumor progression by a quantitative proteomic approach and immunhistochemical validation. *Journal of Proteome Research* **2009**, *8*, 1647-1656, doi:10.1021/pr800890j.

[229] Rozengurt, E., Sinnett-Smith, J. & Eibl, G. Yes-associated protein (YAP) in pancreatic cancer: at the epicenter of a targetable signaling network associated with patient survival. *Signal Transduct Target Ther* **2018**, *3*, 11, doi:10.1038/s41392-017-0005-2.

[230] Shang, M., Zhang, L., Chen, X. & Zheng, S. Identification of hub genes and regulators associated with pancreatic ductal adenocarcinoma based on integrated gene expression profile analysis. *Discovery Medicine* **2019**, *28*, 159-172.

[231] Kapoor, A., Yao, W., Ying, H., Hua, S., Liewen, A., Wang, Q., Zhong, Y., Wu, C. J., Sadanandam, A., Hu, B., Chang, Q., Chu, G. C., Al-Khalil, R., Jiang, S., Xia, H., Fletcher-Sananikone, E., Lim, C., Horwitz, G. I., Viale, A., Pettazzoni, P., Sanchez, N., Wang, H., Protopopov, A., Zhang, J., Heffernan, T., Johnson, R. L., Chin, L., Wang, Y. A., Draetta, G. & DePinho, R. A. Yap1 activation enables bypass of oncogenic Kras addiction in pancreatic cancer. *Cell* **2014**, *158*, 185-197, doi:10.1016/j.cell.2014.06.003.

[232] Rademaker, G., Hennequière, V., Brohée, L., Nokin, M. J., Lovinfosse, P., Durieux, F., Gofflot, S., Bellier, J., Costanza, B., Herfs, M., Peiffer, R., Bettendorff, L., Deroanne, C., Thiry, M., Delvenne, P., Hustinx, R., Bellahcène, A., Castronovo, V. & Peulen, O. Myoferlin controls mitochondrial structure and activity in pancreatic ductal adenocarcinoma, and affects tumor aggressiveness. *Oncogene* **2018**, *37*, 4398-4412, doi:10.1038/s41388-018-0287-z.

[233] Chung, W.-C., Challagundla, L., Zhou, Y., Li, M., Atfi, A. & Xu, K. Loss of Jag1 cooperates with oncogenic Kras to induce pancreatic cystic neoplasms. *Life Science Alliance* **2020**, *4*, e201900503, doi:10.26508/lsa.201900503.

[234] Dahlem, C., Barghash, A., Puchas, P., Haybaeck, J. & Kessler, S. M. The Insulin-Like Growth Factor 2 mRNA Binding Protein IMP2/IGF2BP2 is Overexpressed and Correlates with Poor Survival in Pancreatic Cancer. *International Journal of Molecular Sciences* **2019**, *20*, 3204, doi:10.3390/ijms20133204.

[235] Yan, W., Liu, X., Wang, Y., Han, S., Wang, F., Liu, X., Xiao, F. & Hu, G. Identifying Drug Targets in Pancreatic Ductal Adenocarcinoma Through Machine Learning, Analyzing Biomolecular Networks, and Structural Modeling. *Frontiers in Pharmacology* **2020**, *11*, 534-534, doi:10.3389/fphar.2020.00534.

[236] Li, J., Li, H., Zhu, W., Zhou, B., Ying, J., Wu, J., Zhang, H., Sun, H. & Gao, S. Deubiquitinase inhibitor degrasyn suppresses metastasis by targeting USP5-WT1-E-cadherin signalling pathway in pancreatic ductal adenocarcinoma. *Journal of Cellular and Molecular Medicine* **2020**, *24*, 1370-1382, doi:10.1111/jcmm.14813.

[237] Yang, Y., Zheng, Y., Liu, X., Ji, R., Chen, Z., Guo, Q., Wu, G., Wang, Y. & Zhou, Y. Comprehensive analysis of gene regulation network and immune signatures of prognostic biomarker YAP1 in pancreatic cancer. *Journal of Cancer* **2020**, *11*, 6960-6969, doi:10.7150/jca.49117.

[238] Birnbaum, D. J., Finetti, P., Lopresti, A., Gilabert, M., Poizat, F., Raoul, J.-L., Delpero, J.-R., Moutardier, V., Birnbaum, D., Mamessier, E. & Bertucci, F. A 25-gene classifier predicts overall survival in resectable pancreatic cancer. *BMC Medicine* **2017**, *15*, 170-170, doi:10.1186/s12916-017-0936-z.

[239] Sarkar Bhattacharya, S., Mandal, C., Albiez, R. S., Samanta, S. K. & Mandal, C. Mahanine drives pancreatic adenocarcinoma cells into endoplasmic reticular stress-mediated apoptosis through modulating sialylation process and Ca(2+)-signaling. *Scientific Reports* **2018**, *8*, 3911-3911, doi:10.1038/s41598-018-22143-w.

[240] Meng, M., Liu, S., Wang, C., Gu, X., Linghu, E. & Xue, X. Mass spectrum analysis of membrane proteins reveals that CASK, CD36 and EPB42 are differentially expressed in pancreatic adenocarcinoma. *Oncology Letters* **2020**, *20*, 376-376, doi:10.3892/ol.2020.12239.
[241] Kim, Y., Han, D., Min, H., Jin, J., Yi, E. C. & Kim, Y. Comparative proteomic profiling of pancreatic ductal adenocarcinoma cell lines. *Molecules and cells* **2014**, *37*, 888-898, doi:10.14348/molcells.2014.0207.
[242] Hong, J. Y., Cho, H. J., Kim, S. T., Park, Y. S., Shin, S. H., Han, I. W., Lee, J., Heo, J. S. & Park, J. O. Comprehensive molecular profiling to predict clinical outcomes in pancreatic cancer. *Therapeutic Advances in Medical Oncology* **2021**, *13*, 17588359211038478, doi:10.1177/17588359211038478.
[243] Storr, S. J., Zaitoun, A. M., Arora, A., Durrant, L. G., Lobo, D. N., Madhusudan, S. & Martin, S. G. Calpain system protein expression in carcinomas of the pancreas, bile duct and ampulla. *BMC Cancer* **2012**, *12*, 511-511, doi:10.1186/1471-2407-12-511.
[244] Pistoni, L., Gentiluomo, M., Lu, Y., López de Maturana, E., Hlavac, V., Vanella, G., Darvasi, E., Milanetto, A. C., Oliverius, M., Vashist, Y., Di Leo, M., Mohelnikova-Duchonova, B., Talar-Wojnarowska, R., Gheorghe, C., Petrone, M. C., Strobel, O., Arcidiacono, P. G., Vodickova, L., Szentesi, A., Capurso, G., Gajdán, L., Malleo, G., Theodoropoulos, G. E., Basso, D., Soucek, P., Brenner, H., Lawlor, R. T., Morelli, L., Ivanauskas, A., Kauffmann, E. F., Macauda, A., Gazouli, M., Archibugi, L., Nentwich, M., Loveček, M., Cavestro, G. M., Vodicka, P., Landi, S., Tavano, F., Sperti, C., Hackert, T., Kupcinskas, J., Pezzilli, R., Andriulli, A., Pollina, L., Kreivenaite, E., Gioffreda, D., Jamroziak, K., Hegyi, P., Izbicki, J. R., Testoni, S. G. G., Zuppardo, R. A., Bozzato, D., Neoptolemos, J. P., Malats, N., Canzian, F. & Campa, D. Associations between pancreatic expression quantitative traits and risk of pancreatic ductal adenocarcinoma. *Carcinogenesis* **2021**, *42*, 1037-1045, doi:10.1093/carcin/bgab057.
[245] Rikiishi, H. Possible role of autophagy in the treatment of pancreatic cancer with histone deacetylase inhibitors. *Cancers* **2010**, *2*, 2026-2043, doi:10.3390/cancers2042026.
[246] Zhang, Y., Liu, Q., Cui, M., Wang, M., Hua, S., Gao, J. & Liao, Q. Comprehensive Analysis of Expression, Prognostic Value, and Immune Infiltration for Ubiquitination-Related FBXOs in Pancreatic Ductal Adenocarcinoma. *Frontiers in Immunology* **2021**, *12*, 774435, doi:10.3389/fimmu.2021.774435.
[247] Lu, Y., Yi, Y., Liu, P., Wen, W., James, M., Wang, D. & You, M. Common human cancer genes discovered by integrated gene-expression analysis. *PLOS ONE* **2007**, *2*, e1149-e1149, doi:10.1371/journal.pone.0001149.
[248] Zhang, Z., Li, W., Yang, G., Lu, X., Qi, X., Wang, S., Cao, C., Zhang, P., Ren, J., Zhao, J., Zhang, J., Hong, S., Tan, Y., Burchfield, J., Yu, Y., Xu, T., Yao, X., James, D., Feng, W. & Chen, Z. CASK modulates the assembly and function of the Mint1/Munc18-1 complex to regulate insulin secretion. *Cell discovery* **2020**, *6*, 92-92, doi:10.1038/s41421-020-00216-3.
[249] Padden, J., Ahrens, M., Kälsch, J., Bertram, S., Megger, D. A., Bracht, T., Eisenacher, M., Kocabayoglu, P., Meyer, H. E., Sipos, B., Baba, H. A. & Sitek, B. Immunohistochemical Markers Distinguishing Cholangiocellular Carcinoma (CCC) from Pancreatic Ductal Adenocarcinoma (PDAC) Discovered by Proteomic Analysis of Microdissected Cells. *Molecular & cellular proteomics : MCP* **2016**, *15*, 1072-1082, doi:10.1074/mcp.M115.054585.
[250] Shang, M., Weng, L., Xu, G., Wu, S., Liu, B., Yin, X., Mao, A., Zou, X. & Wang, Z. TRIM11 suppresses ferritinophagy and gemcitabine sensitivity through UBE2N/TAX1BP1 signaling in pancreatic ductal adenocarcinoma. *Journal of Cell Physiology* **2021**, *236*, 6868-6883, doi:10.1002/jcp.30346.
[251] Musa, G., Cazorla-Vázquez, S., van Amerongen, M. J., Stemmler, M. P., Eckstein, M., Hartmann, A., Braun, T., Brabletz, T. & Engel, F. B. Gpr126 (Adgrg6) is expressed in cell

types known to be exposed to mechanical stimuli. *Annals of the New York Academy of Sciences* **2019**, *1456*, 96-108, doi:10.1111/nyas.14135.
[252] Zubair, H., Patel, G. K., Khan, M. A., Azim, S., Zubair, A., Singh, S., Srivastava, S. K. & Singh, A. P. Proteomic Analysis of MYB-Regulated Secretome Identifies Functional Pathways and Biomarkers: Potential Pathobiological and Clinical Implications. *Journal of Proteome Research* **2020**, *19*, 794-804, doi:10.1021/acs.jproteome.9b00641.
[253] Bandaru, S., Zhou, A. X., Rouhi, P., Zhang, Y., Bergo, M. O., Cao, Y. & Akyurek, L. M. Targeting filamin B induces tumor growth and metastasis via enhanced activity of matrix metalloproteinase-9 and secretion of VEGF-A. *Oncogenesis* **2014**, *3*, e119, doi:10.1038/oncsis.2014.33.
[254] Iguchi, Y., Ishihara, S., Uchida, Y., Tajima, K., Mizutani, T., Kawabata, K. & Haga, H. Filamin B Enhances the Invasiveness of Cancer Cells into 3D Collagen Matrices. *Cell Structure and Function* **2015**, *40*, 61-67, doi:10.1247/csf.15001.
[255] Surcel, A., Schiffhauer, E. S., Thomas, D. G., Zhu, Q., DiNapoli, K. T., Herbig, M., Otto, O., West-Foyle, H., Jacobi, A., Krater, M., Plak, K., Guck, J., Jaffee, E. M., Iglesias, P. A., Anders, R. A. & Robinson, D. N. Targeting Mechanoresponsive Proteins in Pancreatic Cancer: 4-Hydroxyacetophenone Blocks Dissemination and Invasion by Activating MYH14. *Cancer Research* **2019**, *79*, 4665-4678, doi:10.1158/0008-5472.CAN-18-3131.
[256] Bremer, S. C. B., Conradi, L. C., Mechie, N. C., Amanzada, A., Mavropoulou, E., Kitz, J., Ghadimi, M., Ellenrieder, V., Strobel, P., Hessmann, E., Gaedcke, J. & Bohnenberger, H. Enhancer of Zeste Homolog 2 in Colorectal Cancer Development and Progression. *Digestion* **2019**, 1-9, doi:10.1159/000504093.
[257] Li, J., Choi, P. S., Chaffer, C. L., Labella, K., Hwang, J. H., Giacomelli, A. O., Kim, J. W., Ilic, N., Doench, J. G., Ly, S. H., Dai, C., Hagel, K., Hong, A. L., Gjoerup, O., Goel, S., Ge, J. Y., Root, D. E., Zhao, J. J., Brooks, A. N., Weinberg, R. A. & Hahn, W. C. An alternative splicing switch in FLNB promotes the mesenchymal cell state in human breast cancer. *Elife* **2018**, *7*, doi:10.7554/eLife.37184.
[258] Brandenberg, N., Hoehnel, S., Kuttler, F., Homicsko, K., Ceroni, C., Ringel, T., Gjorevski, N., Schwank, G., Coukos, G., Turcatti, G. & Lutolf, M. P. High-throughput automated organoid culture via stem-cell aggregation in microcavity arrays. *Nature Biomedical Engineering* **2020**, *4*, 863-874, doi:10.1038/s41551-020-0565-2.
[259] Muñoz, J. J. & Zapata, A. G. in *Histology* (IntechOpen London, 2018).
[260] Co, J. Y., Margalef-Català, M., Li, X., Mah, A. T., Kuo, C. J., Monack, D. M. & Amieva, M. R. Controlling Epithelial Polarity: A Human Enteroid Model for Host-Pathogen Interactions. *Cell Rep* **2019**, *26*, 2509-2520.e2504, doi:10.1016/j.celrep.2019.01.108.
[261] Sean, d. l. O., Liu, Z., Sun, H., Yu, S. K., Wong, D. M., Chu, E., Rao, S. A., Eng, N., Peixoto, G., Bouza, J., Shen, Y., Knox, S. M., Tward, A. D., Gloyn, A. L. & Sneddon, J. B. Single-Cell Multi-Omic Roadmap of Human Fetal Pancreatic Development. *bioRxiv* **2022**, 2022.2002.2017.480942, doi:10.1101/2022.02.17.480942.
[262] Veres, A., Faust, A. L., Bushnell, H. L., Engquist, E. N., Kenty, J. H., Harb, G., Poh, Y. C., Sintov, E., Gurtler, M., Pagliuca, F. W., Peterson, Q. P. & Melton, D. A. Charting cellular identity during human in vitro beta-cell differentiation. *Nature* **2019**, *569*, 368-373, doi:10.1038/s41586-019-1168-5.
[263] Krentz, N. A. J., Lee, M. Y. Y., Xu, E. E., Sproul, S. L. J., Maslova, A., Sasaki, S. & Lynn, F. C. Single-Cell Transcriptome Profiling of Mouse and hESC-Derived Pancreatic Progenitors. *Stem Cell Reports* **2018**, *11*, 1551-1564, doi:10.1016/j.stemcr.2018.11.008.
[264] Petersen, M. B. K., Azad, A., Ingvorsen, C., Hess, K., Hansson, M., Grapin-Botton, A. & Honoré, C. Single-Cell Gene Expression Analysis of a Human ESC Model of Pancreatic Endocrine Development Reveals Different Paths to β-Cell Differentiation. *Stem Cell Reports* **2017**, *9*, 1246-1261, doi:10.1016/j.stemcr.2017.08.009.

[265] Wang, J., Yuan, R., Zhu, X. & Ao, P. Adaptive Landscape Shaped by Core Endogenous Network Coordinates Complex Early Progenitor Fate Commitments in Embryonic Pancreas. *Scientific Reports* **2020**, *10*, 1112, doi:10.1038/s41598-020-57903-0.
[266] Chen, C., Shiota, C., Agostinelli, G., Ridley, D., Jiang, Y., Ma, J., Prasadan, K., Xiao, X. & Gittes, G. K. Evidence of a developmental origin for β-cell heterogeneity using a dual lineage-tracing technology. *Development* **2019**, *146*, doi:10.1242/dev.164913.
[267] Larsen, H. L., Martín-Coll, L., Nielsen, A. V., Wright, C. V. E., Trusina, A., Kim, Y. H. & Grapin-Botton, A. Stochastic priming and spatial cues orchestrate heterogeneous clonal contribution to mouse pancreas organogenesis. *Nature communications* **2017**, *8*, 605, doi:10.1038/s41467-017-00258-4.
[268] Vujasinovic, M., Dugic, A., Maisonneuve, P., Aljic, A., Berggren, R., Panic, N., Valente, R., Pozzi Mucelli, R., Waldthaler, A., Ghorbani, P., Kordes, M., Hagström, H. & Löhr, J. M. Risk of Developing Pancreatic Cancer in Patients with Chronic Pancreatitis. *Journal of Clinical Medicine* **2020**, *9*, doi:10.3390/jcm9113720.
[269] Vujasinovic, M., Valente, R., Del Chiaro, M., Permert, J. & Löhr, J. M. Pancreatic Exocrine Insufficiency in Pancreatic Cancer. *Nutrients* **2017**, *9*, 183, doi:10.3390/nu9030183.
[270] Delon, L. C., Guo, Z., Oszmiana, A., Chien, C. C., Gibson, R., Prestidge, C. & Thierry, B. A systematic investigation of the effect of the fluid shear stress on Caco-2cells towards the optimization of epithelial organ-on-chip models. *Biomaterials* **2019**, *225*, 119521, doi:10.1016/j.biomaterials.2019.119521.
[271] Flitney, E. W., Kuczmarski, E. R., Adam, S. A. & Goldman, R. D. Insights into the mechanical properties of epithelial cells: the effects of shear stress on the assembly and remodeling of keratin intermediate filaments. *FASEB Journal* **2009**, *23*, 2110-2119, doi:10.1096/fj.08-124453.
[272] Kulthong, K., Hooiveld, G., Duivenvoorde, L., Miro Estruch, I., Marin, V., van der Zande, M. & Bouwmeester, H. Transcriptome comparisons of in vitro intestinal epithelia grown under static and microfluidic gut-on-chip conditions with in vivo human epithelia. *Scientific Reports* **2021**, *11*, 3234, doi:10.1038/s41598-021-82853-6.
[273] Lindner, M., Laporte, A., Block, S., Elomaa, L. & Weinhart, M. Physiological Shear Stress Enhances Differentiation, Mucus-Formation and Structural 3D Organization of Intestinal Epithelial Cells In Vitro. *Cells* **2021**, *10*, doi:10.3390/cells10082062.
[274] Molladavoodi, S., Robichaud, M., Wulff, D. & Gorbet, M. Corneal epithelial cells exposed to shear stress show altered cytoskeleton and migratory behaviour. *PLOS ONE* **2017**, *12*, e0178981, doi:10.1371/journal.pone.0178981.
[275] Xu, M., He, J., Zhang, C., Xu, J. & Wang, Y. Strategies for derivation of endothelial lineages from human stem cells. *Stem Cell Res Ther* **2019**, *10*, 200, doi:10.1186/s13287-019-1274-1.
[276] Olmer, R., Engels, L., Usman, A., Menke, S., Malik, M. N. H., Pessler, F., Gohring, G., Bornhorst, D., Bolten, S., Abdelilah-Seyfried, S., Scheper, T., Kempf, H., Zweigerdt, R. & Martin, U. Differentiation of Human Pluripotent Stem Cells into Functional Endothelial Cells in Scalable Suspension Culture. *Stem Cell Reports* **2018**, *10*, 1657-1672, doi:10.1016/j.stemcr.2018.03.017.
[277] Sun, H., Zhang, B. & Li, H. The Roles of Frequently Mutated Genes of Pancreatic Cancer in Regulation of Tumor Microenvironment. *Technology in Cancer Research & Treatment* **2020**, *19*, 1533033820920969, doi:10.1177/1533033820920969.
[278] Orth, M., Metzger, P., Gerum, S., Mayerle, J., Schneider, G., Belka, C., Schnurr, M. & Lauber, K. Pancreatic ductal adenocarcinoma: biological hallmarks, current status, and future perspectives of combined modality treatment approaches. *Radiation Oncology* **2019**, *14*, 141, doi:10.1186/s13014-019-1345-6.
[279] Morris, J. P., Wang, S. C. & Hebrok, M. KRAS, Hedgehog, Wnt and the twisted developmental biology of pancreatic ductal adenocarcinoma. *Nature Reviews Cancer* **2010**, *10*, 683-695, doi:10.1038/nrc2899.

[280] Wang, S., Huang, S. & Sun, Y. L. Epithelial-Mesenchymal Transition in Pancreatic Cancer: A Review. *BioMed research international* **2017**, *2017*, 2646148-2646148, doi:10.1155/2017/2646148.
[281] Wakiya, T., Ishido, K., Yoshizawa, T., Kanda, T. & Hakamada, K. Roles of the nervous system in pancreatic cancer. *Annals of Gastroenterological Surgery* **2021**, *5*, 623-633, doi:10.1002/ags3.12459.
[282] Jaworski, J. J., Morgan, R. D. & Sivakumar, S. Circulating Cell-Free Tumour DNA for Early Detection of Pancreatic Cancer. *Cancers* **2020**, *12*, 3704, doi:10.3390/cancers12123704.
[283] Müller, J. A., Groß, R., Conzelmann, C., Krüger, J., Merle, U., Steinhart, J., Weil, T., Koepke, L., Bozzo, C. P., Read, C., Fois, G., Eiseler, T., Gehrmann, J., van Vuuren, J., Wessbecher, I. M., Frick, M., Costa, I. G., Breunig, M., Grüner, B., Peters, L., Schuster, M., Liebau, S., Seufferlein, T., Stenger, S., Stenzinger, A., MacDonald, P. E., Kirchhoff, F., Sparrer, K. M. J., Walther, P., Lickert, H., Barth, T. F. E., Wagner, M., Münch, J., Heller, S. & Kleger, A. SARS-CoV-2 infects and replicates in cells of the human endocrine and exocrine pancreas. *Nature Metabolism* **2021**, *3*, 149-165, doi:10.1038/s42255-021-00347-1.

8 Supplement

8.1 Material list

Material	Company	Product number
254 nm UV light	NK-Optik	/
3-Isobutyl-1-methylxanthine	Sigma	I5879
Accutase	Sigma	A6964
Activin A	PeproTech	120-14
Agarose	Sigma	A9539
Antibody Diluent	Zytomed	ZUC025
Asiga PICO2 HD 27 UV385	Asiga	/
Axio Observer LSM 880	Zeiss	2042220
bFGF	Novoprotein	C046
C18 reversed phase analytical column	Waters	/
C18 trap column	LC Packings	/
Caerulein	Sigma	C9026
Chromium Single Cell 3' library and gel bead kit v3.1	10x Genomics	PN-1000121
Citrate buffer	Vector Laboratories	H-3300
Citric acid	Sigma	251275
DAPI	Sigma	D9542
DMEM	Gibco	41966052
DMEM/F12	Gibco	12634010
DMSO	Schuber und Weiss	APP A3672,0250
Dorsomorphin	Sigma	P5499
Dulbecco's Phosphate Buffered Saline	Gibco	10010056
EGF	R&D	236-EG-200
Envision FLEX HRP Magenta high pH kit	Dako	GV900
Fatty acid free (FAF) Bovine Serum Albumin (BSA)	Proliant and Roche	68700
FGF10	R&D	345-FG
FGF10	Peprotech	100-26
FLNB ELISA kit	MyBioSource	MBS451921
Fluoromount-G	SouthernBiotech	0100-01
4% PFA	Thermo Fisher Scientific	15670799
Forskolin	Abcam	ab120058
Fully automated OMNIS staining device	Dako	/
Glucose	Sigma	G7528
Glutamax	Gibco	35050038
Glycin	Roth	0079.1

Material	Company	Product number
Growth factor reduced (GFR) Matrigel	Corning	354230
GSK3β-inhibitor (CHIR99021)	Axon MedChem	1386
Haematoxylin	Dako	CS700
Heat-inactivated FBS	Thermo Fisher Scientific	Corning Media Tech 35-079-CV
hESC Matrigel	Corning	354277
Hydroxypropylmethylcellulose	Fluka Analytical	09963
Indolactam V	StemCell Technologies	72312
Insulin-transferrin-selenium-X	Gibco	51500056
KGF	PeproTech	100-19
L-ascorbic acid	Sigma	A4544
LDN-193189	Sigma	SML0559
MCDB131	Thermo Fisher Scientific	10372019
Mouse Wnt3a	PeproTech	315-20
MSC2530818	Selleckchem	S8387
mTeSR1	Stemcell Technologies	85850
Nano-RSLC, Ultimate 3000 RSLC	Dionex	/
Nicotinamide	Sigma	N0636
NovaSeq 6000 S2 flow cell	Illumina	/
Otoflash G171	NK-Optik	644900
PDMS, SYLGARD™ 184 Silicone Elastomer Kit	Dow Chemical Company	39100000
Penicillin/Streptomycin	Sigma and Thermo	P4333
Pluronic F-127	Sigma	P2443
Polyglactin coated vicryl suture	Ethicon	/
Q-Exactive HF-X mass spectrometer	Thermo Fisher Scientific	/
Retinoic acid	Sigma	R2625
RIPA buffer	Thermo Fisher Scientific	89900
ROCK inhibitor Y-27632	abcam	ab120129
SANT-1	Sigma	S4572
Sodium bicarbonate	Sigma	S5761
Sodium phosphate	Sigma	71649
Stage top incubator	Tokai Hit	/
Sucrose	Sigma	S0389
SuperFrost Ultra Plus microscope slides	Thermo Fisher Scientific	1255015
TBS	Duolink	82048
TBS-T	Duolink	82047
Tramadol	Grünenthal	/
Tris buffer	Vector Laboratories	H3301250
TrypLE Select	Gibco	11588846
Tween 20	Roth	9127.1

Material	Company	Product number
Ultra-pure SDS	Invitrogen	24730020
X-CLARITY Mounting Solution	Logos Biosystems	LGBED0004
$ZnSO_4$	Sigma	Z0251

8.1.1 Antibody list

The antibody list is adapted from Wiedenmann, et al. [1] and used with "author permission rights" from Nature.

Antibody	Clone	Staining method	Condition	Dilution	Company	Catalog	Lot	Antibody validation
AcTub (aa K40 acetylated)	EPR16772	IF-p	steamer Citrat	1000	Abcam	ab179484	GR3240369-6	[2]
AMY2A	polyclonal	IF-p	steamer Citrat	1000	Sigma	A8273-1VL	068K4796	[109]
AQP5	EPR3747	IF-p	steamer Citrat	200	Abcam	ab92320	GR3273694-1	[1]
ARL13B	N295B/66	IF-p	steamer Citrat	1000	Abcam	ab136648	GR3272548-1	[2]
BICC1	polyclonal	IF-p	steamer Citrat	75	Sigma	NBP194171	NA	[1]
CA2	EPR5195	IF-p	steamer Citrat	500	Abcam	ab124687	GR155503-7	[2]
CDH1	24E10	IF-p	steamer Citrat	200	Cell Signaling	3195	13	[2]
CDH1	36	IF-p	steamer Citrat	1000	BD Bioscience	610182	9315423	[2]
CFTR	D6W6L	IF-p	steamer Citrat/ steamer Tris	200/ 400	Cell Signaling	78335	1	[2]
CFTR	13-1	IF-p	steamer Tris	200	R&D	MAB1660	BLG022005A	[2]
CHGA	DAK-A3	IF-p	steamer Citrat	200	Dako	M0869	20081824	[283]
CLDN1	polyclonal	IF-p	steamer Tris	100	Abcam	ab15098	GR282937-1	[2]
COL4A1	polyclonal	IF-p	steamer Citrat	500	Abcam	ab6586	GR3350938-1/ GR322984-1	[1]
FLNB	polyclonal	IF-p	steamer Citrat	50	Merck	HPA004886	000018297	[1]
GATA6	D61E4	IF-p	steamer Tris	300	Cell Signaling	5851	5	[1]
HNF1B	CL0374	IF-p	steamer Citrat	100	Abcam	ab236759	GR3279363-6	[2]
Human Nucleoli antibody	NM95	IF-p	steamer Citrat	200	Abcam	ab190710	GR3269017-3	[2]
Ki-67	MIB-1	IF-p	steamer Citrat	200	DAKO	M7240	20083387	[2]
KRT19	RCK108	IF-p	steamer Citrat or Tris	100	DAKO	M0888	20062456/ 41236534	[2]

Antibody	Clone	Staining method	Condition	Dilution	Company	Catalog	Lot	Antibody validation
KRT7	OV-TL	IF-p	steamer Citrat	200	DAKO	M7018	20064378	[2]
KRT8	CAM5.2	IF-p	steamer Tris	100	BD Bioscience	345779	5292988	[109]
MMP1	EP1247Y	IF-p	steamer Tris	150	Abcam	ab52631	GR3261996-3	[1]
MUC1	VU4H5	IF-p	steamer Citrat	100	Santa Cruz	sc-7313	A2114	[2]
MUC1	D908K	IF-p	steamer Tris	200	Cell Signaling	14161	1	[1]
MUC13	TCC16	IF-p	steamer Citrat	500	Biolegend	363902	B190123	[1]
MUC2	Ccp58	IF-p	steamer Tris	200	Santa Cruz	sc-15334	00920	[2]
MUC5AC	CLH2	IF-p	steamer Citrat	100	Santa Cruz	sc-33667	J1408	[2]
MUC6	CLH5	IF-p	steamer Tris	100	Santa Cruz	sc-33668	B0520	[1]
NKX6-1	FF5A12	IF-p	steamer Citrat or Tris	150	DSHB Hybridoma	SH30349	AD18110292/ AE29446913	[109]
OCT4	C-10	IF-p	steamer Citrat	100	Santa Cruz	sc-5279	C2014	[1]
PDX1	polyclonal	IF-p	steamer Citrat or Tris	500	R&D	AF2419	UNY0119031	[109]
SCTR	polyclonal	IF-p	steamer Citrat	100	Atlas Antibodies/ Sigma	HPA007269/ SAB4502719	A119297/ 61742	[1]
SOX2	245610	IF-p	steamer Citrat	300	R&D	MAB2018	NA	[1]
SOX9	polyclonal	IF-p	steamer Citrat	500	Millipore	AB5535	3249418/ 3282152	[109]
TFF1	GE2	IF-p	steamer Tris	100	Novus Biologicals	NBP2-34293	7031-1P180627	[1]
VIM	D21H3	IF-p	steamer Citrat	500	Cell Signaling	5741	6	[2]
ZEB1	H-3	IF-p	SKT or steamer Tris	300	Santa Cruz	sc-515797	C0520	[2]
ZO-1	A12	IF-p	steamer Citrat	100	Invitrogen	33-9100	TL277395	[2]
FLNB	polyclonal	IHC-p	EnVision FLEX HRP Magenta, High pH (Dako Omnis)	50	Merck	HPA004886	000018297	[1]
CDH1	24E10	ICC/IF	Organoid/ tissue slices	200	Cell Signaling	3195	13	[2]
CFTR	D6W6L	ICC/IF	Organoid/ tissue slices	800	Cell Signaling	78335	1	[2]
CLDN1	421203	ICC/IF	Organoid/ tissue slices	200	R&D	MAB4618	ZZY031912B	[1]
COL4A1	polyclonal	ICC/IF	Organoid/ tissue slices	500	Abcam	ab6586	GR3350938-1/GR322984-1	[1]

Antibody	Clone	Staining method	Condition	Dilution	Company	Catalog	Lot	Antibody validation
KRT19	RCK108	ICC/IF	Organoid/ tissue slices	100	DAKO	M0888	20062456/ 41236534	[2]
MUC13	TCC16	ICC/IF	Organoid/ tissue slices	500	Biolegend	363902	B190123	[1]
PDX1	polyclonal	ICC/IF	Organoid/ tissue slices	500	R&D	AF2419	UNY0119031	[109]
SOX9	D8G8H	ICC/IF	Organoid/ tissue slices	400	Cell Signaling	82630	1	[1]
SOX9	polyclonal	ICC/IF	Organoid/ tissue slices	500	Millipore	AB5535	3249418/ 3282152	[109]
ZO-1	A12	ICC/IF	Organoid/ tissue slices	200	Invitrogen	339100-A555	TI277386	[2]
c-KIT	104D2	FC	surface staining	100	Invitrogen	CD11705	2086609	[109]
CXCR4	12G5	FC	surface staining	50	Invitrogen	MHCXCR404	2153692	[109]
NKX6-1	FF5A12	FC	Intra-cellular staining	150	DSHB Hybridoma	SH30349	AD18110292/ AE29446913	[109]
NKX6-1-APC	R11-560	FC	Intra-cellular staining	35	BD Bioscience	563338	1062126	[2]
PDX1	polyclonal	FC	Intra-cellular staining	500	R&D	AF2419	UNY0119031	[109]
PDX1-PE	658A5	FC	Intra-cellular staining	35	BD Bioscience	562161	0058961	[2]

8.2 Protocols developed for the thesis

8.2.1 PDMS microwell chip molding

1. Pre-coat the mold with a citric acid sodium phosphate buffer with 0.1% (Hydroxypropyl)methylcellulose for 10 min.
2. Store in fridge ((Hydroxypropyl)methylcellulose is more soluble in low temperatures).
3. Remove bubbles with a vacuum pump.
4. Rinse with deionized water.
5. Dry with nitrogen.
6. Prepare 1:10 curing agent: PDMS (about 10 g per chip in 6-well).
7. Mixing PDMS with the program: 3 min both directions with 1500 rpm.

8. Put a little drop of PDMS in a six-well, then press the chip mold in it and fill PDMS over it completely.
9. Remove bubbles by evacuating under the vacuum, stay with the vacuum pump for the first minutes and open it carefully if necessary to avoid boiling.
10. Open the vacuum all 10min until no bubbles appear anymore from the pillars.
11. Carefully add the coverglass in the middle and let it sink, do not push it because it will cause bubbles.
12. Push the coverglass from left to right to remove all the PDMS underneath.
13. Bake for at least 1.5 h at 80°C.
14. Put isopropanol on top of the PDMS and circle with a scooper to get the chip out
15. Turn it around and add isopropanol again
16. Carefully remove the printed mold by lifting it slightly away from all sides. Make sure isopropanol is underneath.
17. Turn the chip around again, cut it to the glass, and then remove it.
18. Cut the rest overlapping PDMS of the chip for better imaging.

8.2.2 Cell seeding onto the microwell duct-on-chip technology

Sterilization and coating

1. Coating with 10% pluronic acid overnight
2. Use the vacuum pump to fill all the wells with pluronic acid.
3. Put with pluronic under the hood and sterilize with sterilizer for 30 min.
4. Aspirate the pluronic acid.
5. Wash with PBS, and pipet a few times up and down (you will see some "fog").
6. Wash with media, pipet a few times up and down.
7. Aspirate media and ensure all liquid is gone around the stamps (DON’T go inside the stamps).
8. Try to put 20 µl drop of media in the stamp to check if it is leaking or not. If yes, redo the previous step.
9. When all stamps are fine, continue to prepare the cells.

Cell seeding

1. Count cells, calculate per array and well number. E.g., the standard conditions:

600 cells per well in the 300 µm well diameter for one chip. Calculate with one more array than you want to seed that you have enough cell suspension.

$$cell\ number\ (600) * well\ number\ (61) * array\ number\ (4+1) = 183{,}000\ \text{cells}$$

	150 µm chip	300 µm chip	600 µm chip
Number of wells per array	251	61	19

2. Centrifuge the cells with 300x g for 5 min.
3. Dilute that you have the correct number of cells in 20 µl per array.
   For the previous example, it would be 100 µl (5 * 20 µl).
4. Aspirate the media in the stamps (do not touch the ground. Do not use the pump.).
5. Before you seed, pipet once up and down, then seed the cells onto the chip.
6. Let them settle at room temperature for 20min**.**
7. Put in an incubator for 30 min.
8. Add ~600 µl of media carefully in the corner, and make sure there are no bubbles in the wells.

8.2.3 HiPSC differentiation to PDLOs

The differentiation protocol for PPs was developed and published before[109,145]. The differentiation protocol for PDLOs was developed by Breunig, et al. [2] and adapted for the PDLO on-chip application.

Well plate coating

1. Thaw GFR-Matrigel on ice.
2. Coat the wells (24 well plate) with 220 µl GFR-Matrigel in DMEM:F12 (1:18 mix on ice and cool down DMEM:12 before).
   Make sure that the entire surface of the well is covered and does not dry out.
3. Incubate the well plate for 1 h at 37°C.

4. Aspirate Matrigel and add 200 µl mTesR+ROCK (1:1000)

Cell seeding for differentiation

5. Wash hiPSCs once with PBS before splitting.
6. Add 700 µl TrypLE Select for 3 to a maximum of 5 min at 37°C.
   → hiPSCs should detach when you slightly move the plate.
7. Add 2 ml DMEM:F12 to detach the hiPSCs.
   Resuspend by gently pipetting up and down 2-3 times with a 5 ml pipette.
   → Avoid shear stress from too much pipetting, shaking and moving.
8. Centrifuge at 200x g for 4 min.
9. Resuspend in mTesR + ROCK (1:1000) by gently pipetting up and down 2-3 times with 5 ml pipette.
10. Plate 25,000 hiPSCs per well in the pre-coated 24-well plate.
11. Change media 4 h before differentiation start to pure mTesR.
12. According to the table "Differentiation protocol until pancreas progenitors", change media every day.
13. Check the definitive endoderm (day 3), pancreatic endoderm (day 10), and pancreas progenitor (day 13) stage with FACS stainings.

	Base media 1 (BE1)		Base media 3 (BE3)	
Compound	**Final concentration**	**Volume (µl)**	**Final concentration**	**Volume (µl)**
75g/l Sodium Bicarbonate	1.174 g	782.7	1.754 g	1169.3
100x Glutamax	1x	500	1x	500
200g/l Glucose	0.8 g	200	3.3 g	825
75g/l FAF-BSA	5 g	3333.3	20 g/l	13333.3
ITS-X				250
MCDB131		45684		35091.7
Total in µl		**50000**		**50000**

Table 1 | Media composition of the base media for the differentiation.

The media composition is according to Breunig, et al. [2].

Differentiation protocol until pancreas progenitors			
	Compound	**Final concentration**	**Volume in µl**
Stage 1 (day 0) Media day 0	**BE1**		9986
	Act A	100 ng/ml	10
	CHIR	2 µM	4
	Total in µl		10000
Stage 1 (days 1-2) Media change every day	**BE1**		9989
	Act A	100 ng/ml	10
	bFGF	5 ng/ml	1
	Total in µl		10000
Stage 2 (days 3-5) Media change every day	**BE1**		9986
	FGF10	50 ng/ml	10
	DorsoM	0,75 µM	1
	Wnt3a	3 ng/ml	1
	Total in µl		10000
Stage 3 (days 6-8) Media change every day	**BE3**		9965,5
	FGF10	50 ng/ml	10
	LDN	200 nM	10
	SANT-1	0,25 µM	2,50
	RA	2 µM	2
	Ascorbic Acid	0,25mM	10
	Total in µl		10000
Stage 4 (days 9-12) Media change every day	**BE3**		9863
	LDN	200 nM	2
	EGF	100 ng/ml	20
	NA	10 mM	100
	ILV	330 nM	5
	Ascorbic Acid	0,25mM	10
	Total in µl		10000

Table 2 | Media composition of the differentiation toward PPs.

The media composition is according to Breunig, et al. [2].

Differentiation transfer to the microwell chip

Follow the protocol “Cell seeding onto the microwell duct-on-chip technology”.

For detaching the PPs:

1. Wash PPs once with PBS before splitting.
2. Add 220 µl TrypLE Select for 5-10 min at 37°C.
   → PPs should detach when you slightly move the plate.
3. Add 500 µl DMEM:F12 to detach the PPs.

Resuspend by gently pipetting up and down 2-3 times.

→ Avoid shear stress from too much pipetting, shaking and moving.

4. Centrifuge at 200x g for 5 min.
5. Continue with protocol “Cell seeding onto the microwell duct-on-chip technology” at cell seeding.

Ductal two-phase differentiation media			
Phase 1: day 13-20 media change at d13 & d17	**Compound**	**Final concentration**	**Volume in µl**
	BE3		9739.9
	Nicotinamide	10 mM	100
	ZnSO4	10 µM	10
	Rock Inhibitor (just for the first media change)	10 µM	10
	EGF	50 ng/ml	10
	FGF10	50 ng/ml	10
	KGF	50 ng/ml	10
	MSC	50 nM	0.1
	Ascorbic Acid	0.044 g/L	10
	Pen/Strep	1%	100
	Total in µl		**10000**
Phase 2: day 20 until day 27 or longer media change twice per week	**Compound**	**Final concentration**	**Volume in µl**
	BE3		9760
	Nicotinamide	10 mM	100
	ZnSO4	10 µM	10
	EGF	50 ng/ml	10
	FGF10	50 ng/ml	10
	Ascorbic Acid	0.044 g/L	10
	Pen/Strep		100
	Total in µl		**10000**

Table 3 | Media composition of the 2 phase ductal differentiation protocol.

The media composition is according to Breunig, et al. [2].

8.2.4 Fast acrylamide free tissue clearing and immunofluorescence staining on-chip

Fixation

1. Wash with PBS.
2. Add 4% PFA.
3. Three days fixing at 4°C.

Clearing

4. 1-24 h of 8% SDS in 1x PBS (10% Ultra pure SDS + MilliQ+ 1x PBS pill).
5. For the duration, check when the orgnoids get invisible.
6. Wash once with PBS.

Staining primary antibody

7. Wash 2x 1 h with PBST on a shaker.
8. Blocking with 1% BSA, 22.52 mg/ml Glycin and 0.1% Tween20 for 1 h.
9. 1st antibody in 1% BSA and 0.1% Tween20.
10. Incubate for 1-4 days.

Staining secondary antibody

11. Wash 2x 10 min Wash A.
12. Secondary antibody in 1% BSA for 4 h at room temperature in the dark or at 4°C overnight.
13. Wash 2x 10 min Wash B.
14. Add DAPI 1:1000 for 15 min.
15. Wash 3x Wash A.
16. Postfixation with 4% PFA for 30 min
17. Store in PBS.

Imaging

18. Cut chip and put in ibidi (can also be done before staining).
    a. Remove all of the PBS.
    b. Then cut with a scalpel the arrays.
    c. Put the parts with a tweezer to a 8-well ibidi.
19. Add 40 µl X-CLARITY.
20. Go for measurement.

8.2.5 Proteome and secretome sample extraction from the microwell chip

1. Wash chip with DMEM:F12 three times:
    a. Remove carefully complete media (be careful not to take out the organoids).

b. Add 3 ml DMEM:F12 to the pipetting help.
c. Incubate for 1 h at 37°C.
d. Repeat a-c three times.

2. Critical step: try to take out the complete media, but avoid taking out the organoids.
3. Add 700µl carefully DMEM:F12 on the organoids, avoiding that the pipetting help is filled.
4. Keep it for 8 h in an incubator at 37°C.

Supernatant for Secretome

You should use protein-low binding tubes.

5. Take all of the supernatant (very carefully, avoid aspiration of any organoids).

   Do step 8. before you continue here.

6. Centrifuge the supernatant (short, maximum 1 min with 200xg).
7. Freeze the supernatant at -80°C (to ensure there are no organoids or dead cells in anymore).

Organoid Pellet for Proteome

You should use protein-low binding tubes.

8. Add ice-cold PBS to the organoids (directly after taking the supernatant away).
9. Pipet up and down with 1000µl pipet a few times to remove the organoids from the chip.

   Before you pipet the organoids, make sure you coated the pipet tip with PBS (otherwise, you might lose more organoids).

10. Repeat steps 7 and 8 until you get almost all of the organoids (check under the microscope).
11. Wash organoids with PBS at least three times.
    a. Wait 10min in between.
    b. Centrifuge 5min 200x g.
12. Freeze organoid pellet at -80°C until measured.

8.3 Author contribution

Sandra Wiedenmann, Markus Breunig, Meike Hohwieler, Alexander Kleger and Matthias Meier designed the study Wiedenmann, et al. [1]. ***Sandra Wiedenmann*** designed and produced the microwell chips, based on work from Michel Moussus. ***Sandra Wiedenmann***, Markus Breunig, Jessica Merkle and Meike Hohwieler executed the biological experiments. ***Sandra Wiedenmann***, Markus Breunig, Meike Hohwieler and Tihomir Georgiev did the imaging and image analysis. ***Sandra Wiedenmann***, Michael Sterr and Heiko Lickert performed the scRNA-seq processing and ***Sandra Wiedenmann*** did the analysis. Christine von Törne and Stefanie M. Hauck did the mass spectrometric measurements and data processing. ***Sandra Wiedenmann***, Markus Breunig and Matthias Meier analyzed the MS/MS results. Stephanie E. Weißinger and Peter Möller stained and evaluated the FLNB patient cohort and ***Sandra Wiedenmann*** analyzed the results. Lucas Schulte and Thomas Seufferlein took the serum samples of the PDAC patient cohort, Meike Hohwieler performed the ELISA, and ***Sandra Wiedenmann*** analyzed the results. Meike Hohwieler, Alexander Kleger and Matthias Meier received the funding and supervised the study. The manuscript for the publication Wiedenmann, et al. [1] was written by ***Sandra Wiedenmann***, Markus Breunig, Meike Hohwieler, Alexander Kleger and Matthias Meier.